

LIQUID-LIQUID TWO-PHASE FLOW AND MASS TRANSFER IN MICROCHANNELS

By

MAYUR RAMESH DAREKAR

Registration no. ENGG01201404004

Bhabha Atomic Research Centre, Trombay

*A thesis submitted to the
Board of Studies in Engineering Sciences*

*In partial fulfillment of requirements
for the Degree of*

DOCTOR OF PHILOSOPHY

of

HOMI BHABHA NATIONAL INSTITUTE



July, 2020



Homi Bhabha National Institute

Report of Ph.D. Viva-Voce

Board of Studies in Engineering Sciences

A. General Details:

1. **Name of the Constituent Institution:** Bhabha Atomic Research Centre

2. **Name of the Student:** Mayur Ramesh Darekar

3. **Enrolment Number:** ENGG01201404004

4. **Date of Enrolment in HBNI:** August 2014

5. **Date of Submission of Thesis:** 18-12-2019

6. **Title of the Thesis:** "Liquid-liquid two-phase flow and mass transfer in microchannels"

7. **Number of Doctoral Committee Meetings held with respective dates:**

Review Period	Date	Review Period	Date
1. August 2014 to July 2015	14-10-2015	2. August 2015 to July 2016	17-08-2016
3. August 2016 to July 2017	21-08-2017	4. August 2017 to July 2018	31-07-2018
5. August 2018 to July 2019	08-08-2019	6. Presynopsis	23-09-2019

8. **Name and Affiliation of the Thesis Examiner 1:** Prof. H.-J. Bart, Chair of Separation Science & Technology, TU Kaiserslautern, Germany.

Recommendations of the Examiner 1 (Thesis Evaluation) (i) ~~accepted~~, (ii) accepted after revisions, or (iii) ~~rejected~~: Accepted after revisions

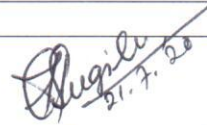
9. **Name and Affiliation of the Thesis Examiner 2:** Prof. S. Pushpavanam, Chemical Engineering Department, Indian Institute of Technology Madras, Chennai-600036, India.

Recommendations of the Examiner 2 (Thesis Evaluation) (i) accepted, (ii) ~~accepted after revisions~~, or (iii) ~~rejected~~: Accepted

B. Record of the Viva-Voce Examination

1. **Date of Viva Voce Examination:** 21/07/2020
2. **Name and affiliation of External Examiner:** Prof. S. Pushpavanam, Chemical Engineering Department, Indian Institute of Technology Madras, Chennai-600036, India.
3. **Whether there were other experts / faculty/students present? Please enclose a soft copy of attendance sheet indicating participation in person/over video as per proforma given below at (5)**
4. **Recommendations for the award of the Ph.D. degree: Recommended / Not Recommended**
The research work titled "Liquid-liquid two-phase flow and mass transfer in microchannels" was carried out to understand liquid-liquid two-phase flow hydrodynamics and various aspects of solvent extraction in microchannels using liquid-liquid systems relevant to solvent extraction in nuclear fuel cycle. Experimental methodology to identify an optimum configuration for solvent extraction in microchannel at a desired throughput for a given liquid-liquid system is proposed. A novel monoblock distributor having in-built microfluidic junctions for realizing higher throughputs using numbering-up approach is conceptualized and evaluated. Intensification of phase separation of a liquid-liquid dispersion generated at a microfluidic junction is explored using an in-line phase separator housing a metallic mesh. Finally, a complete process of recovery of uranium from lean streams comprising of extraction, and direct precipitation is demonstrated using microchannels.
Overall quality of thesis: ~~Excellent~~ / Very Good / Good / Satisfactory
(If recommended, give summary of main findings and overall quality of thesis)
(If not recommended, give reasons for not recommending and guidelines to be communicated by Convener of the Doctoral committee to the student for further work)
5. **Attendance at Viva Voce (Doctoral Committee, External Examiner, others):**

Sr No	Composition	Name	Attended in person or through video; if in person, signature
1.	Chairman	Prof. G. Sugilal	Attended through video conference
2.	Convener (Guide)	Prof. Sulekha Mukhopadhyay	Attended through video conference
3.	External Examiner	Prof. S. Pushpavanam	Attended through video conference
4.	Member	Prof. S. B. Roy	Attended through video conference
5.	Member	Prof. R.N. Singh	Attended through video conference
6.	Member	Prof. Deep Prakash	Attended through video conference
7.	The Technology Adviser , if any	Dr K. K. Singh	Attended through video conference
Others: list in separate sheet			


(Chairman, Doctoral Committee III)

Other participants

S.No.	Name	Designation/ Affiliation
1	Dr. T.L. Prasad	SO/G, DD, BARC
2	Smt. Deepa Thomas	ChED, BARC
3	Dr. (Smt.) Smita Mishra	SO/F, ChED, BARC
4	Shri Gaurav Varshney	SO/F, ChED, BARC
5	Kum Garima Pandey	SO/D, ChED, BARC
6	Shri Sourav Sarkar	SO/D, ChED, BARC
7	Dr. Nirvik Sen	SO/E, ChED, BARC
8	Shri Rajnesh Chaurasiya	DDFS, PhD Student, HBNI
9	Shri Snehasis Dutta	SO/D, ChED, BARC
10	Shri Vijay Mamtani	SO/E, MDS, BARC
11	Kum Ritu Parashar	DDFS PhD student
12	Shri Mihir Chatterjee	SO/G, ChTD, BARC
13	Dr. Soumitra Kar	SO/F, MDS, BARC
14	Shri Sujeesh	SO/E, ChTD, BARC
15	Shri Soumya Sarkar	SO/G, NRB
16	Shri Ankit Badiwal	SO/C, ChED, BARC
17	Dr. A.K. Ghosh	SO/G, MDS, BARC

STATEMENT BY AUTHOR

This dissertation has been submitted in partial fulfillment of requirements for an advanced degree at Homi Bhabha National Institute (HBNI) and will be deposited in the Library to be made available to borrowers under rules of the HBNI.

Brief quotations from this dissertation are allowable without special permission, provided that accurate acknowledgement of source is made. Requests for permission for extended quotation from or reproduction of this manuscript in whole or in part may be granted by the Competent Authority of HBNI when in his or her judgment the proposed use of the material is in the interests of scholarship. In all other instances, however, permission must be obtained from the author.

Mayur Darekar

Name & Signature
of the student

DECLARATION

I, hereby declare that the investigation presented in the thesis has been carried out by me. The work is original and has not been submitted earlier as a whole or in part for a degree / diploma at this or any other Institution / University.


28/07/2019.

Prof. (Smt.) Sulekha Mukhopadhyay
Guide & Head, PES/ChED,
BARC, Mumbai

Mayur Darekar
28/07/2019
(Mayur Darekar)
Registration no. ENGG01201404004

List of publications

Publications in refereed journals:

1. Darekar, M.; Singh, K. K.; Mukhopadhyay, S.; Shenoy, K. T. Single-stage micro-scale extraction: Studies with single microbore tubes and scale-up. *Separation and Purification Technology*, (2016) 158, 160-170.
2. Darekar, M.; Singh, K. K.; Joshi, J. M.; Mukhopadhyay, S.; Shenoy, K. T. Single-stage microscale solvent extraction in parallel microbore tubes using a monoblock distributor with integrated microfluidic junctions. *Separation Science and Technology*, (2017) 52(14), 2213-2223
3. Darekar, M.; Singh, K. K.; Mukhopadhyay, S.; Shenoy, K. T. Liquid-Liquid Two-Phase Flow Patterns in Y-Junction Microchannels. *Industrial & Engineering Chemistry Research*, (2017) 56(42), 12215-12226.
4. Darekar, M., Sapkale, P.; Singh, K. K.; Goswami, A. K.; Mukhopadhyay, S.; Shenoy, K. T. On microfluidic solvent extraction of uranium. *Chemical Engineering & Processing: Process Intensification*, (2018) 132, 65-74
5. Sen, N.; Darekar, M.; Sirsat, P.; Singh, K. K.; Mukhopadhyay, S.; Shirsath, S. R.; Shenoy, K. T. Recovery of uranium from lean streams by extraction and direct precipitation in microchannels, *Separation and Purification Technology*, (2019) 227, 115641
6. Darekar, M.; Chaurasiya R.K.; Singh, K. K.; Mukhopadhyay, S.; Shenoy, K. T. In-line Phase Separator for Microfluidic Solvent Extraction of Uranium. *Journal of Radioanalytical and Nuclear Chemistry*, (2020) 324, 123-133

Publications in conferences:

1. Darekar, M.; Singh, K. K.; Mukhopadhyay, S.; Shenoy, K. T. Single-stage micro-scale solvent extraction in parallel microbore tubes using MDIMJ. SESTEC-2016. IIT Guwahati. Best Poster Award by Royal Society of Chemistry. (Poster Presentation)
2. Darekar, M.; Thakur, P.; Singh, K.K.; Patil N.; Mukhopadhyay, S.; Shenoy, K. T. Numerical simulation of liquid-liquid two-phase flow at different microfluidic junctions. 8th DAE-BRNS biennial symposium on Emerging Trends in Separation Science and Technology (SESTEC-2018), 23-26 May (2018). Goa. India. (Poster Presentation)
3. Darekar, M.; Singh, K. K.; Mukhopadhyay, S.; Shenoy, K. T. Inline phase separation of microfluidic liquid-liquid dispersions, National Symposium on Recent Advances on Nuclear Fuel Cycle Activities (NUFUC-2018). 26-27 October (2018), Tarapur, India. (Paper Presentation)

4. Darekar, M.; Singh, K. K.; Mukhopadhyay, S.; Shenoy, K. T. Liquid-liquid extraction of uranium using microchannels. DAE-BRNS Conference on Indigenous Nuclear Fuel Program in India: Achievements, Status and Prospects (INFPIN-2019), 31 January – 2 February (2019), Mumbai, India. INFPIN-2019. BARC. (Poster Presentation)

Mayur Darekar

(Mayur Darekar)

Date: 23/07/2020

Dedicated to.....

.....My Mentor

Dr. KK Singh

ACKNOWLEDGEMENTS

I would like to express my gratitude to Dr. Sulekha Mukhopadhyay, my guide, for their continuous support, encouragement, patience and for the freedom they provided for free thinking.

I am especially grateful to Dr. K.K. Singh, ChED, BARC, my mentor who is also my technology advisor, for his continuous support, encouragement, and guidance (which ranged from technical/scientific aspects to grooming) without which timely completion of my research work would simply had been impossible.

I am also grateful to Shri K.T. Shenoy, Head ChED for his constant encouragement to pursue my research work.

I would like to express my gratitude to members of doctoral committee. for their valuable suggestion for improvement of my PhD work, I am also grateful to Chairman of doctoral committee for giving me opportunity for improvement of my research work.

Finally mention must be made of my family for their support, understanding and blessings

Mayur Darekar
(Mayur Darekar)

CONTENTS

	Page No.
Summary	xi
List of figures	xiii
List of tables	xx
Nomenclature	xxii
Chapter 1 Introduction and literature survey	1
1.1 Chemical microprocessing	1
1.2 Solvent extraction in microchannels	1
1.3 Literature survey	4
1.3.1 Liquid-liquid two-phase flow in microchannels	4
1.3.2 Miniature devices for separation of microfluidic liquid-liquid dispersions	12
1.3.3 Liquid-liquid extraction in microchannels	15
1.3.4 Gap areas	19
1.4 Relevance of the research work	24
1.5 Outline of research work	26
Chapter 2 Assesment of feasibility of intensification of solvent extraction process in single microchannels.	28
2.1 Introduction	28
2.2 Experimental	29
2.2.1 Setup	29
2.2.2 Phases used in the experiments	30
2.2.3 Calculations	31
2.2.4 Experiments for measuring distribution coefficient	32
2.3 Results and discussion	33
2.3.1 Effect of flow rate	34
2.3.2 Effect microbore tube diameter	39
2.3.3 Effect of microbore tube length	41
2.4 Methodology for identifying an optimum configuration of single microbore tubes	43
2.5 Comparison of microbore tube contactor with a mixer- settler	47
2.6 Conclusions	49
Chapter 3 Effect of flow pattern and layout of microchannel on mass transfer and settling behavior	51
3.1 Introduction	51
3.2 Experimental	52
3.2.1 Setup	52
3.2.2 Phases used in the experiments	53
3.2.3 Calculations	53

3.2.4 Experiments for measuring distribution coefficient	54
3.3 Result and discussion	55
3.3.1 Effect of flow rate and flow pattern on mass transfer	55
3.3.2 Effect of flow rate and flow pattern on settling	60
3.3.3 Effect of coiling on mass transfer	61
3.4 Conclusions	64
Chapter 4 Studies on liquid-liquid two phase flow patterns in Y-junction microchannels	65
4.1 Introduction	65
4.2 Experimental	66
4.2.1 Setup	66
4.2.2 Phases used in the experiments	67
4.3 Result and discussion	69
4.3.1 Typical flow patterns	69
4.3.2 Effect of flow rate on the flow regime map	73
4.3.3 Effect of microchannel diameter on flow regime map	74
4.3.4 Effect of interfacial tension on flow regime map	77
4.3.5 Effect of hydrophobicity of channel on flow regime map	79
4.3.6 Generalized flow regime map	81
4.4 Conclusions	85
Chapter 5 Scale-up for achieving larger throughput	86
5.1 Introduction	86
5.2 Scale-up by using Y structural bifurcation	87
5.2.1 Experimental setup	87
5.2.2 Phases used in the experiments	89
5.2.3 Scale-up for 1 LPH total throughput	89
5.3 Scale-up by using MDIMJ	91
5.3.1 CFD modeling of MDIMJ	91
5.3.2 Effect of flow rate	94
5.3.3 Effect of inlet channel diameter	96
5.3.4 Effect of outlet channel diameter	97
5.3.5 Effect of distance between outlet channels	98
5.3.6 Effect of pressure imbalance at the outlets	99
5.3.7 Selection of final design	101
5.4 Solvent extraction using MDIMJ at 3 LPH	103
5.4.1 Experimental setup	103
5.4.2 Calculations	104
5.4.3 Flow distribution	105
5.4.4 Solvent extraction experiments	106
5.5 Two stage solvent extraction at 10 LPH using MDIMJ	109
5.5.1 Experimental setup	109
5.5.2 Solvent extraction experiments	111
5.6 Conclusions	113

Chapter 6	Metallic mesh based devices for in-line phase separation of microfluidic dispersion	115
6.1	Introduction	115
6.2	Experimental study	118
6.2.1	Metallic membrane based device	118
6.2.2	Setup for inline phase separation	120
6.3	Hydrodynamics studies in inline phase separator	121
6.3.1	Flow regimes	121
6.3.2	Effect of volumetric flow rate	123
6.3.3	Effect of design of flow channels	124
6.3.4	Effect of mesh thickness	127
6.3.5	Effect of mesh pore size	128
6.3.6	Effect of back pressure	129
6.4	Microcontactor with in-line phase separator	130
6.5	Conclusions	132
Chapter 7	Recovery of uranium from lean streams by extraction and direct precipitation in microchannels	134
7.1	Introduction	134
7.2	Experiments	135
7.2.1	Materials	135
7.2.2	Setup and procedure	135
7.3	Extraction using microbore tube	137
7.4	Direct precipitation using microbore tubes	138
7.4.1	Effect of residence time	139
7.4.2	Effect of O/A ratio	143
7.4.3	Effect of concentration of ammonium hydroxide	146
7.4.4	Reusability of organic phase	148
7.5	Conclusions	150
Chapter 8	Conclusions and future work	152
8.1	Conclusions	152
8.2	Future work	156
References		158

LIST OF FIGURES

Figure No.	Details	Page No.
S.1	Effect of volumetric flow rate on overall volumetric mass transfer coefficient (750 μm Y-junction, diameter of microbore tube = 800 μm , $O/A = 1/1$, residence time = 1.36 s)	xiv
S.2	Generalized liquid-liquid flow regime map for a Y-junction microchannel (the closed curve encloses the region of uncertainty of the flow pattern)(PF- Parallel Flow, SF-Slug Flow, SDF-Slug and Droplet Flow, DF-Droplet Flow)	xvii
S.3	(a) MDIMJ feeding 6 microbore tubes (b) Samples collected at the outlets of 6 microbore tubes showing almost equal flow distribution	xix
S.4	Schematic diagram of in-line phase separator (top) and experimental setup (bottom)	xx
1.1	Schematics diagram of experimental setup for experiments with single microbore tubes	3
1.2	Microchannel glass chip with three inlets (Sarkar et al., 2012)	4
1.3	Effect of channel size and velocity on inertial, gravity and viscous forces (Gunther and Jensen, 2006)	6
1.4	Various types of microfluidic junctions (Wang et al., 2017)	6
1.5	Flow visualization for the case when the phase getting dispersed comes from the center (Sarkar et al., 2012)	7
1.6	Flow visualization for the case when the phase getting dispersed comes from the sides(Sarkar et al., 2012)	8
1.7	Representative photographs of stable flow patterns in the 0.4mm diameter rectangular microchannel (Zhao et al., 2006)	9
1.8	Flow regime map in terms of Weber number of kerosene and waterphase (Zhao et al., 2006)	10
1.9	Flow regimes observed for liquid–liquid systems in microstructure reactor. (Kashid et al., 2011)	10
1.10	Flow regimes map for T-square microchannel (\square , slug; \diamond , slug-drop; Δ , deformed interface; O, annular/parallel) (Kashid et al., 2011)	11
1.11	Comparison of flow regimes maps for all microchannels (\square , slug;	11

	◇, slug-drop; Δ, deformed interface; O, annular/parallel) (Kashid et al., 2011)	
1.12	Miniaturized phase separators based on differences in wetting properties. (a) Y-junction phase separator (Kashid et al., 2007b) (b) T-junction phase separator (Wang et al., 2017) (c) Y-Y microchannel with a coated section for phase separation, (Logtenberg et al. 2011) (d) A high-capacity mini extraction system using a plate phase separator, (Kolehmainen and Turunen 2007)	13
1.13	Microflow phase separators based on capillary pressure. (a) Tubular member phase separator (Bannock et al., 2013) (b) liquid-liquid extraction using a capillary membrane (Breisig et al., 2017)	14
1.14	Multistage countercurrent extraction based on microflow. Schematic and actual photograph of the experimental setup (Lan et al., 2016)	18
1.15	Two-stage counter-current setup (Holbach and Kockmann, 2013)	19
2.1	Experimental setup used in the experiments with single microbore tube	29
2.2	Schematics diagram of experimental setup for experiments with single microbore tubes	29
2.3	Repeatability of experimental results (750 μm Y-junction, $D_T = 800 \mu\text{m}$, $O/A = 1/1$, $Q = 0.5 \text{ LPH}$)	34
2.4	Effect of flow rate on flow pattern and settling behavior (750 μm Y-junction, $D_T = 800 \mu\text{m}$, $O/A = 1/1$, $\tau = 1.36 \text{ s}$)	36
2.5	Effect of flow rate on stage efficiency and percentage extraction (750 μm Y-junction, $D_T = 800 \mu\text{m}$, $O/A = 1/1$, $\tau = 1.36 \text{ s}$)	38
2.6	Effect of flow rate on overall volumetric mass transfer coefficient (750 μm Y-junction, $D_T = 800 \mu\text{m}$, $O/A = 1/1$, $\tau = 1.36 \text{ s}$)	39
2.7	Effect of diameter of microbore tube on stage efficiency and percentage extraction (750 μm Y-junction, $O/A = 1/1$, $Q = 0.5 \text{ LPH}$, $\tau = 0.45 \text{ s}$)	40
2.8	Effect of diameter of microbore tube on overall volumetric mass transfer coefficient (750 μm Y-junction, $O/A = 1/1$, $Q = 0.5 \text{ LPH}$, $\tau = 0.45 \text{ s}$)	40
2.9	Effect of tube length on stage efficiency and percentage extraction (750 μm Y-junction, $D_T = 800 \mu\text{m}$, $O/A = 1/1$, $Q = 0.5 \text{ LPH}$)	42
2.10	Quality of dispersion at end of different length microbore tube	43

(750 μm Y-junction, $D_T = 800 \mu\text{m}$, $O/A = 1/1$, $Q = 0.5 \text{ LPH}$)

2.11	Methodology for identifying an optimum configuration for extraction in parallel microbore tubes	46
3.1	Schematic diagram of the experimental setup	53
3.2	Effect of flow rates on (a) aqueous and organic phase on flow pattern flow pattern (b) percentage efficiency ($O/A=2/1$) and (c) overall volumetric mass transfer coefficient ($O/A=2/1$) at a constant residence time ($\tau_m = 1.5 \text{ s}$)	56
3.3	Flow patterns at different flow rates of the aqueous and organic phases ($O/A=2/1$)	57
3.4	Effect of flow rate on (a) stage efficiency and (b) overall volumetric mass transfer coefficient at a constant length of microbore tube ($L = 30 \text{ cm}$, $O/A=1/1$)	59
3.5	Images of flow pattern inside microbore tube at different flow rate of aqueous and organic phase ($O/A=1/1$)	59
3.6	Variation of dispersion band thickness with total flow rate for (a) $O/A=2/1$ and (b) $O/A=1/1$	61
3.7	Effect of flow rate on (a) efficiency and (b) overall volumetric mass transfer coefficient for straight and coiled microbore tube ($O/A=1/1$, $L=30 \text{ cm}$, $C_R=13 \text{ mm}$)	62
3.8	(a)Comparison of stage efficiency in straight and coiled microbore tubes of different lengths ($Q_T = 4 \text{ ml/min}$, $O/A=1/1$, $C_R=5 \text{ mm}$, $P=1.6 \text{ mm}$) (b) Effect of coiling radius on mass transfer coefficient and stage efficiency ($Q_T = 4 \text{ ml/min}$, $O/A=1/1$, $L=60 \text{ cm}$, $P=1.6 \text{ mm}$)	64
4.1	Schematic diagram of the experimental setup	67
4.2	a) Microchannel chip with holder for microbore tubing (b) Cross-section of the microchannel having $D_H = 260 \mu\text{m}$ (c) Cross-section of the microchannel having $D_H = 760 \mu\text{m}$	68
4.3	Different liquid-liquid two-phase flow patterns observed in the experiments (images from uncoated microchannel, $D_H = 760 \mu\text{m}$)	69
4.4	Slugs formed for different continuous phase (organic phase) flow rates at a constant dispersed phase (aqueous phase) flow rate (phase system: water– butyl acetate, $D_H = 760 \mu\text{m}$, uncoated microchannel)	70
4.5	Slugs formed for different dispersed phase (aqueous phase) flow ratee at a constant continuous phase (organic phase) flow rate (phase system: water– butyl acetate, $D_H = 760 \mu\text{m}$, uncoated	71

	microchannel)	
4.6	Effect of the continuous phase (organic phase) flow rate on the size of the droplet in droplet flow regime. (phase system: water – butanol, $D_H=760\ \mu\text{m}$, coated microchannel)	72
4.7	Effect of the continuous phase (organic phase) flow rate on the position of the interface between the two liquids in parallel flow. (phase system: water – butyl acetate, $D_H = 760\ \mu\text{m}$, uncoated microchannel)	73
4.8	Effect of flow rate on flow pattern in coated microchannel. $D_H=260\ \mu\text{m}$, $Q_{A, \text{max}} = 3\ \text{ml/min}$, $Q_{O, \text{max}}=3\ \text{ml/min}$ (a) water – butyl acetate (b) water – toluene	74
4.9	Effect of microchannel diameter on flow regime map. (a) phase system: water – butyl acetate, $D_H= 760\ \mu\text{m}$, uncoated microchannel, $Q_{A, \text{max}} = 10\ \text{ml/min}$, $Q_{O, \text{max}} = 10\ \text{ml/min}$ (b) phase system: water – butyl acetate, $D_H= 260\ \mu\text{m}$, uncoated microchannel, $Q_{A, \text{max}} = 3\ \text{ml/min}$, $Q_{O, \text{max}} = 3\ \text{ml/min}$ (c) Phase system: water – toluene, $D_H = 760\ \mu\text{m}$, uncoated microchannel, $Q_{A, \text{max}} = 10\ \text{ml/min}$, $Q_{O, \text{max}} = 10\ \text{ml/min}$ (d) phase system: water – toluene, $D_H= 260\ \mu\text{m}$, uncoated microchannel, $Q_{A, \text{max}} = 3\ \text{ml/min}$, $Q_{O, \text{max}} = 3\ \text{ml/min}$.	77
4.10	Effect of interfacial tension between the two liquids on the flow regime maps in uncoated microchannels of $760\ \mu\text{m}$ diameter (a) phase system: water – butanol, $Q_{A, \text{max}} = 2\ \text{ml/min}$, $Q_{O, \text{max}} = 2\ \text{ml/min}$ (b) phase system: water – butyl acetate, $Q_{A, \text{max}} = 10\ \text{ml/min}$, $Q_{O, \text{max}} = 10\ \text{ml/min}$ (c) phase system: water – toluene system, $Q_{A, \text{max}} = 10\ \text{ml/min}$, $Q_{O, \text{max}} = 10\ \text{ml/min}$)	79
4.11	Flow regime map for uncoated microchannel and coated microchannel of $760\ \mu\text{m}$ diameter (a) phase system: water – butanol, uncoated microchannel, $Q_{A, \text{max}} = 2\ \text{ml/min}$, $Q_{O, \text{max}} = 2\ \text{ml/min}$. (b) phase system: water – butanol, coated microchannel, $Q_{A, \text{max}} = 2\ \text{ml/min}$, $Q_{O, \text{max}} = 2\ \text{ml/min}$ (c) phase system: water – butyl acetate, uncoated microchannel, $Q_{A, \text{max}} = 10\ \text{ml/min}$, $Q_{O, \text{max}}=10\ \text{ml/min}$. (d) phase system: water – butyl acetate, coated microchannel, $Q_{A, \text{max}} = 10\ \text{ml/min}$, $Q_{O, \text{max}} = 10\ \text{ml/min}$. (e) phase system: water – toluene, uncoated microchannel, $Q_{A, \text{max}} = 10\ \text{ml/min}$, $Q_{O, \text{max}} = 10\ \text{ml/min}$. (f) phase system: water – toluene, coated microchannel, $Q_{A, \text{max}} = 10\ \text{ml/min}$, $Q_{O, \text{max}} = 10\ \text{ml/min}$.	80
4.12	Generalized flow regime map for (a) uncoated microchannels with We as the dimensionless number (b) uncoated microchannels with $We \cdot Oh$ as the dimensionless number (c) uncoated microchannels with velocity as the dimensionless number (d) uncoated microchannels with Ca as the dimensionless number (e) uncoated microchannels with Ca and Re as the dimensionless number (f)	84

	data of Kashid et al.(2011)	
5.1	Experimental setup for conducting experiments at 1 LPH total throughput by using two microbore tubes connected in parallel	87
5.2	Schematic diagram of experimental setup used for conducting experiments at 1 LPH total throughput by using two microbore tubes connected in parallel	88
5.3	Pipe settler used in the experiments with two parallel microbore tubes	88
5.4	Meshed computational domain representing MDIMJ (top) and a closer view of the mesh near one of the microfluidic junctions (shown in bottom. The dimensions shown are some typical dimensions used in the CFD simulations)	92
5.5	Schematic of the flow path of MDIMJ	93
5.6	Spatial variation of velocity in the inlet channel and the outlet channels of MDIMJ contour for different flow rates. Direction of flow in the inlet channel is from left to right.($D_h = 4$ mm, $D_m = 2$ mm, $L = 30$ mm)	95
5.7	Effect of flow rate on % flow non-uniformity ($D_h = 4$ mm, $D_m = 2$ mm, $L = 30$ mm)	96
5.8	Effect of inlet channel diameter on % flow non-uniformity ($D_m = 2$ mm, $Q_T = 3$ LPH, $L = 30$ mm)	97
5.9	Effect of outlet channel diameter on % flow non-uniformity ($D_h = 4$ mm, $Q_T = 3$ LPH, $L = 30$ mm)	98
5.10	Effect of distance between outlet channels on % flow non-uniformity ($D_h = 4$ mm, $D_m = 2$ mm, $Q_T = 3$ LPH)	99
5.11	Effect of outlet pressure imbalance on % flow non-uniformity ($D_h = 4$ mm, $D_m = 1$ mm, $Q_T = 3$ LPH, $L = 30$ mm)	100
5.12	Effect of outlet pressure imbalance on % flow non-uniformity ($D_h = 4$ mm, $D_m = 2$ mm, $Q_T = 3$ LPH, $L = 30$ mm)	101
5.13	Comparison of experimentally measured flow non-uniformity with predicted flow non-uniformity ($D_h = 4$ mm, $D_m = 0.75$ mm, $Q_T = 3$ LPH, $L = 10$ mm)	102
5.14	Schematic diagram of the experimental setup used for solvent extraction at total throughput of 3 LPH by using MDIMJ	103
5.15	The MDIMJ (left) and the settler (right)	104
5.16	Samples collected at each outlet during a fixed interval of time to	106

	check the flow distribution by MDIMJ	
5.17	Effect of flow rate on percentage efficiency and percentage extraction (O/A=1/1)	107
5.18	Effect of flow rate on overall volumetric mass transfer coefficient	108
5.19	Schematic diagram of a MDIMJ	109
5.20	The MDIMJ with 20 microbore tubes connected to it	110
5.21	The schematic of two-stage microfluidic solvent extraction	111
6.1	Metallic membrane based device (Willersinn and Bart, 2015)	119
6.2	(a) Metallic mesh, (b) straight flow channel, (c) flow channel with two-bends and (d) flow channel with 6 bends	119
6.3	Schematic diagram of in-line phase separator (top) and experimental setup (bottom)	121
6.4	Different flow regime observed in the experiments (a) annular flow at $Q_A = 4$ ml/min & $Q_O = 10$ ml/min, (b) slug flow at $Q_A = 4$ ml/min & $Q_O = 1$ ml/min, (c) droplet flow at $Q_A = 3$ ml/min & $Q_O = 3$ ml/min, (d) slug-droplet flow at $Q_A = 4$ ml/min & $Q_O = 5$ ml/min, (e) dispersed flow at $Q_A = 7$ ml/min & $Q_O = 10$ ml/min	122
6.5	Effect of volumetric flow rate on phase separation characteristics with 100 μm thick mesh, straight, 3 mm width flow channels. (Partial separation \blacktriangle , complete separation \blacktriangle , transition line ---)	123
6.6	Effect of layout of the channels on phase separation characteristics. --- straight channels, --- 2-bend channels, --- 6-bend channels. Flow channels are 3 mm wide, 1 mm in height and mesh is 100 μm thick having 5 μm pore size	125
6.7	Effect of width of flow channels on phase separation characteristics- --- 3 mm width channel, --- 5 mm width channel. Flow channels are 6-bend channels. Height of flow channels is 1 mm, mesh is 200 μm thick with 5 μm pore size.	126
6.8	Effect of mesh thickness on phase separation- --- 100 μm thick mesh, --- 200 μm thick mesh, --- 300 μm thick mesh. Flow channels are 3 mm wide 6-bend channels and mesh is of 5 μm pore size	127
6.9	Effect of mesh pore size on phase separation- --- 5 μm pore size, --- 500 μm pore size. Flow channels are 3 mm wide 6-bend channels and mesh is 300 μm thick.	128
6.10	Effect of back pressure on phase separation- --- without back	130

pressure, —with back pressure. Flow channels are 3 mm wide 6-bend channels and mesh is 300 μm thick.

6.11	Effect of residence time on percentage extraction	131
6.12	Effect of residence time on stage efficiency	132
7.1	Schematic diagram for experimental setup	136
7.2	Effect of O/A ratio on (a) % uranium extraction and (b) uranium concentration in the raffinate	137
7.3	Effect of percent uranium recovery from loaded organic with residence time (O/A=6; $D_T=0.8$ mm; $L=7.35$ m)	141
7.4	Effect of velocity on (a) percent uranium recovery from the organic phase (b) uranium concentration in lean organic phase (c) recovery rate (d) space-time-recovery. (O/A=6; $D_T=0.8$ mm; $L=7.35$ m)	142
7.5	Effect of O/A ratio on (a) percentage uranium recovery from loaded organic (b) recovery rate (c) space time recovery ($v=0.037$ m/sec; $D_T=0.8$ mm; $L=7.35$ m)	143
7.6	Effect of O/A and flow velocity on percent uranium recovery	145
7.7	Effect of O/A ratio and ammonium hydroxide concentration on (a) percent uranium recovery from loaded organic (b) recovery rate and (c) space time recovery ($v=0.037$ m/sec; $D_T=0.8$ mm; $L=7.35$ m)	147
7.8	Distribution coefficient value measured after repeated contact of organic phase with ammonium hydroxide solution	149
7.9	FT-IR spectrum of the fresh and recycled organic phase	150

LIST OF TABLES

Table No.	Details	Page No.
1.1	Dimensionless number and their physical significance	5
1.2	Overall volumetric mass transfer coefficient of different types of contactors (Tsaoulidis, 2014)	15
1.3	Summary of some of previously reported studies on solvent extraction in microchannels	17
2.1	Physical properties of the phases	30
2.2	Distribution coefficient of nitric acid	33
2.3	Effect of flow rate on stage efficiency, pressure drop and settling behavior in microbore tube (750 μm Y-junction, $D_T = 800 \mu\text{m}$, $O/A = 1/1$, $\tau = 1.36 \text{ s}$)	38
2.4	Effect of tube diameter on stage efficiency, pressure drop and settling behavior (750 μm Y-junction, $O/A = 1/1$, $Q = 0.5 \text{ LPH}$, $\tau = 0.45 \text{ s}$)	41
2.5	Effect of tube length on stage efficiency, pressure drop and settling behavior (750 μm Y-junction, $D_T = 800 \mu\text{m}$, $O/A = 1/1$, $Q = 0.5 \text{ LPH}$)	43
2.6	Comparison of microbore tube contactor with a mixer-settler	49
3.1	Distribution coefficient of uranium	54
3.2	Overall volumetric mass transfer coefficient and observed SRV for different flow patterns	60
3.3	Overall volumetric mass transfer coefficient in different types of microchannels	61
4.1	Physical properties of the test systems used in the experiments at 20°C	68
4.2	Comparison of the experimental and estimated values of the organic phase flow rate (Q_2) at which transition from slug flow to droplet flow occurs at the lowest flow rate of the aqueous phase in 260 μm (D_{H2}) microchannel ($Q_1 = 3.5 \text{ ml/min}$ for water – butyl acetate system, $Q_1 = 6.5 \text{ ml/min}$ for water – toluene system, $D_{H1} = 760 \mu\text{m}$)	76
4.3	Comparison of estimated and experimental value of organic flow rate (Q_2) at which transition from slug flow to droplet flow occurs for the lowest flow rate of the aqueous phase ($Q_1 = 3.5 \text{ ml/min}$ for	79

water – butyl acetate system, $D_H = 760 \mu\text{m}$)

5.1	Results of the experiments at 1 LPH total throughput with two optimum configuration microbore tubes in parallel (750 μm Y-junction, $D_T = 800 \mu\text{m}$, $L_T = 300 \text{ cm}$, $Q_T = 1 \text{ LPH}$, $\tau = 10.85 \text{ s}$)	90
5.2	Outlet pressures used in the simulations to study the effect of pressure imbalance at the outlets on flow distribution by an MDIMJ	100
5.3	Flow non-uniformity in the MDIMJ at O/A=1/1	106
5.4	Effect of Flow rate on percentage efficiency and percentage extraction at O/A=1/1	107
5.5	Extraction and stripping studies in parallel microbore tubes at 10 LPH ($\tau_m=2.23 \text{ s}$, $\tau_s=129 \text{ s}$)	112

NOMENCLATURE

a	Specific interfacial area [L^{-1}]
A_S	Settling area [L^2]
B_O	Bond number [-]
C_A^{in}	Solute concentration in the aqueous phase at the inlet [$M L^{-3}$]
$C_{A,Batch}^{Eqb}$	Solute concentration in the aqueous phase in equilibrium with the solute concentration of the organic phase in batch studies [$M L^{-3}$]
$C_{A,Eqb}^{in}$	Solute concentration in the aqueous phase in equilibrium with the solute concentration of the organic phase at the inlet [$M L^{-3}$]
C_A^{out}	Solute concentration in the aqueous phase at the outlet [$M L^{-3}$]
$C_{A,Eqb}^{out}$	Solute concentration in the aqueous phase in equilibrium with the solute concentration in the organic phase at the outlet [$M L^{-3}$]
C_O^{in}	Solute concentration in the organic phase at the inlet [$M L^{-3}$]
C_O^{out}	Solute concentration in the extract [$M L^{-3}$]
$C_{O,Batch}^{Eqb}$	Solute concentration in the organic phase in equilibrium with the solute concentration of the aqueous phase in batch studies [$M L^{-3}$]
C_R	Microbore tube coiling radius [L]
D	Diameter of selected microbore tube [L]
De	Dean number [-]
d_h	Channel hydraulic diameter [L]
D_h	Inlet channel diameter [L]
D_{Hi}	Hydraulic diameter of i^{th} microchannel [L]
D_i	Different diameter of microbore tube [L]
D_{max}	Maximum diameter of available microbore tube [L]
D_m	Outlet channel diameter [L]
D_T	Microbore tube diameter [L]

g	Acceleration due to gravity [$M T^{-2}$]
H_D	Dispersion band height or thickness [L]
K_D	Distribution coefficient [-]
K_L	Overall mass transfer coefficient [$M T^{-1}$]
$K_L a$	Overall volumetric mass transfer coefficient [T^{-1}]
L_T	Tube length [L]
L_{min}	Minimum tube length [L]
ΔL	Change in tube length [L]
Δ_{LMC}	Log mean concentration difference [$M L^{-3}$]
N_T	Numbers of tubes [-]
O/A	Ratio of organic flow rate to aqueous flow rate [-]
P	Power input [$M L^2 T^{-3}$]
ΔP	Pressure drop [$M L^{-1} T^{-2}$]
ΔP_{max}	Maximum permissible pressure drop [$M L^{-1} T^{-2}$]
Q	Total flow rate of single microbore tube [$L^3 T^{-1}$]
Q_A	Aqueous flow rate [$L^3 T^{-1}$]
Q_{avg}	Average flow rate [$L^3 T^{-1}$]
$Q_{A, max}$	Maximum aqueous phase flow rate [$L^3 T^{-1}$]
Q_C	Continuous phase flow rate [$L^3 T^{-1}$]
Q_D	Dispersed phase flow rate [$L^3 T^{-1}$]
Q_i	Flow rate for i^{th} system [$L^3 T^{-1}$]
Q_{MeOH}	Methanol phase flow rate [$L^3 T^{-1}$]
Q_o	Organic flow rate [$L^3 T^{-1}$]

Q_{oil}	Oil phase flow rate [$L^3 T^{-1}$]
$Q_{O, max}$	Maximum organic phase flow rate [$L^3 T^{-1}$]
Q_T	Total flow rate [$L^3 T^{-1}$]
Q_W	Water phase flow rate [$L^3 T^{-1}$]
Q_A^{Avg}	Average aqueous phase flow rate [$L^3 T^{-1}$]
Q_O^{Avg}	Average organic phase flow rate [$L^3 T^{-1}$]
Q_T^{Avg}	Average total flow rate [$L^3 T^{-1}$]
Re	Reynolds number [-]
r	Radius of curvature [L]
$t_{desired}$	Desired settling time [T]
t_{set}	Settling time [T]
τ_m	Residence time in microchannel [T]
U_d	Dispersed phase velocity [$L T^{-1}$]
U_T	Superficial velocity of toluene [$L T^{-1}$]
U_W	Superficial velocity of water [$L T^{-1}$]
V_{Total}	Total volume of the contactor [L^3]
V_{mixer}	Mixer volume [L^3]
$V_{settler}$	Settler volume [L^3]
V_r	Reactor volume [L^3]
We	Weber number[-]
We_{ks}	Weber number for kerosene phase flowing in microchannel [-]
We_{ws}	Weber number for water phase flowing in microchannel [-]

Greek letters

α	Constant specific for microfluidic junction [-]
$\Delta\rho$	Density difference [$M L^{-3}$]
η	Stage efficiency [-]
μ	Viscosity [$M L^{-1} T^{-1}$]
ρ	Density [$M L^{-3}$]
σ	Interfacial tension [$M T^{-2}$]
τ	Residence time [L]

Abbreviations

AF	Annular flow
ADU	Ammonium diuranate
AFNi	Percentage aqueous flow non-uniformity
CFD	Computational fluid dynamics
DF	Droplet flow
DPF	Droplets populations flow
D2EHPA	Di-(2-ethylhexyl)phosphoric acid
EFCE	European federation of chemical engineering
FDF	Finely dispersed flow
ICP-AES	Inductively coupled plasma atomic emission spectrometer
ID	Internal diameter
LMCD	Log mean concentration difference
LPH	Liter per hour
MDF	Monodispersed droplets flow

MDIMJ	Monoblock distributor with in-built microfluidic junctions
MS	Mixer-settler
MTC	Microbore tube contactor
OFNi	Percentage organic flow non-uniformity
OD	Outer diameter
PF	Parallel flow
PE	Percentage extraction
PFA	Perfluoroalkoxy alkanes
PTFE	Polytetrafluoroethylene
RR	Recovery rate
SDF	Slug and droplet flow
SE	Stage efficiency
SER	Specific extraction rate
SER _M	Specific extraction rate in mixer
SER _{MS}	Specific extraction rate in mixer and settler
SF	Slug flow
SRV	Settling rate per unit volume
STR	Space–time-recovery
SS	Stainless steel
TBP	Tributyl phosphate
TFNi	Total flow non-uniformity for i th outlet

CHAPTER 8

CONCLUSIONS AND FUTURE WORK

8.1 CONCLUSIONS

Following are the conclusions emanating from the research work reported in this thesis:

1. Experiments in single microchannels can be performed to identify an optimum configuration for carrying out solvent extraction at the desired throughput with a given liquid-liquid system. The optimum configuration is the one which ensures high mass transfer rate, fast settling of ensuing liquid-liquid dispersion and low pressure drop. The experiments can be conducted systematically following the proposed methodology to identify the optimum configuration. Following this methodology, an optimum configuration has been found out for extraction of nitric acid from 3M nitric acid feed using 30% (v/v) TBP in dodecane as the solvent. This is a liquid-liquid system which has significant relevance to solvent extraction processes in nuclear fuel cycle(Chapter-2).
2. Performance of Microcontactor is compared with a mixer-settler which represents a conventional contactor. Specific extraction rate in the microcontactor is estimated to be about 4 times of the same in a mixer-settler. Specific extraction rate per unit power input in the microcontactor is estimated to be about 20 time of the same in a mixer-settler. This highlights the scope of significant process intensification that can be achieved by using a microcontactor (Chapter-2).
3. Liquid-liquid two-phase flow pattern generated at a microfluidic junction significantly affects both mass transfer rate as well as settling rate. Among the flow

patterns observed in the experiments conducted in this research work, maximum and minimum values of overall volumetric mass transfer coefficient were observed for finely dispersed flow ($K_{La} = 4.01 \text{ s}^{-1}$) and slug flow ($K_{La} = 0.38 \text{ s}^{-1}$), respectively. Maximum and minimum values of settling rate per unit volume (SRV) of dispersion band were found to be for slug flow ($\text{SRV} = 118.36 \text{ h}^{-1}$) and finely dispersed flow ($\text{SRV} = 30.35 \text{ h}^{-1}$), respectively. It was found that the flow pattern which is the best for mass transfer is the worst for settling and vice versa. It is also concluded that stage efficiency and overall volumetric mass transfer coefficient can be increased by helically coiling a microbore tube. The effect of coiling on mass transfer becomes more pronounced as coil diameter is reduced (Chapter-3).

4. Considering overwhelming dependence of mass transfer and settling on liquid-liquid two-phase flow pattern generated at a microfluidic junction, it is important to predict the expected flow pattern for a given microfluidic junction, flow rates and physical properties of the two liquids that are contacted at the microfluidic junction. This calls for generalized flow regime maps that can be used to predict the flow pattern. However, due to wide variations possible in the design of the microfluidic junction, flow rates and physical properties of the liquids, it is extremely difficult to identify the generalized flow regime map which is universally applicable. However, generalized flow regime maps can be proposed for different microfluidic junctions. In this research, experiments were conducted and data analyzed to propose a generalized flow regime map for microfluidic Y-junctions. The experiments were conducted using the standard test systems prescribed by the EFCE. Product of Weber number and Ohnesorge number ($We \cdot Oh$) is found to be the best combination of dimensionless

numbers for generalized flow regime map. This finding for microfluidic Y-junctions agrees well with a previously reported study on microfluidic T-junctions (Chapter-4).

5. A new design of distributor for scale-up by numbering-up is conceptualized and tested. This distributor is named as Monoblock Distributor with In-built Microfluidic Junctions (MDIMJ). As the name suggests, the distributor is fabricated using a single block and also houses the microfluidic junctions required to feed several microbore tubes connected to it. Since microfluidic junctions are housed within the same block, flow distribution for numbering-up by this distributor can be achieved in a much compact manner compared to conventional structural bifurcation method. CFD simulations can be very useful for designing such distributors. MDIMJ is found to give very satisfactory two-phase flow distribution among 6 parallel microbore tubes with flow non-uniformity less than $\pm 5\%$. In the experiments carried out with simulated lean stream having 720 ppm of U(VI) concentration, the set up based on MDIMJ and microbore tubes is found to give high stage efficiency (above 90% in most cases) in short contact times (in most cases less than 10 seconds) for O/A ratio 1/1. The contact time required for high stage efficiency is much shorter than typically provided in conventional contactors such as mixer-settlers. Maximum value of $K_L a$ obtained is 0.4 s^{-1} which is at least an order of magnitude higher than $K_L a$ value typically observed in conventional contactors. This demonstrates the process intensification achieved by using micro-scale extraction as well as confident scale-up by following numbering-up approach using properly designed compact distributors. Scale-up of single-stage microfluidic extraction is demonstrated up to 4.8 LPH of total flow rate. MDIMJ could be successfully used for carrying out multistage extraction and stripping at 10 LPH total throughput using 20 parallel microbore tubes (Chapter-5).

6. To have a compact setup for microfluidic extraction, intensification of phase separation is as important as the intensification of mass transfer. Intensification of settling of dispersion generated at a microfluidic junction can be achieved by replacing gravity settler with an in-line phase separator. The inline phase separator comprises of two flow channels separated by a metallic mesh which is sandwiched between the two flow channels. The upper channel receives the dispersion. The continuous phase passes to the lower flow channel through the mesh. The clear continuous phase is obtained from the outlet of the lower flow channel while the clear dispersed phase is obtained from the outlet of the upper flow channel. Metallic mesh is particularly attractive for applications in the back-end of nuclear fuel cycle where materials to be used must have high radiation resistance. Experiments conducted with metallic mesh based in-line phase separator show that the size of the operating window in which complete phase separation can be achieved depends on factors such as the length of the flow channels, mesh thickness, mesh pore size and back-pressure on the outlets of the flow channels. One or more of these factors may be altered to alter the size of the window of complete phase separation. Specific settling rate are compared for the inline phase separator ($112 - 224 \text{ h}^{-1}$) and gravity settler ($30 - 120 \text{ h}^{-1}$). It is concluded that the use of inline phase separator leads to intensification of the settling process (Chapter-6).

7. Unlike previously reported studies in which focus has been either on extraction and stripping, a complete solvent extraction process was demonstrated through microfluidic route. This involved, microfluidic extraction of uranium from a lean stream using 30% (v/v) TBP in dodecane as the solvent followed by direct precipitation of uranium from loaded organic phase by contacting it with ammonium

hydroxide in another microchannel. Direct precipitation of uranium from the loaded organic phase basically combines two process steps i.e. stripping of loaded organic and precipitation from the strip phase in a single step of direct precipitation from the loaded organic phase. The conditions which lead to maximum overall recovery of uranium were identified. Recyclability of the solvent was also established. The study leads to the conclusion that use of microfluidic devices can lead to process intensification not only by enhancement of mass transfer but also by reducing number of processing steps(Chapter-7).

8.2 FUTURE WORK

Following are the recommendations for the future work:

1. The generalized flow regime maps for liquid-liquid two-phase flow should be developed for different designs of microfluidic junctions. So far generalized flow regime maps have been proposed only for T-junction microchannel (in a previous study) and Y-junction microchannel (in this research work). Availability of generalized flow regime maps for different types of microfluidic junctions will be very useful.
2. To minimize experimentation, computational fluid dynamics modeling of different aspects of microfluidic extraction should be carried out. This will involve, CFD models aimed at predicting liquid-liquid two-phase patterns at different designs of microfluidic junctions for wide range of operating conditions and a broad spectrum of physical properties. Attempts should also be made to perform CFD modelling to predict mass transfer rates for different types of flow patterns. The experimental data and images generated in this research work will be useful for validation of the CFD models for predicting flow patterns and mass transfer.

3. Microbore tube contactors are attractive for extraction of desired materials with high stage efficiency in short contact time and with very low inventory of aqueous and organic phases. The advantage of low inventory is particularly attractive for processes involving radioactive / hazardous/ toxic substances. This advantage of using microbore tube contactor should be harnessed for specific applications involving such substances. Findings reported in this research work should be utilized for designing the systems for such identified specific applications.

SUMMARY

The research work is carried out to understand liquid-liquid two-phase flow hydrodynamics and various aspects of solvent extraction in microchannels using liquid-liquid systems relevant to solvent extraction in nuclear fuel cycle. Mass transfer in a microchannel as well as subsequent phase separation or settling depends on flow pattern generated inside microchannel. Experiments are carried out to study the effects of flow pattern on mass transfer and settling characteristics. Four different liquid-liquid flow patterns - slug flow, slug and droplet flow, droplet flow and finely dispersed flow - are observed. Among all observed flow patterns, maximum and minimum value of overall volumetric mass transfer coefficient are observed for finely dispersed flow ($K_{La} = 4.01 \text{ s}^{-1}$) and slug flow ($K_{La} = 0.38 \text{ s}^{-1}$), respectively. Maximum and minimum value of specific settling rate per unit volume (SRV) of dispersion band are found to be for slug flow (SRV = 118.36 hr^{-1}) and finely dispersed flow (SRV = 30.35 hr^{-1}), respectively. Given the significant dependence of liquid-liquid flow pattern on mass transfer and phase separation, it is important to predict the flow pattern expected to be generated at a microfluidic junction when two immiscible liquid phases are brought into contact at the junction. For this, experiments with standard test systems are performed to study the liquid-liquid two-phase flow pattern generated at Y-junction microchannels and generalized flow regime maps using $We \cdot Oh$ (product of Weber number and Ohnesorge number) as coordinates are obtained. Such flow regime maps can be used to predict the flow pattern for a given set of flow rates, liquid-liquid system and diameter of the microchannel.

Thesis reports experiments on extraction of U(VI) and HNO_3 from nitric acid solution in microchannels by using 30% (v/v) TBP in dodecane as the organic phase. Initially experiments with single microchannels are carried out to identify an optimum configuration that provides high stage efficiency in short contact time with low pressure drop and quick phase separation. The optimum configuration for extraction of nitric acid from aqueous solution of 3 M HNO_3 by 30% (v/v) TBP in dodecane consists of a 750 μm Y-junction having microchannel (microbore tube) of

diameter 800 μm and length 300 cm on its downstream side. This configuration can handle a total throughput of 0.5 LPH and provides 90% stage efficiency in contact time of about 11 seconds. As the throughput of single microbore tube is limited. Throughput is increased by numbering-up approach using a novel compact distributor named as MDIMJ (Monoblock Distributor having In-built Microfluidic Junctions). MDIMJ has been conceptualized and designed using the insights obtained from CFD simulations. MDIMJ is found to give very good two-phase flow distribution in 6 parallel microbore tubes at total flow rate of 3 LPH with non-uniformity in flow distribution being less than $\pm 5\%$. Following this, single-stage microfluidic solvent extraction of uranium from a lean aqueous stream is demonstrated at 3 LPH by using MDIMJ. Along with intensification of extraction, intensification of phase separation is also required. Intensification of phase separation of the liquid-liquid dispersion generated at microfluidic junction is demonstrated by using an inline phase separator housing a metallic mesh. The effects of various parameters (flow rates, design of flow channels, mesh size) on the window of clear phase separation are studied. Experiments on solvent extraction of uranium in a microchannel are performed at the conditions for which complete in-line phase separation is observed by using the in-line phase separator for phase separation. 98% stage efficiency is achieved in total contact time of 9 seconds for O/A ratio 1/1 at aqueous phase flow rate of 0.36 LPH. Thus the use of in-line phase separator along with the microchannel contactor leads to significant process intensification. Intensification of complete process of solvent extraction, which conventionally involves extraction of precious metal from an aqueous phase, stripping of loaded organic and precipitation of precious metal from the strip solution, is demonstrated by replacing two separate stripping and precipitation steps with a single direct precipitation step from loaded organic carried out in a microchannel. Demonstration is done for recovery of uranium from a lean aqueous stream at a total throughput of 10 mL/min (860 ppm uranium and 1N acidity). The set of operating conditions is identified for which more than 90% recovery of uranium from the loaded organic phase in the form of ammonium diuranate (ADU) is achieved.

CHAPTER 1

INTRODUCTION AND LITERATURE SURVEY

1.1 CHEMICAL MICROPROCESSING

The application of a continuous flow microfluidics towards chemical synthesis and processing is called chemical microprocessing. Chemical microprocessing is receiving increasing attention in the fields of both microtechnology and chemical engineering (Hessel et al., 2004). Chemical processing in microchannels enable laboratory-scale studies of large depth, large flexibility, and notable fastness in gaining information.

Chemical processing in microchannels has several distinct advantages. High surface to volume ratio in a microchannel ensures intensified heat transfer and is very useful for carrying out highly exothermic reactions (Rebrov et al., 2001; Schneider et al., 2004; Sen et al., 2013). Numbering up approach followed for scale-up makes the scale-up easy and certain. Small volumes of microchannels lead to low inventory of chemicals in the setups based on microchannels. This makes such setups very useful for carrying out reactions involving toxic and hazardous chemicals (Acke et al., 2007; Veser, 2013, Zhang et al., 2004). Solvent extraction is one the unit operations which can be intensified by use of microchannels.

1.2 SOLVENT EXTRACTION IN MICROCHANNEL

There are several advantages of carrying out solvent extraction in microchannels. Unlike conventional contactors, in microchannels quality of dispersion can be controlled precisely which leads to high mass transfer rate as well as ensure fast settling. High mass transfer rates and fast settling can reduce the size of contactor as

well as phase disengagement section of the contactor eventually resulting in reduction of solvent inventory and footprint area of the contactor. Unlike conventional contactors, dispersion generated in a microchannel can be tailored to have very narrow drop size distributions (Saito et al., 2005; Sugiura et al., 2000). This can avoid the problems of generation of fine droplets and resulting entrainment losses which is often a problem in conventional contactors (Neira et al., 1992). Due to smaller flow cross-sections, the size of the dispersed phase is restricted leading to high specific interfacial area and high overall volumetric mass transfer coefficients (Ji et al., 2010; Kashid et al., 2011; Su et al., 2010). Scale-up is relatively easy and can be done confidently as throughput is increased by numbering-up (Darekar et al., 2014b).

One of the attractive features of solvent extraction in microchannels is that overall volumetric mass transfer coefficient increases with reduction in contact time. High stage efficiencies in contact times of the order of few seconds have been reported (Hotokezaka et al., 2005; Kashid et al., 2007c; Kumar et al., 2012). This makes them particularly attractive for deployment in the back-end of the nuclear fuel cycle where short contact times are required to avoid solvent degradation. Criticality is one of the probable hazards in solvent extraction in the back-end of nuclear fuel cycle (Desigan et al., 2012; Zhao et al., 2014). High surface to volume ratios in microchannels can also keep criticality hazard at bay. Reduction in inventory resulting in compact setup can reduce shielding requirement. As a result there are several studies reported on liquid-liquid extraction in microchannels using phase systems relevant for nuclear fuel cycle (Darekar et al., 2014b; Hellé et al., 2014; Hellé et al., 2015; Hotokezaka et al., 2005; Kumar et al., 2012; Tamagawa and Muto, 2011; Tsaoulidis et al., 2013a; Tsaoulidis et al., 2013b).

A typical experimental setup used for solvent extraction using micro channel (microbore tube) is shown in Fig. 1.1. Both aqueous and organic phases are pumped by respective positive displacement pump to the microfluidic junction. The outlet of the microfluidic junction is connected to a microbore tube. The dispersion is generated at the microfluidic junction, mass transfer takes place while dispersion flows through the microbore tube. Dispersion is then collected in sample bottle. Phase separation of dispersion into clear aqueous and organic phase takes place in sample bottle. Contact time can be varied both by varying flow rate and / or by varying the length of microbore tube. Instead of microbore tubes, microchannel etched in glass or any other suitable substrate can also be used. Fig. 1.2 shows microchannel etched in glass chips some of which are available commercially.

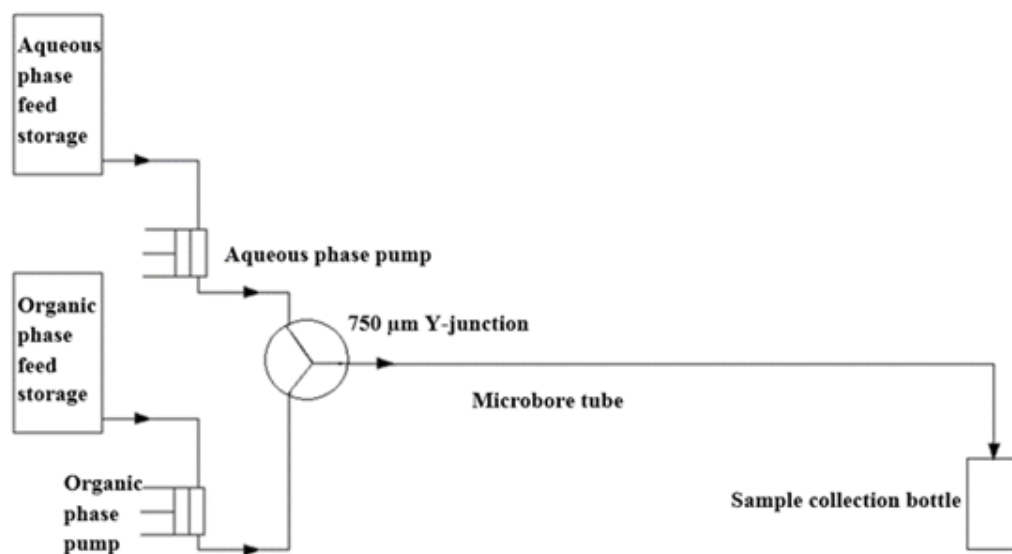


Figure 1.1: Schematics diagram of experimental setup for experiments with single microbore tubes

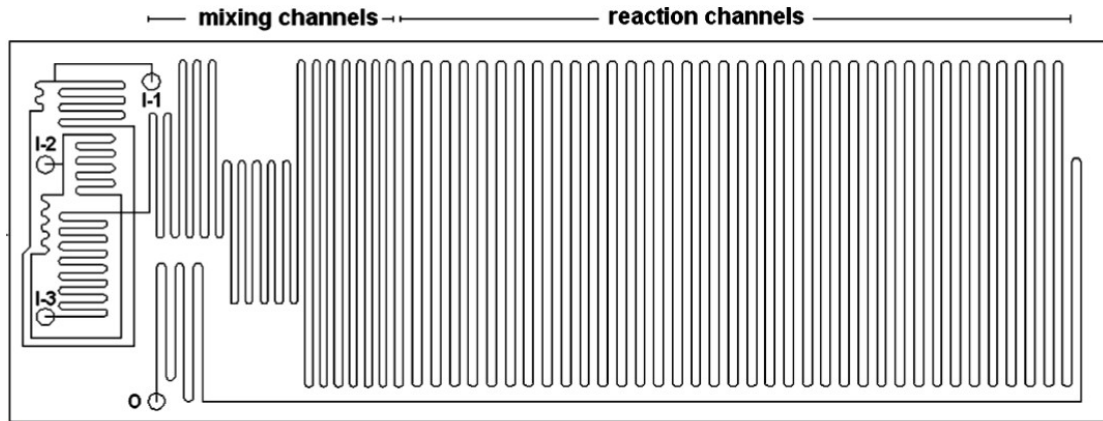


Figure 1.2: Microchannel glass chip with three inlets (Sarkar et al., 2012)

1.3 LITERATURE SURVEY

1.3.1 Liquid-liquid two-phase flow in microchannels

Liquid-liquid two phase flow patterns in microchannel are important as specific interfacial area, overall volumetric mass transfer coefficient and phase separation characteristics depends on type of flow pattern generated in microchannel. Liquid-liquid two phase flow patterns in microchannel are resultant of complex interaction between various forces such as viscous force, inertial force and interfacial tension force and gravitational force acting on fluid inside microchannel (Gunther and Jensen, 2006). These forces depend on physical properties of liquids flowing through microchannel, equivalent diameter of channel and velocity of the liquids inside microchannel. Different dimensionless numbers such as Reynolds number (Re), capillary number (Ca), Weber number (We) and Bonds number (Bo) are used to represent these forces as shown in Table 1.1.

Fig. 1.3 show the effect of channel hydraulic diameter (d_h) and dispersed phase velocity (U_d) on Bond, Capillary, and Weber numbers. In other way Fig. 1.3 represents effect of channel hydraulic diameter (d_h) and dispersed phase velocity (U_d) on gravity force, viscous force and interfacial force w.r.t interfacial tension force.

Table 1.1: Dimensionless number and their physical significance

Dimensionless numbers	Physical significance
$Re = \frac{\rho U_d d_h}{\mu}$	$\frac{\text{inertial forces}}{\text{viscous forces}}$
$Ca = \frac{\mu U_d}{\sigma}$	$\frac{\text{viscous forces}}{\text{interfacial forces}}$
$We = \frac{\rho U_d^2 d_h}{\sigma}$	$\frac{\text{inertial forces}}{\text{Interfacial forces}}$
$B_o = \frac{(\Delta\rho)gd_h^2}{\sigma}$	$\frac{\text{buoyancy forces}}{\text{Interfacial forces}}$

In other way Fig. 1.3 represents effect of channel hydraulic diameter (d_h) and dispersed phase velocity (U_d) on gravity force, viscous force and interfacial force w.r.t interfacial tension force. The thickness of the planes represents the practical range for fluid properties. At low velocities and small channel sizes interfacial forces dominate over gravity, inertia, and viscous ones, This condition is represented by yellow plane in Fig 1.3. If U_d is of the order of several meters per second, or in the presence of very large accelerations of liquids, drops much smaller than d_h can be formed.

The microfluidic junction shown in Fig. 1.1 is simple Y-junction. Two-phase liquid-liquid dispersion is generated when the two immiscible liquids are brought into contact at the microfluidic junction. Many designs of microfluidic junctions are possible (Sarkar et al., 2014). In literature various types of junctions are explored for generation of liquid-liquid dispersion. Some of them are shown in Fig. 1.4.

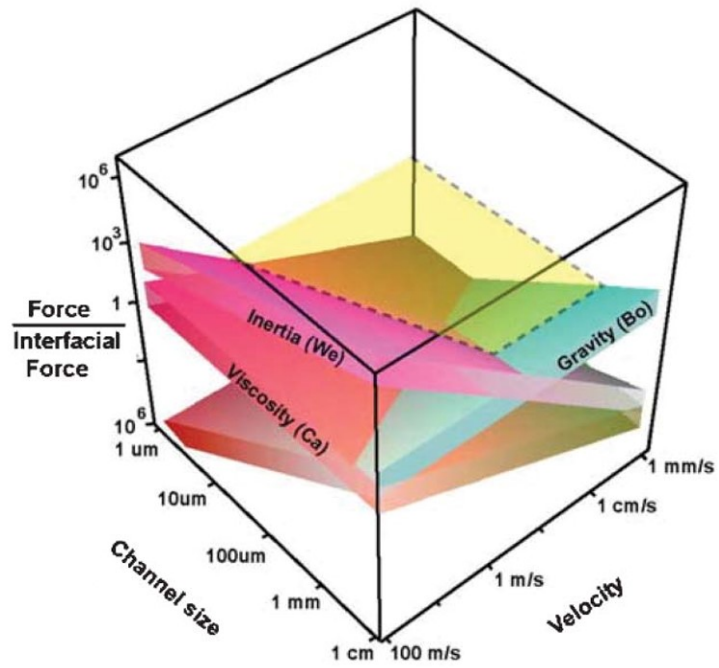


Figure 1.3: Effect of channel size and velocity on inertial, gravity and viscous forces (Gunther and Jensen, 2006)

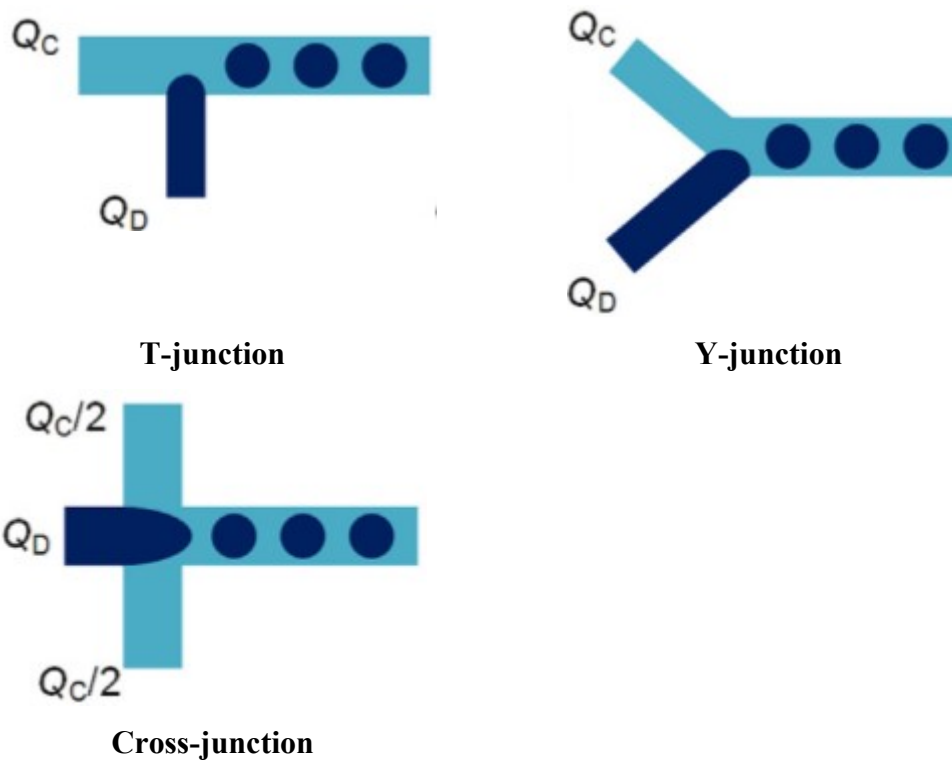


Figure 1.4: Various types of microfluidic junctions (Wang et al., 2017)

Three distinct regimes - squeezing, dripping, and jetting - are identified in microchannel (De Menech et al.,2008). At very low flow rates the squeezing regime prevails, in which slug-in-the-making at the junction grows in size leading to reduction in flow area available for the continuous phase. Due to constriction in the flow area the pressure starts building up on the upstream side of the slug and it is gradually squeezed in downstream direction. Gradually the neck connecting the slug in the making to its bulk phase becomes thin and finally it is broken and a slug is formed. On further increasing the flow rates, dripping regime is observed. In this, breakup appears to occur when the interfacial force is nearly balanced by the shear force though pressure effect as in squeezing regimes might also be contributing to the breakup. Compared to the squeezing regime, point of breakup of the droplet being formed from its bulk phase moves in downstream direction. On further increase in flow rate inertial forces completely dominate over the interfacial forces resulting in parallel flow or stratified flow or annular flow. This is called jetting. Similar kind of regimes are reported for other junctions also.

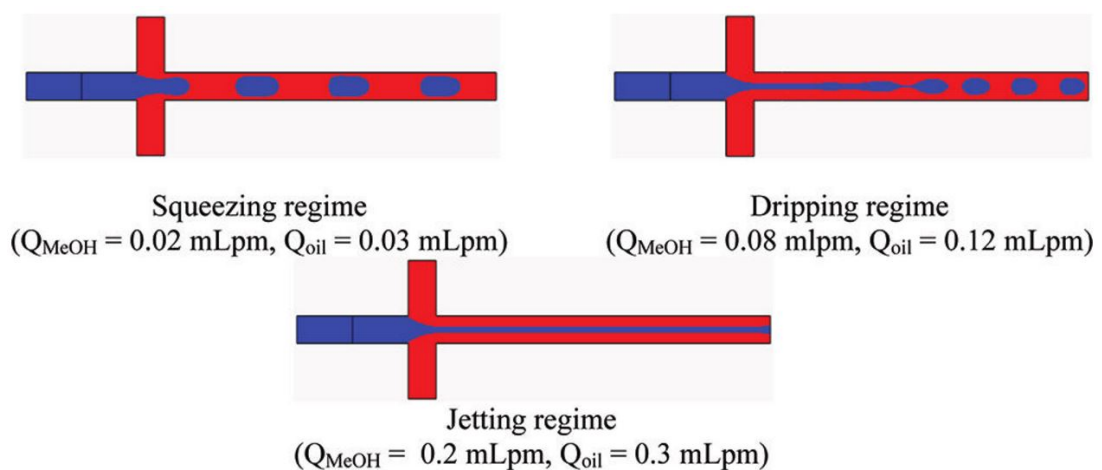


Figure 1.5: Flow visualization for the case when the phase getting dispersed comes from the center (Sarkar et al., 2012)

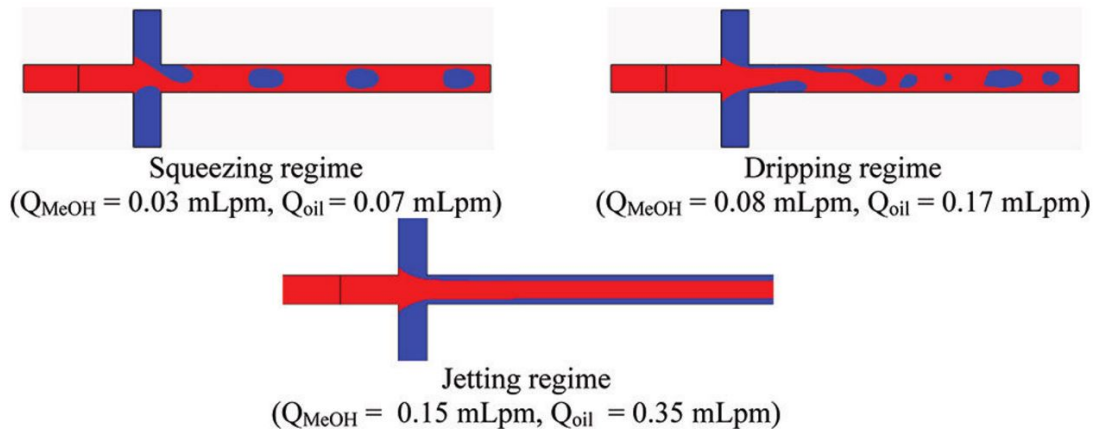


Figure 1.6: Flow visualization for the case when the phase getting dispersed comes from the sides (Sarkar et al., 2012)

The flow patterns shown in Fig. 1.5 and Fig. 1.6 are based on the results obtained from numerical simulations of liquid–liquid two-phase flow at a microfluidic junction (Sarkar et al., 2012). The blue and red colors indicate methanol phase and oil phase, respectively. Though these observations are for a different phase system, the transition from one regime to another will be observed for all phase systems and probably in all kinds of microfluidic junctions. The squeezing regime will give slug flow. When the flow rates are small, a slug will grow to occupy almost full cross-section of the channel before getting detached from its bulk phase. As the flow rate increases, slug will become smaller. Dripping regime in which point of breakage will go further inside the channel will give slug and droplet flow and droplet flow. The jetting regime will give annular flow and unstable annular flow.

Several experimental studies on liquid-liquid two phase flow patterns in different types of microfluidic junctions and micro channels have been reported. In an experimental study conducted by using kerosene and water in 0.4 mm diameter rectangular microchannel the different flow patterns such as Slug flow (SF), Monodispersed droplets flow (MDF), Droplets populations flow (DPF), Parallel flow

(PF), Annular flow (AF) are obtained (Zhao et al., 2006). These flow patterns are shown in Fig. 1.7. Flow regime map in terms of Weber number is shown in Fig. 1.8. Flow regime map as shown in Fig. 1.8 is divided into three zones I, II and III. In zone I, We_{ks} and We_{ws} are less than 1. In this region interfacial tension forces are higher than other forces. In zone II We_{ks} and We_{ws} are greater than 1 and less than 10. In this region inertial force is comparatively higher than interfacial tension force. In zone III We_{ks} and We_{ws} are greater than 10. In this region inertial force is dominating force.

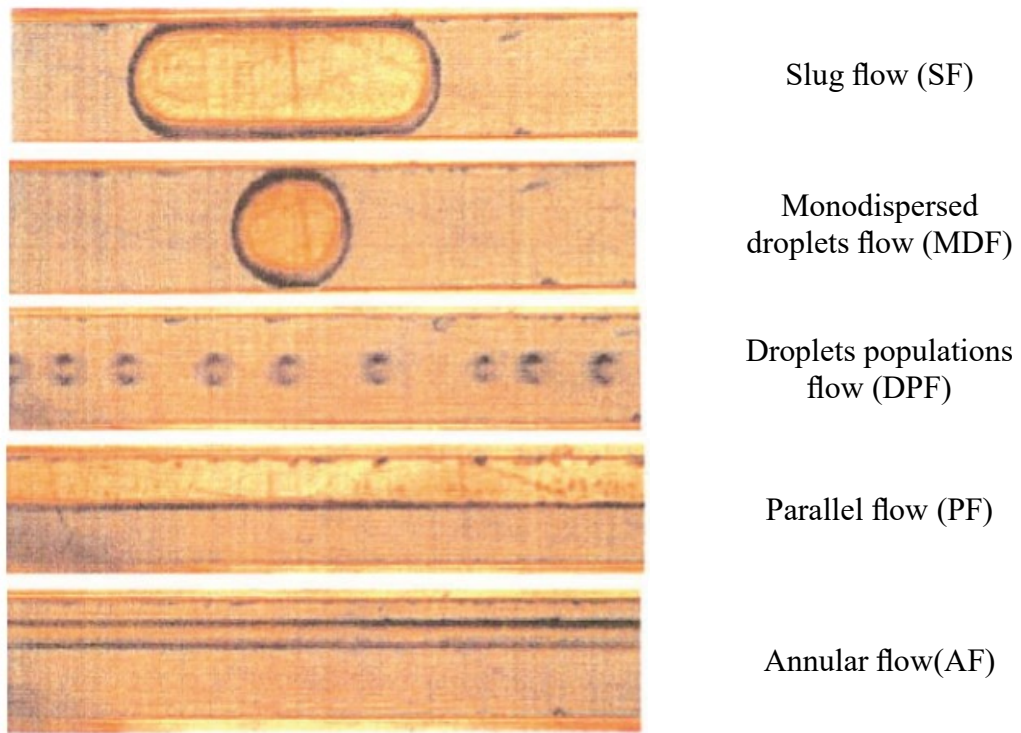


Figure 1.7: Representative photographs of stable flow patterns in the 0.4mm diameter rectangular microchannel (Zhao et al., 2006)

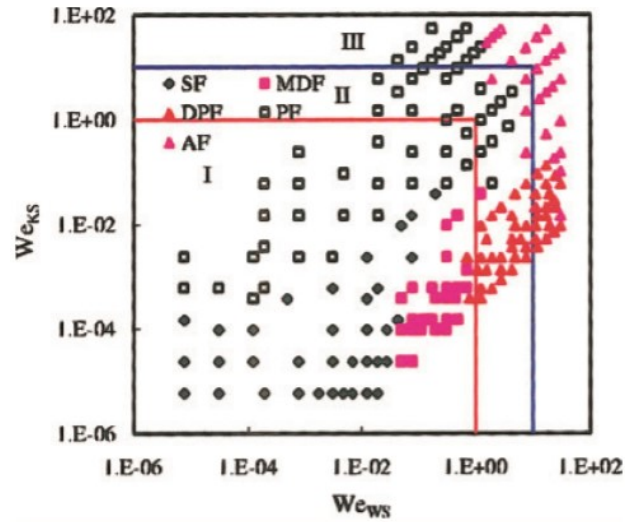


Figure 1.8: Flow regime map in terms of Weber number of kerosene and water phase (Zhao et al., 2006)

In literature similar studies have been carried out for different phase systems and different types of microchannels. Flow pattern observed in these studies depends upon physical properties of phase system, geometrical parameters of microchannels and operating conditions. Fig. 1.9 shows the flow patterns observed by Kashid et al. (2011). In this study flow regime map is plotted in terms of flow rate, superficial velocity and capillary numbers as shown in Fig. 1.10 and Fig. 1.11, respectively. Thus in literature flow regime maps are plotted in different ways (Sarkar et al., 2012).

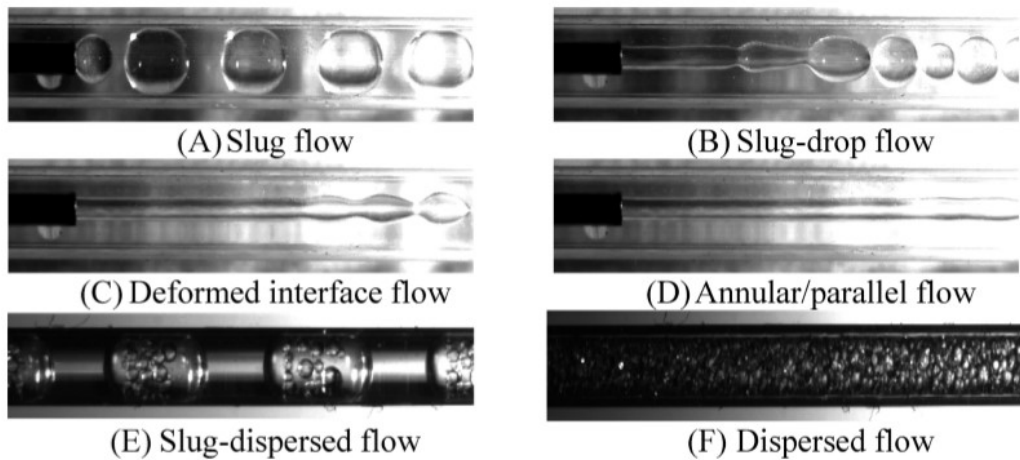


Figure 1.9: Flow regimes observed for liquid–liquid systems in microstructure reactor. (Kashid et al., 2011)

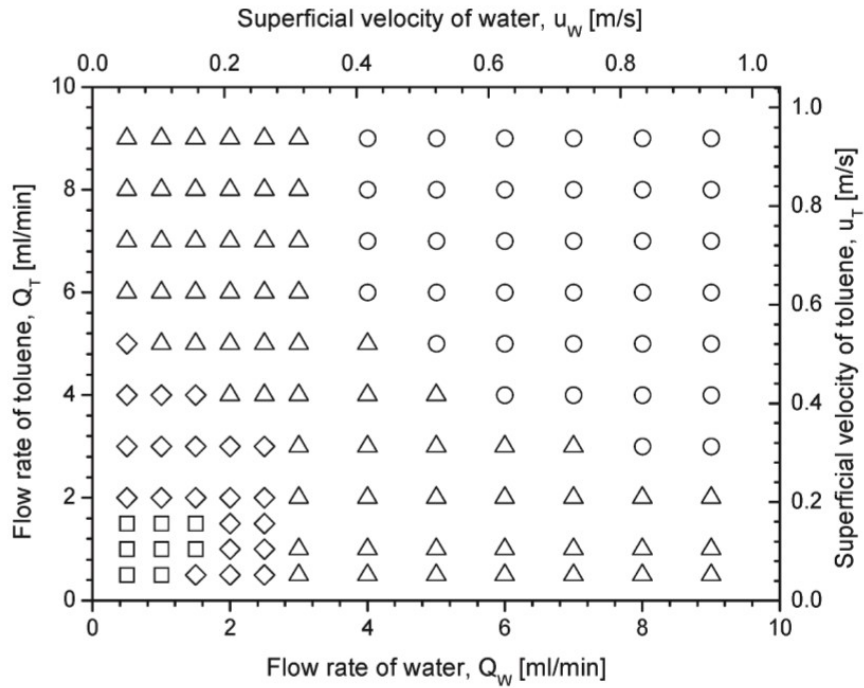


Figure 1.10: Flow regimes map for T-square microchannel (□, slug; ◇, slug-drop; △, deformed interface; O, annular/parallel) (Kashid et al., 2011)

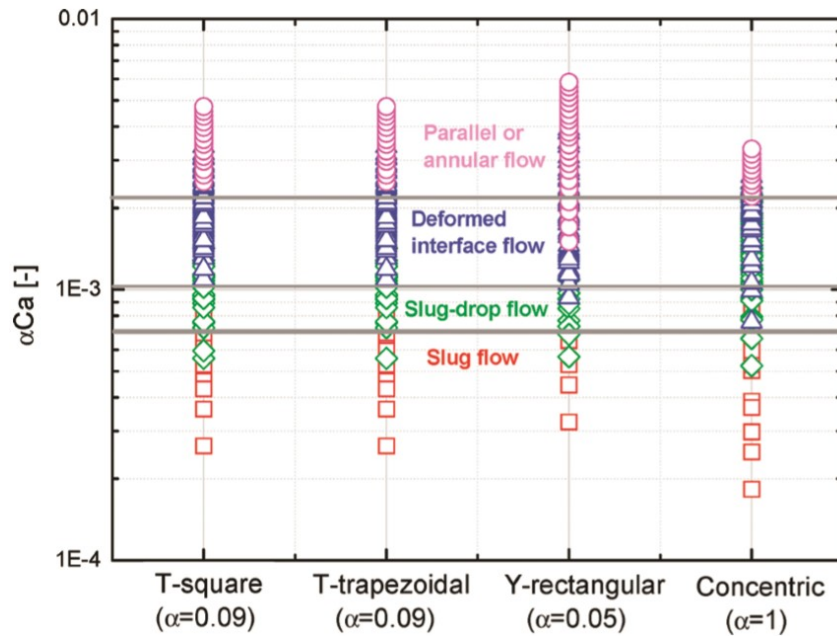


Figure 1.11: Comparison of flow regimes maps for all microchannels (□, slug; ◇, slug-drop; △, deformed interface; O, annular/parallel) (Kashid et al., 2011)

1.3.2 Miniature devices for separation of microfluidic liquid-liquid dispersions

In order to reduce inventory in settler and make setup compact miniature devices are required for separation of microfluidic liquid-liquid dispersions coming from microfluidic devices. Several efforts have been made in literature to realize such devices (Bannock et al., 2013; Breisig et al., 2017; Kashid et al., 2007c; Wang et al., 2017, Logtenberg et al., 2011; Kolehmainen and Turunen, 2007). Fig. 1.12 shows the miniaturized devices used in literature for separation of liquid-liquid dispersion. Most of these devices separate phases by exploiting the difference in the wetting properties of the two liquids. As shown in Fig. 1.12 (a), a hydrophilic SS tube and a hydrophobic PTFE tube are used in a Y-shaped phase separator (Kashid et al., 2007c). The aqueous phase of the inlet dispersion preferentially moves in to hydrophilic SS tube, while organic phase moves into hydrophobic PTFE outlet. Thus phase separation is achieved. Such a device will work for the conditions in which slug flow is generated (at low flow rate). However, over a wide operational range in which different flow patterns may result, to have complete phase separation is a challenge and entrainment may exist in one or both phases (Scheiff et al., 2011). The same principle of wetting of phases by using different materials has been used in a T-junction separator (Wang et al., 2017). In Y-Y junction microchannel, surface modification by applying hydrophobic coating on part of the length has also been used for phase separation (Logtenberg et al., 2011). In some studies parallel plates having difference in wetting properties, schematically shown in Fig. 1.12 (c), have been used for phase separation by converting dispersed flow pattern to stratified flow pattern at comparatively higher throughput (Kolehmainen and Turunen, 2007; Okubo et al., 2004).

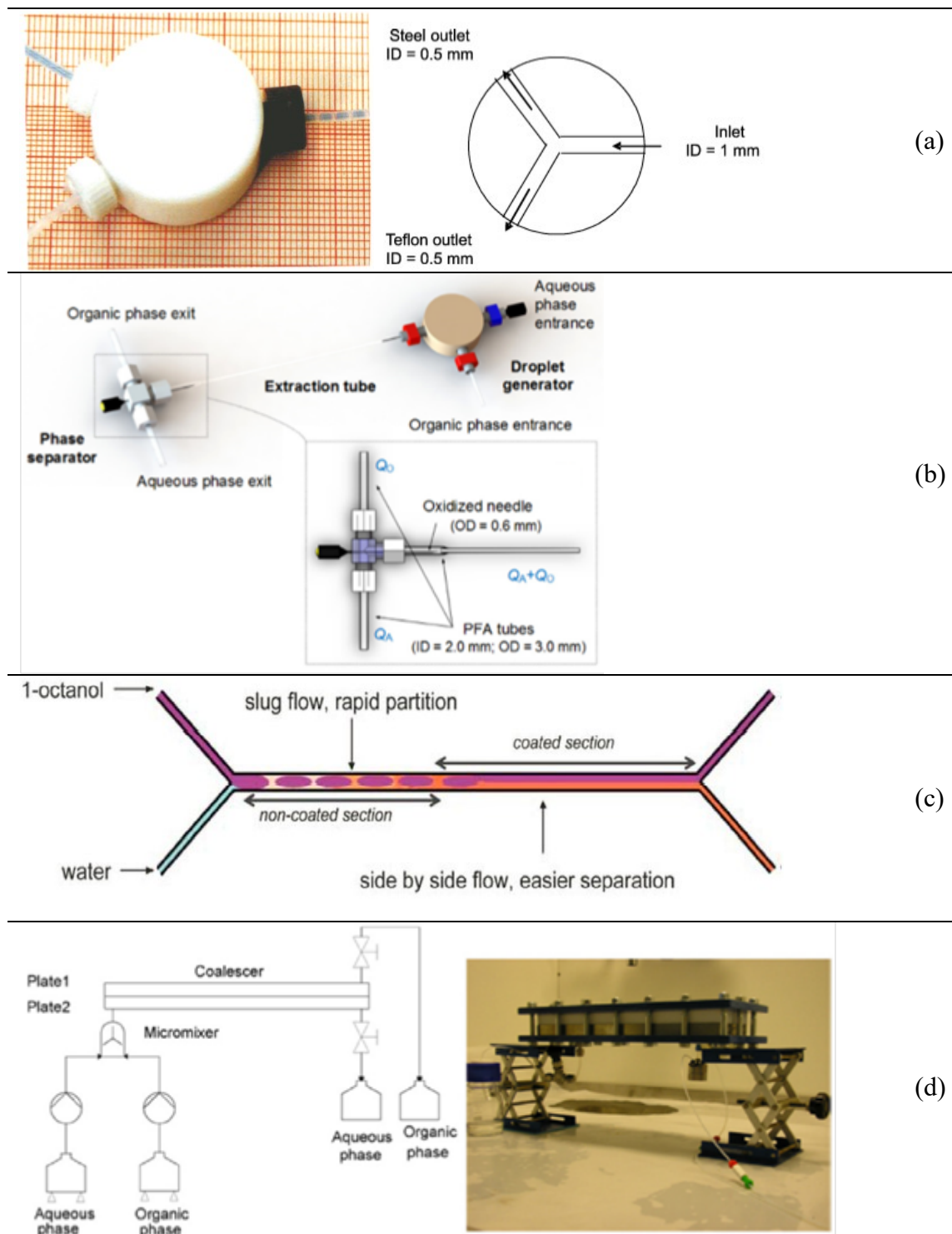


Figure 1.12: Miniaturized phase separators based on differences in wetting properties.

- (a) Y-junction phase separator (Kashid et al., 2007c) (b) T-junction phase separator (Wang et al., 2017) (c) Y-Y microchannel with a coated section for phase separation, (Logtenberg et al., 2011) (d) A high-capacity mini extraction system using a plate phase separator, (Kolehmainen and Turunen, 2007)

Apart from exploiting difference in wettability, modifications in the geometry can also be done to have phase separation. Since the capillary force is significantly stronger in smaller microchannels, microchannel arrays can be used to rapidly draw the continuous phase from the two-phase mixture, as shown in Fig. 1.13 (a) and Fig. 1.13(b) (Bannock et al., 2013; Breisig et al., 2017).

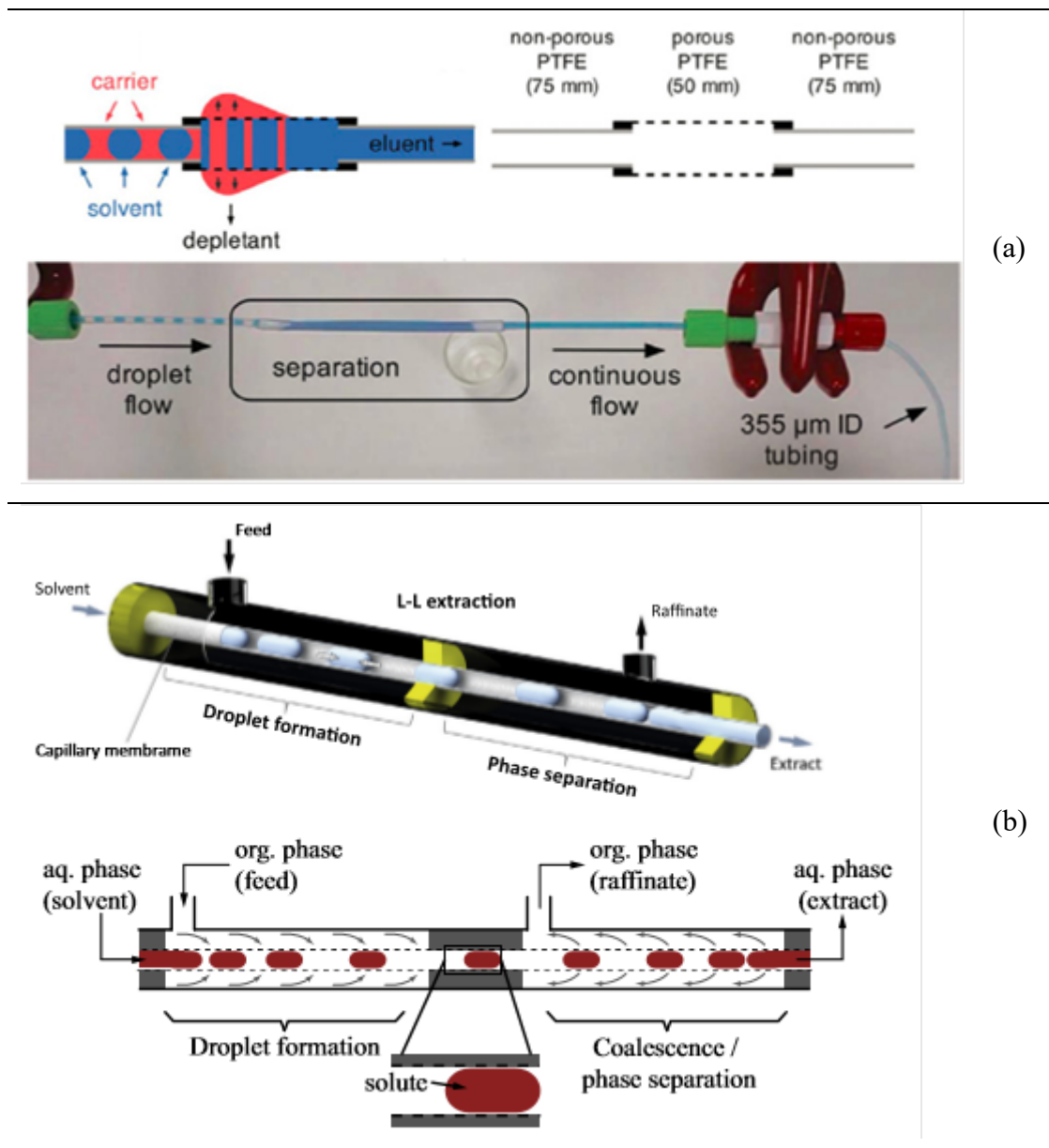


Figure 1.13: Microflow phase separators based on capillary pressure. (a) Tubular member phase separator (Bannock et al., 2013) (b) liquid-liquid extraction using a capillary membrane (Breisig et al., 2017)

1.3.3 Liquid-liquid extraction in microchannels

Table 1.2 shows that specific interfacial area and overall volumetric mass transfer coefficients in micro-reactors are much higher than those obtained in conventional contactors. Overall volumetric mass transfer coefficients in microchannel is 2 orders of magnitude higher than conventional contactor. Thus intensification of mass transfer can be achieved using microchannel (Tsaoulidis, 2014)

Table 1.2: Overall volumetric mass transfer coefficient of different types of contactors (Tsaoulidis, 2014)

References	Contactor	α (m ² /m ³)	$k_L\alpha$ (s ⁻¹)
Fernandes and Sharma, 1967	Agitated contactor	32–311	$(48–83) \times 10^{-3}$
Verma and Sharma, 1975	Packed bed column	80–450	$(3.4–5) \times 10^{-3}$
Charpentier, 1981	Bubble column	50–600	$(5–240) \times 10^{-3}$
Kies et al., 2004	• Spray column • Stirred tank	75–170 100–2000	$(15–2.2) \times 10^{-3}$ $(30–400) \times 10^{-3}$
Dehkordi, 2001; Dehkordi, 2002	• Two impinging jets reactor • Air operated two impinging reactors	1000– 3400 350–900	0.28 0.075
Kashid et al., 2007b	Capillary microchannel, ID = 0.5–1 mm	830–3200	0.88–1.67

Some of the reported studies on solvent extraction in microchannels are summarized in Table 1.3. Studies on liquid-liquid extraction in different types of microchannels and micromixer – commercially available as well as fabricated in-house have been reported (Hotokezaka et al., 2005; Kumar et al., 2012). While there are studies with phase systems of interest of the authors, there are several studies in which standard

phase systems recommended by EFCE ([Benz et al., 2001](#);[Darekar et al., 2014a](#);[Zhao et al., 2007](#)) have been used. While most of the studies are with single microchannels, there are only few studies focusing on achieving higher flow rates using parallel microchannels or micromixer or specially designed microchannels ([Liu et al., 2014](#)).

Table 1.3: Summary of some of previously reported studies on solvent extraction in microchannels

Reference	Microchannel(s)	Phase system	Maximum flow rate	Remarks
Benz et al., 2001	A commercially available design of micromixer	Water-Acetone-Toluene; Water-Acetone-n-Butyl acetate; Water-Succinic acid-Butanol; Water-Dipantolactone-Methyl isobutylketone	6.4 LPH	Micromixer array is used. Though settler is used in the experimental setup, the details of settling behavior are not discussed. Pressure drop is not reported.
Hotokezaka et al., 2005	Y-junction microchannel chip	Nitric acid -Uranium-Tributyl phosphate (TBP)	0.00044 LPH	Single microchannel is used. Pressure drop is not reported. Settler was not used as experiments were conducted in parallel flow regime.
Kralj et al., 2007	Microchannel chip with integrated T-mixer, contactor and phase separator	Water-N,N Dimethylformamide (DMF) - Methylene chloride	0.12 LPH	Single microchannels were used. Pressure drop is not reported. Phase separator is used but settling behavior is not discussed.
Zhao et al., 2007	Opposed T-junction and cross T-junction microchannels	Water-Succinic acid-n Butanol	2.59LPH	Single microchannels were used. Pressure drop and settling characteristics are not studied.
Okubo et al., 2008	Y-shaped microchannel and a commercial design of micromixer	Water -Phenol-Dodecane	0.3 LPH for single microchannel and 10 LPH for micromixer	Pressure drop is given as low or high but not quantified. Separation time in segmented flow was found to be negligible whereas the same in emulsification flow was about 1 h.
Zhao et al., 2010	Opposed T-junction and cross T-junction microchannels	Water-Succinic acid-n Butanol	1.56 LPH	Single microchannels are used. Pressure drop and settling behavior not discussed.
Aoki et al., 2011	Opposed T-junction microchannel	Water-Phenol-Dodecane	1.2 LPH	Single microbore tube is used. Mass transfer in only slug flow is studied. Pressure drop and settling behavior not discussed.
Tamagawa et al., 2011	Y-junction	Water- Cesium nitrate- Cyclohexane	0.1 LPH	Single microchannel is used. Settler is used in the experimental setup. Pressure drop study and settling behavior not described.
Kumar et al., 2012	Y- junction with microbore tubing	Water-Nitric acid -30% TBP in n-Dodecane	0.072 LPH	Single microbore tube is used. Micro-settler is used in the setup. Studies on pressure drop and settling behavior not reported.
Priest et al., 2012	The glass microfluidic chips	Water -Copper-Sulphuric acid	0.01 LPH	Single microchannels are used. Pressure drop and settling behavior not discussed.

Usually the solvent extraction in a microchannel takes place during co-current flow of the two liquid phases. Thus a microchannel typically represents a single stage. For complete or almost complete extraction of desired material by liquid-liquid extraction, multistage extraction is required. However, multistage extraction using microchannels is challenging though some efforts have been put in this direction. Fig. 1.14 shows a multistage extraction system using microchip extractors. In this setup gravity settler is used for phase separation. Syringe pumps are used to pump liquids at controlled flow rates in microchannel chips (Lan et al., 2016; Li et al., 2012). Fig. 1.15 shows two-stage counter current extraction system. Inter-stage pumping is provided in this two-stage extraction process (Holbach and Kockmann, 2013).

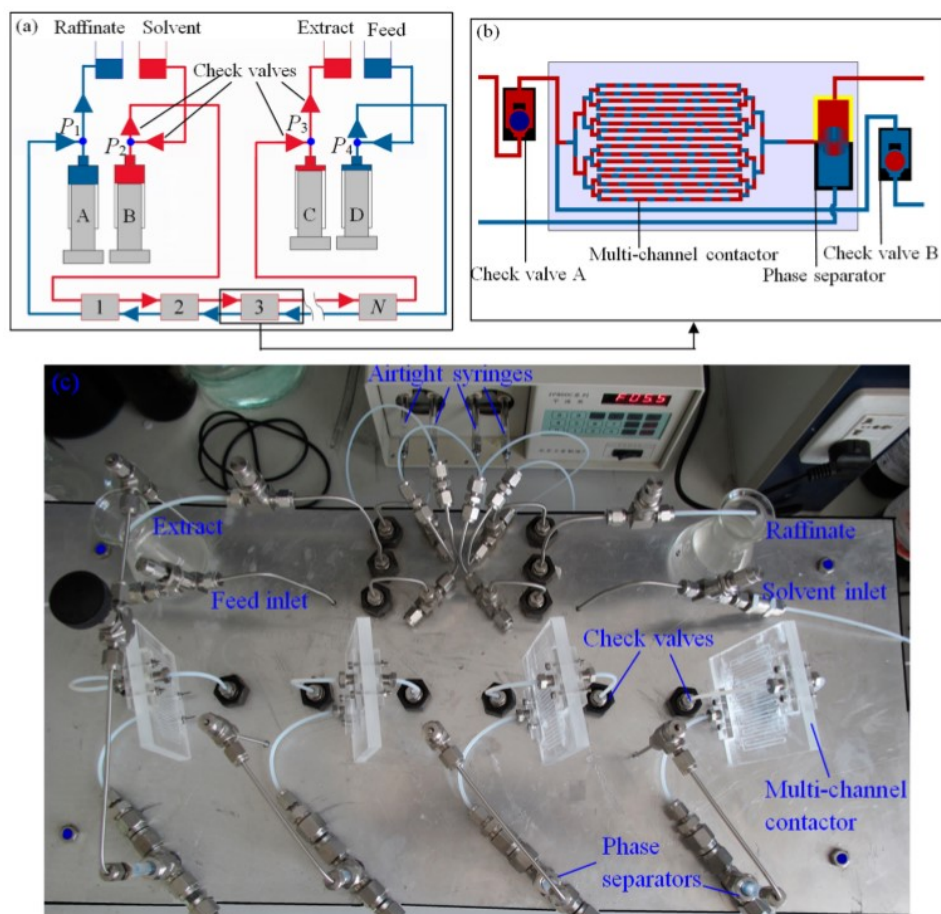


Figure 1.14: Multistage countercurrent extraction based on microflow. Schematic and actual photograph of the experimental setup (Lan et al., 2016)



Figure 1.15: Two-stage counter-current setup (Holbach and Kockmann, 2013)

1.3.4 Gap areas

Intensification of mass transfer can be achieved using microchannel contactor due to high specific interfacial area and high overall volumetric mass transfer coefficients (Darekar et al., 2014a; Darekar et al., 2014c; Ji et al., 2010; Kashid et al., 2011; Sen et al., 2014; Su et al., 2010; Zhu et al., 2014). In majority of the studies on liquid-liquid extraction in microchannels focus is on mass transfer in single microbore tube (Aoki et al., 2011; Hotokezaka et al., 2005; Kumar et al., 2012; Priest et al., 2012). Single microchannel handles limited flow rate. To handle larger throughput numbering up approach is required to be used, where numbers of microbore tubes are connected in parallel. Each microbore tube has optimum configuration that ensures fast mass transfer along with quick phase separation and low pressure drop. In literature methodology to identify an scalable optimum configuration that ensures fast mass transfer along with quick phase separation and low pressure drop for a given

throughput and given phase system. This gap area has been addressed in Chapter 2 of this thesis.

In literature, several studies have been reported on liquid-liquid two-phase flow patterns in microchannels (Cherlo et al., 2010; Fu et al., 2015; Kashid and Agar, 2007a; Salim et al., 2008; Sarkar et al., 2012; Zhao et al., 2006). However, the studies reporting the effect of flow pattern on mass transfer are just a few (Darekar et al., 2014b; Dessimoz et al., 2008; Zhao et al., 2010). The flow pattern generated at the microfluidic junction also affects the settling of phases after extraction. But the studies on the effect of flow pattern on settling are scarce. In Chapter 3 of this thesis, the effect of flow pattern on mass transfer is studied to address this gap area in literature.

The performance of a microchannel for solvent extraction depends on the specific interfacial area available for mass transfer which, in turn, depends on the flow pattern generated at the junction of the microchannel. In literature experiments with different test systems in different types of microchannels have been reported (Cherlo et al., 2010; Dessimoz et al., 2008; Fu et al., 2015; Kashid et al., 2011; Salim et al., 2008; Sarkar et al., 2012; Yagodnitsyna et al., 2016; Zhao et al., 2006; Zhao et al., 2010). Condition for using a particular flow regime map is that, the expected flow regime should be able to predict by available flow regime maps. However, considering wide variations in the design of microfluidic junction and physical properties of the liquids, it is very difficult to prescribe generalized flow regime map. Previously an attempt has been made for the generalized flow regime map for a T-junction. In this work, we have taken that work forward to present the generalized flow regime maps for Y-junctions microchannels. This gap area in the literature is addressed in Chapter 4.

In literature, most of the studies on micro-scale solvent extraction are on single microchannels or single microbore tubes (Aoki et al., 2011; Hotokezaka et al., 2005; Kumar et al., 2012; Priest et al., 2012). The studies on micro-scale extraction using parallel microchannels to achieve high throughputs are just a few (Al-Rawashdeh et al., 2012a; Al-Rawashdeh et al., 2012b; Tonkovich et al., 2005). These few studies involve commercial designs in which the length of the microchannels is fixed. For feeding parallel microchannels, a properly designed distributor is essential to distribute flow equally among microbore tubes connected to the distributor. In literature various designs of distributors are reported. Most of them are for distributing a single fluid into parallel channels. Manifold type distributor is used for flow distribution in heat exchangers (Fang et al., 2008). Inlet dividing distributors are reported for flow distribution in shell and tube heat exchangers (Kannan et al., 2010). Flow equalization is also tried by using constructal distributors (Luo et al., 2008; Zhiwei et al., 2009). Distributors which are having structural bifurcations are used in fuel distributors and fuel processing chemical reactors (Liu et al., 2010). Studies on distributors which have in-built microfluidic junctions for flow distributions as well as generation of dispersion are scant. This gap area is addressed by designing a distributor named Monoblock Distributor with In-built Microfluidic Junctions (MDIMJ) using CFD for equal distribution of two phases and in situ generation of liquid-liquid dispersion, as described in Chapter 5. Also in this chapter MDIMJs along with 20 parallel microbore tubes are used to achieve maximum throughput of 10 LPH in multistage extraction and stripping.

In literature different methods have been used for separation of liquid-liquid dispersion such as gravity settler working on the principle of density difference

(Kumar et al., 2017), separation based on selective wettability of different phases on microchannel surface/membrane (Bannock et al., 2013; Castell et al., 2009; Cervera-Padrell et al., 2012; Holbach and Kockman, 2013; Kralj et al., 2007; Weeranoppanant et al., 2017;) and retardation of flow (Bremond et al., 2008). In some cases, non-dispersive parallel flow is used and in such cases, the phases can be separated by providing a Y-junction at the outlet (Hellé et al., 2014; Hellé et al., 2015; Hotokezaka et al., 2005; Zhang et al., 2016). The flow rates possible in such configurations are relatively less ($\sim 10^{-2}$ mL/min) as at higher flow rate the parallel flow may develop instabilities. Also to ensure parallel flow some kind of surface treatment is necessary on one part of the wall of microchannel. This surface treatment may not remain effective after prolonged use. Use of commercially available membrane phase separators has also been reported (Vansteene et al., 2018). But typically the flow rates handled are much less ($\sim 10^{-2}$ mL/min). Flow splitter having two channels one of SS and other PTFE to separate the phases based on wettability has also been reported (Tsaoulidis et al., 2013 a). However, this method also can be used for less flow rates and for the conditions when slug flow pattern is achieved. For other flow patterns, such a flow splitter will not work. These gap areas are addressed proposing metallic mesh based in-line phase separator that can work for larger flow rates (flow rates of the order of 10 mL/min) and can handle different types of flow patterns generated in microcontactors, as described in Chapter 6.

In literature there are many studies on non-dispersive counter-current extraction. Mostly they are in hollow fibers. Membrane based devices are hardly used for extraction of radioactive material due to degradation of membrane at high radiation. Non-dispersive countercurrent solvent extraction is demonstrated using

microchannel with metal mesh sandwiched between parallel microchannels. Metal mesh do not suffer from degradation problem at high radiation. In Chapter 6 countercurrent device with metallic mesh is used for extraction of uranium from lean stream.

In literature several studies on extraction and/ or stripping studies have been reported in microchannels ([Aoki et al., 2011](#); [Darekar et al., 2014b](#); [Sen et al., 2014](#); [Tsaoulidis et al., 2013a](#), [Willersinn and Bart, 2015](#)). However, most of the studies are limited to extraction or stripping in co-current flow which essentially represents a single-stage in extraction or stripping. [Smirnov et al. \(2013\)](#) recently reported a method to strip uranium directly from loaded organic in the form of uranium peroxide. The authors contacted organic phase loaded with uranium directly with hydrogen peroxide (along with ammonium hydroxide) to obtain uranium peroxide precipitate. They studied the effects of different parameters like solution pH, hydrogen peroxide concentration and reaction temperature on the precipitation process. They also studied the kinetics of the process and reported the time necessary for near complete uranium recovery (99.4%). They used an organic phase having 78 gm/L of uranium. However, the authors did not report the reusability of the organic phase. The method reported by [Smirnov et al. \(2013\)](#) differs from the traditional method which employs water (or diluted nitric acid) for stripping uranium from the loaded organic phase to the aqueous phase as uranyl nitrate and then contact of aqueous phase containing uranyl nitrate with ammonium hydroxide/sodium hydroxide/hydrogen peroxide to precipitate uranium from the aqueous phase. This method of direct precipitation from organic phase leads to process intensification by combining two different steps (stripping and precipitation) in a single step. However, the feasibility of direct precipitation of value metal ion from

loaded organic has not been demonstrated in microchannels. This hitherto unreported implementation of direct precipitation of value material from loaded organic in microchannel is the subject matter of chapter 7. Feasibility of implementation of this method in microchannels is demonstrated by recovering uranium from lean streams using 30% TBP in dodecane as the organic phase and thereafter contacting loaded organic obtained from extraction stage directly with ammonium hydroxide to precipitate out uranium as ammonium diuranate. The direct stripping removes the equilibrium limitation typically associated with a stage-wise contactor for stripping.

Most of the studies done in this thesis are with the liquids relevant for solvent extraction processes in nuclear fuel cycles. Though there are several studies on solvent extraction in microchannel with test systems relevant to nuclear fuel cycle, work on all aspects of solvent extraction such as mass transfer, settling, flow patterns, scale-up, multi-staging using test systems relevant to nuclear fuel cycle are scarce. (Darekar et al., 2014b; Hellé et al., 2014; Hellé et al., 2015; Hotokezaka et al., 2005; Kumar et al., 2012; Tamagawa and Muto, 2011; Tsaoulidis et al., 2013b).

1.4 RELEVANCE OF RESEARCH WORK

In the front-end of nuclear fuel cycle, solvent extraction is used for separation and purification of uranium (Edwards and Oliver, 2000; Fan et al., 2014; Gupta et al., 1997; Mathuthu et al., 2019; Sivaramakrishna et al., 2019), thorium (Menzies and Rigby, 1961), zirconium, hafnium (Amaral and Morais, 2016) and other nuclear materials. In the back-end of nuclear fuel cycle, reprocessing of spent nuclear fuel is also carried out by using solvent extraction as the separation process (Veliscek-Carolan et al., 2016). Mixer-settlers, slurry extractors, centrifugal extractors and air

pulsed columns are commonly used for solvent extraction in nuclear industry. Mixer-settlers are used for the systems requiring longer residence time and easily separable by gravity (Ban et al., 2016). Slurry extractors offer the advantage of handling the feed containing solids (Gupta et al., 1997). Centrifugal extractors are most appropriate when extraction is to be achieved in short contact times but require frequent maintenance due to parts rotating at high speeds (Duan et al., 2014). Air pulsed columns have the advantage of being maintenance-free and are suited for spent fuel reprocessing (Torab et al., 2011).

The prerequisite for a solvent extraction equipment to be suitable for deployment in the back-end of nuclear fuel cycle is that it should not have moving parts as maintenance is difficult in high radiation environment. Another requirement which assumes importance during recovery of value material from high burn-up nuclear fuels is that the contact time in the solvent extraction equipment should be as small as possible to avoid the degradation of solvent which is used for extraction. None of the available types of contactors can meet both the requirements (Wang et al., 2019). For example, centrifugal extractor which can significantly reduce the contact time and thus avoid solvent degradation is considered suitable for high burn-up fuels (Natarajanand Raj, 2007). But it suffers from the limitation of having the parts rotating at very high speeds. Air pulsed columns which do not have moving parts typically involve large contact time and thus may be suitable for low burn-up fuel but not suitable for high burn-up fuels. Thus the quest of having an extractor which can meet both the requirement is still relevant. Of late, there has been significant interest in micro-scale contactors or microfluidic contactors. Such contactors have advantages such as high extraction efficiency in short contact times due to high overall volumetric

mass transfer coefficients and precise control on quality of dispersion. There are several studies which report use of microfluidic contactors for solvent extraction in diverse processes (Ciceri et al., 2014; Sattari-Najafabadi et al., 2018). Use of microfluidic contactors for extraction of nuclear materials has also been reported extensively (Darekar et al., 2014b; Hellé et al., 2014; Hellé et al., 2015; Hotokezaka et al., 2005).

1.5 OUTLINE OF RESEARCH WORK

The outline of the research work is mentioned below.

- Introduction and literature survey presents current state of art of using microchannels for solvent extraction and identification of gap areas (Chapter 1).
- Assesment of feasibility of intensification of solvent extraction in single microchannels and optimization of configuration of the microchannel for achieving high mass transfer with fast phase separation and low pressure drop (Chapter 2).
- Experimental studies on the effect of flow patterns and layout of microchannel on mass transfer and settling (phase separation) characteristics. Mass transfer and settling characteristics for different flow patterns were quantified and compared. The effect of coiling of microchannel on mass transfer was also studied(Chapter 3).
- Generalized flow regime map of liquid-liquid two phase flow in Y-junction microchannels. Generalized flow regime map was generated by utilizing the data of the experiments conducted with different standard test systems and Y-junctions of different diameters. (Chapter 4).

- Scale-up of solvent extraction in micro channels for achieving larger throughputs using Monoblock Distributor with In-built Microfluidic Junctions (MDIMJ). MDIMJ was conceptualized, evaluated using CFD, fabricated and tested for scale-up by numbering-up. Multistage solvent extraction in microchannels was demonstrated at 10 LPH using MDIMJs (Chapter 5).
- Metallic membrane based device was tested for inline phase separation of dispersion generated in a microchannel as well as for mass transfer. Intensification of settling (phase separation) was demonstrated by using inline phase separator. Feasibility of non-dispersive solvent extraction by using metallic membrane based counter current device was also demonstrated (Chapter 6).
- Feasibility of process of direct precipitation of solute from loaded organic in microchannels was also demonstrated. The complete process involved extraction of uranium from a lean aqueous stream to an organic phase in a microchannel followed by direct precipitation of uranium from loaded organic in another microchannel. The proposed process combines two different steps – multi-stage stripping step using dilute acid and precipitation step - in a single step and thus simplifies and intensifies the conventional process (Chapter 7).
- Conclusions of the studied conducted in microchannel and future work are also presented (Chapter 8).

CHAPTER 2

ASSESSMENT OF FEASIBILITY OF INTENSIFICATION OF SOLVENT EXTRACTION PROCESS IN SINGLE MICROCHANNELS

2.1 INTRODUCTION

Single microchannel handles limited flow rate. If throughput in a single microbore tube is increased, the dispersion will tend to become finer. At the same time film coefficients will also increase causing the mass transfer rates to increase. But as the dispersion become finer, the settling tends to become slow. Thus considering both mass transfer and settling, there exists a limit on the throughput a single microbore tube can handle.

In real life application, besides mass transfer phase disengagement or settling is equally important. If the phase disengagement of the dispersion generated in the contactor is not quick, much of the inventory will be locked in the settling device or settler. This will defeat the very concept of miniaturization.

Though there are many studies on liquid-liquid extraction in microchannels, studies with a holistic view considering both mass transfer and settling are very few. The requirement of fast mass transfer and quick settling often conflicts. In this chapter we take the holistic view of the solvent extraction process and propose a simple methodology which can be used to decide an optimum configuration that ensures fast mass transfer along with quick phase separation and low pressure drop. This chapter is focused on experiments with single microbore tubes to identify a configuration that gives high stage efficiency in short contact times, quick settling of resulting dispersion with low pressure drop.

2.2 EXPERIMENTAL

2.2.1 Setup

Fig. 2.1 shows image and Fig. 2.2 shows schematic diagram of the experimental setup used for the experiments with single microbore tubes. This setup consists of a Y-junction of 750 μm diameter drilled in a polytetrafluoroethylene (PTFE) disk. The included angle between the two inlets of Y-junction is 120° . A replaceable microbore tube of PTFE is connected to the disk using a threaded connector. Dispersion generated at the Y- junction passes through the microbore tube and collects in a glass sample bottle.

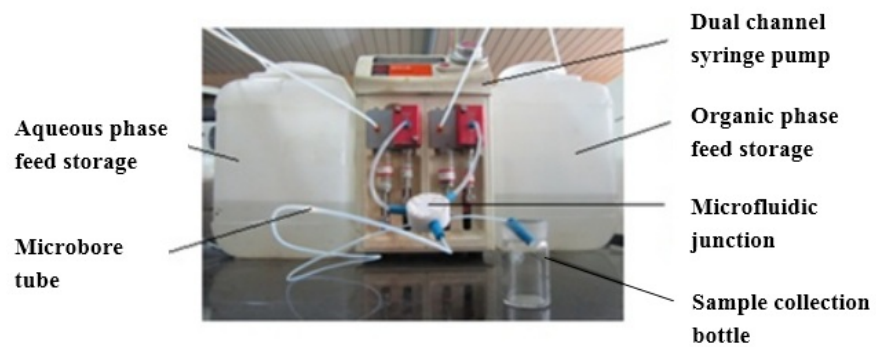


Figure 2.1: Experimental setup used in the experiments with single microbore tube

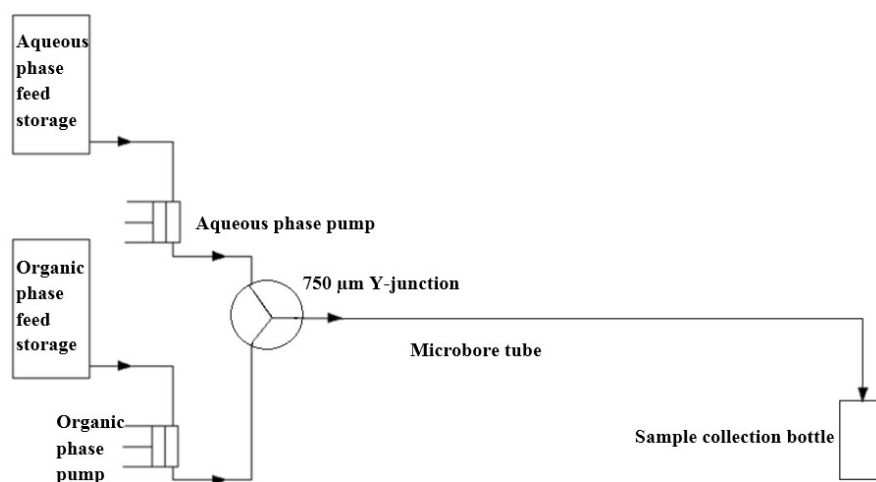


Figure 2.2: Schematic diagram of experimental setup for experiments with single microbore tubes

Glass sample bottle allows visual observation of settling behavior of the dispersion. The aqueous and organic phases are pumped at the desired flow rates by a dual channel syringe pump (Model ASP-3.0, Syrris Ltd. UK).

In this chapter, the focus is on finding an optimum configuration (flow rate, diameter and length of microbore tube) which can provide high stage efficiency with low pressure drop and quick settling.

2.2.2 Phases used in the experiments

The aqueous phase is 3 M nitric acid and the organic phase is 30% (v/v) TBP in dodecane. Demineralized water and organic phases are equilibrated with each other to minimize mass transfer due to mutual solubility. Solute (nitric acid) is added to the equilibrated demineralized water to prepare the feed. The system is chosen for its relevance in nuclear fuel cycle wherein solvent extraction is often performed in nitrate media (Darekar et al., 2014c; Desigan et al., 2012; Hotokezaka et al., 2005; Kumar et al., 2012). Physical properties of the phases are given in Table 2.1 (Sen et al., 2014, Roy et al., 2018). The aqueous samples are analyzed for nitric acid concentration using acid base titration using 1 N NaOH solution.

Table 2.1: Physical properties of the phases

Phase	Density (kg/m ³)	Viscosity (cP)	Interfacial Tension (mN/m)
Organic phase	810	1.800	10.99
Aqueous phase	1098	1.142	

2.2.3 Calculations

Eqs. (2.1-2.9) are used to quantify the experimental results. Eq. (2.1) is used to calculate percentage stage efficiency ($\% \eta$), Eq. (2.2) for calculating percentage extraction (PE), Eq. (2.3) for evaluating SER_M (Specific Extraction Rate in Mixer). SER represents the number of moles of solute extracted per unit time per unit volume of the contactor and is thus a measure of process intensification. If the same amount of solute is extracted in shorter contact time and with smaller contactor volume, SER will be high which will indicate process intensification. Comparison based on SER is similar to the comparison of microreactor and macroreactor based on space time yield (Sen et al., 2013; Takebayashia et al., 2012). Eq. (2.4) is used for evaluating SER_{MS} (Specific Extraction Rate in Mixer and Settler). Unlike SER_M , SER_{MS} accounts the inventory locked in settler also.

The driving force for mass transfer in general vary from the entrance to the exit of the contactor and hence in a way analogous to log mean temperature difference in a heat exchanger, a log mean concentration difference (LMCD) can be defined by Eq. (2.8). This LMCD is used in Eq. (2.9) to calculate overall volumetric mass transfer coefficient.

$$\% \eta = \frac{C_A^{in} - C_A^{out}}{C_A^{in} - \frac{C_O^{out}}{K_D}} \times 100 \quad (2.1)$$

$$PE = \frac{C_A^{in} - C_A^{out}}{C_A^{in}} \times 100 \quad (2.2)$$

$$SER_M = \frac{(C_A^{in} - C_A^{out})Q_A}{V_{mixer}} \quad (2.3)$$

$$SER_{MS} = \frac{(C_A^{in} - C_A^{out})Q_A}{V_{Total}} \quad (2.4)$$

$$K_D = \frac{C_O^{Eqb}}{C_A^{Eqb}} \quad (2.5)$$

$$C_{A,Eqb}^{in} = \frac{C_O^{in}}{K_D} \quad (2.6)$$

$$C_{A,Eqb}^{out} = \frac{C_O^{out}}{K_D} \quad (2.7)$$

$$\Delta_{LMC} = \frac{(C_A^{in} - C_{A,Eqb}^{in}) - (C_A^{out} - C_{A,Eqb}^{out})}{\ln \left\{ \frac{C_A^{in} - C_{A,Eqb}^{in}}{C_A^{out} - C_{A,Eqb}^{out}} \right\}} \quad (2.8)$$

$$K_L a = \frac{C_A^{in} - C_A^{out}}{\frac{V_{mixer}}{Q_A} \Delta_{LMC}} \quad (2.9)$$

2.2.4 Experiments for measuring distribution coefficient

Experiments were conducted to find out the distribution coefficient. In these experiments 3M nitric acid and 30% TBP in dodecane are taken in different volume ratios and stirred by using a magnetic stirrer for 30 minutes. The phases are disengaged and concentration of nitric acid is measured to estimate the distribution coefficient. The distribution coefficient defined as the ratio of nitric acid concentration in the organic phase to nitric acid concentration in the aqueous phase at equilibrium is found to vary as shown in [Table 2.2](#). The variation of K_D indicates that the distribution coefficient value is not constant over the range of aqueous and organic concentration concerned. In this chapter extraction of nitric acid is studied and extraction of uranium is studied in subsequent chapters. Distribution coefficient values for uranium are reported in subsequent chapters.

Table 2.2: Distribution coefficient of nitric acid

$C_{O,Batch}^{Eqb}$ (ppm)	$C_{A,Batch}^{Eqb}$ (ppm)	K_D
0.48	2.76	0.17
0.47	2.53	0.19
0.43	2.14	0.20

2.3 RESULTS AND DISCUSSION

The parameters that affect performance of a microbore tube for solvent extraction are tube diameter, length and flow rates of the aqueous and organic phases. All these parameters affect the performance by affecting the quality of dispersion, film coefficients and pressure drop. Here the performance for solvent extraction has a larger connotation and goes beyond the extraction of the desired species from one phase to another. Though extraction is definitely the first requirement, it must be achieved in such a way that subsequent phase disengagement must be quick otherwise much of the solvent inventory will lock in the settler nullifying the minimization of the inventory achieved in the microbore tube. Another parameter to keep under check is the pressure drop. A very long tube can ensure very high stage efficiency but at the cost of excessive pressure drop. Thus finding an appropriate or optimum configuration of a microbore tube contactor is not trivial as the configuration must meet the three requirements – high stage efficiency, quick settling of resulting dispersion and low pressure drop. Experiments with single microbore tubes were focused on finding this optimum configuration. To identify the optimum configuration, experiments were carried out sequentially to quantify the effect of each relevant parameter on stage efficiency, settling behavior of resulting dispersion, and pressure drop.

Before conducting actual experiments, repeatability of experimental data was ascertained. For this experiments were carried out in 800 μm microbore tubes of three different lengths. Experiments were conducted twice. Fig. 2.3 shows the repeatability of the experimental data by comparing percentage efficiency obtained in the two sets of experiments. Error bars in Fig. 2.3 are $\pm 10\%$ error bars. Fig. 2.3 thus leads us to conclude that experimental results are repeatable.

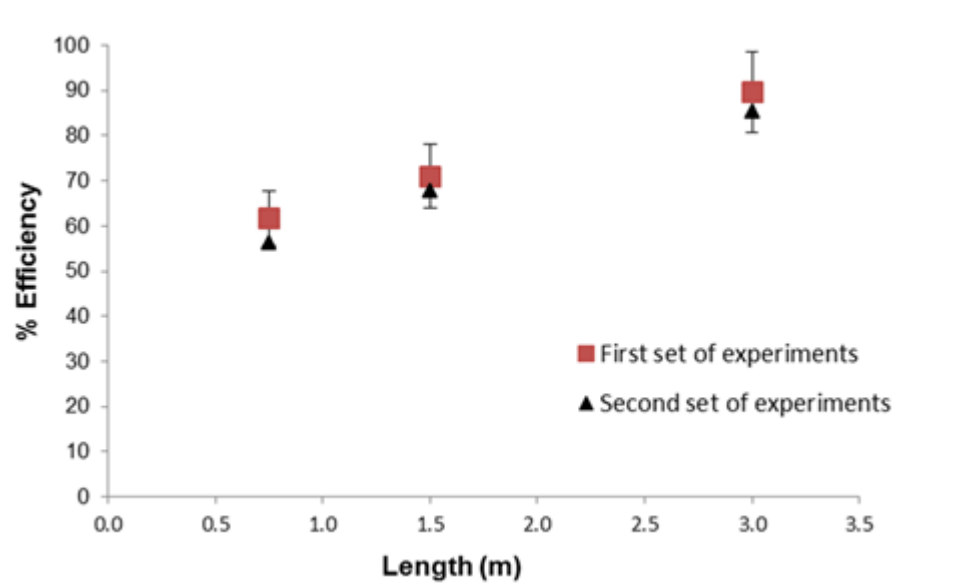


Figure 2.3: Repeatability of experimental results

(750 μm Y-junction, $D_T = 800 \mu\text{m}$, $O/A = 1/1$, $Q = 0.5 \text{ LPH}$)

2.3.1 Effect of flow rate

Here we qualitatively define three types of settling behavior. The first is instantaneous settling in which dispersion, when collected in 1 inch diameter sample bottle, separates very fast and the dispersion band, if at all present, consists of a single layer of droplets. The second is quick settling in which the settling time of the dispersion in a 1 inch diameter sample bottle is less than 1 min. The third type of settling behavior is slow settling in which settling time in a 1 inch diameter sample bottle is more than a minute or both the phases are hazy and the haze takes very long time to disappear.

The first set of experiments was carried out to decide the maximum flow rate a single microbore tube can handle while giving quick phase separation. Microbore tubes of three different diameters (300 μm , 500 μm and 800 μm) were available. Of these, the microbore tube with the largest diameter was chosen for finding the maximum flow rate a single microbore tube can handle at $O/A=1/1$. This is because the maximum flow rate a microbore tube can handle with quick settling is likely to reduce with reduction in tube diameter. For a given flow rate, with reduction in microbore tube diameter the velocities will increase causing the dispersion to become finer and leading to difficulty in settling. Mass transfer was also estimated for different flow rates. Tube length is varied in such a way that the residence time of the liquid inside the microbore tube remains the same for each flow rate so that difference in mass transfer can solely be attributed to the quality of dispersion and film coefficients. It is presumed that mass transfer predominantly takes place in microbore tube. During phase separation the quality of dispersion is much coarser than in a microbore tube. Owing to much larger cross-section of the sample bottle compared to a microbore tube, the velocities during phase separation are much less compared to the velocities in the confined environment of a microbore tube. For these reasons the mass transfer during phase separation is likely to be much less compared to the mass transfer in a microbore tube.

The flow patterns observed in the microbore tube and corresponding settling behavior are shown in [Fig. 2.4](#). As can be seen, for the lowest flow rate i.e. 0.25 LPH long slugs separated by droplets were observed. For this flow pattern, the size of the dispersed phase was large enough to ensure quick phase separation such that no dispersion band is seen in the sample bottle. There were no fines as evident by the clarity of the

aqueous layer and organic layer in the sample bottle. As the flow rate is increased to 0.5 LPH, dispersion becomes finer and the slug and droplet flow changes to droplet flow. A dispersion band is now seen in the sample bottle. For the highest flow rate i.e. 1 LPH, finely dispersed (or thoroughly dispersed) flow was observed. For this flow pattern, no dispersion band is seen immediately in the sample bottle but both the phases are hazy. It takes very long time for the haze to vanish and to get clear aqueous and organic layers.

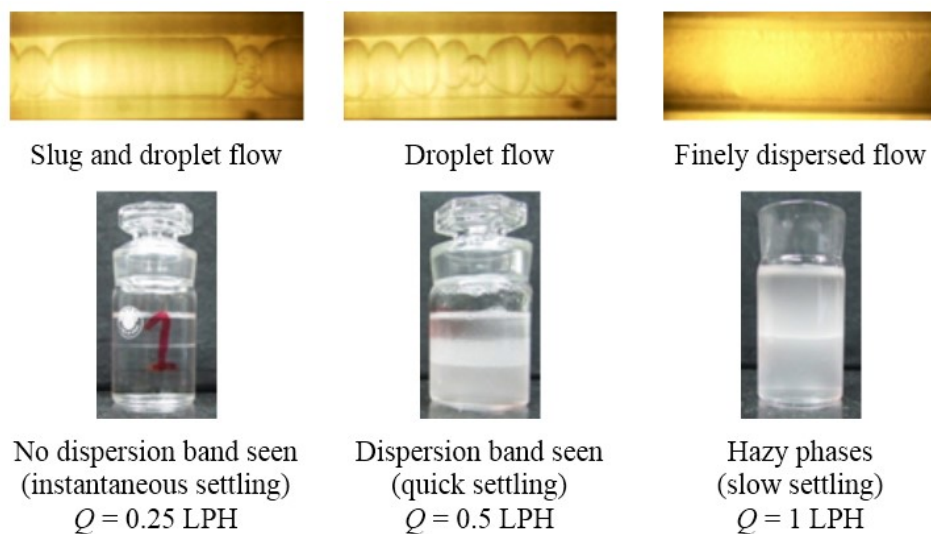


Figure 2.4: Effect of flow rate on flow pattern and settling behavior (750 μm Y-junction, $D_T = 800 \mu\text{m}$, $O/A = 1/1$, $\tau = 1.36 \text{ s}$)

It is concluded that when flow rate is more than 0.5 LPH settling becomes very slow. Therefore 0.5 LPH is considered as the maximum total flow rate a microbore tube of 800 μm diameter can handle. Fig. 2.5 shows the variation of stage efficiency with flow rate. As flow rate increases from 0.25 LPH to 1 LPH, stage efficiency monotonically increases. Increase in stage efficiency can partly be attributed to flow pattern transitions leading to increase in specific interfacial area with increase in flow rate. Increase in stage efficiency with flow rate can also be attributed to increase in film coefficients and hence mass transfer coefficient due to enhanced velocities. Thus

increase in stage efficiency can be attributed to increase in overall volumetric mass transfer coefficient which is product of mass transfer coefficient and specific interfacial area. Fig. 2.6 shows variation of overall volumetric mass transfer coefficient with flow rate and corresponding flow patterns. As can be seen as dispersion becomes finer, overall volumetric mass transfer coefficient increases. If mass transfer alone was the criterion, 1 LPH total throughput in a single microbore tube would have been the obvious choice. Table 2.3 summarizes the results of the experiments carried out to observe the effect of flow rate on mass transfer, settling behavior and pressure drop. As expected, it shows that pressure drop increases with increase in flow rate. Though the highest stage efficiency is obtained at flow rate of 1 LPH, it is not acceptable due to high pressure drop and slow settling. For flow rate of 0.25 LPH settling is quick and pressure drop is also less but stage efficiency is very low and due to this flow rate of 0.25 LPH is also not acceptable. Thus of the three flow rates evaluated, 0.5 LPH is observed to be optimum as it gives faster settling with lower pressure drop and good stage efficiency. Hence 0.5 LPH is concluded to be the maximum flow rate a single microbore tube of 800 μm diameter can handle. Though stage efficiency at 0.5LPH is only about 50% it can be increased by using longer tubes.

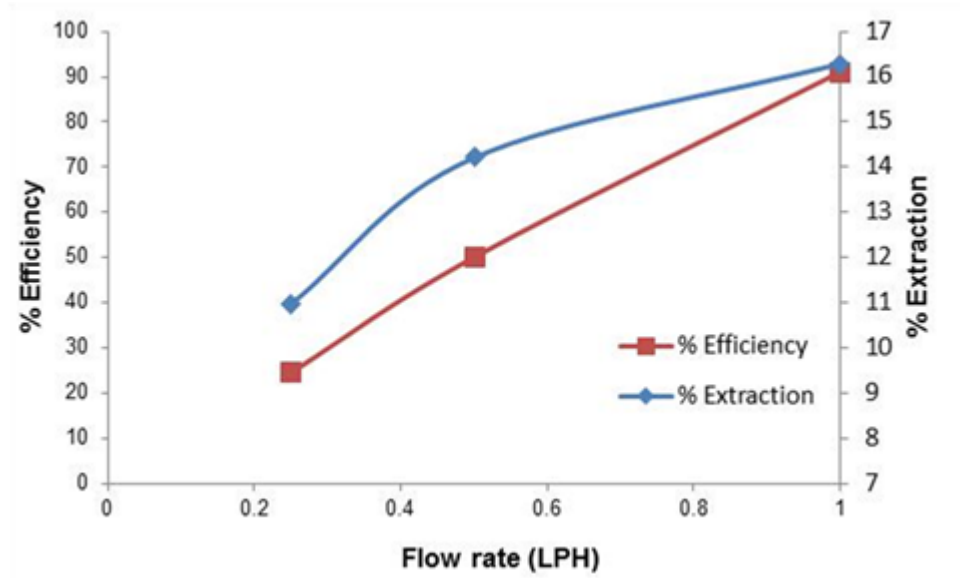


Figure 2.5: Effect of total flow rate on stage efficiency and percentage extraction (750 μm Y-junction, $D_T = 800 \mu\text{m}$, $O/A = 1/1$, $\tau = 1.36 \text{ s}$)

Table 2.3: Effect of flow rate on stage efficiency, pressure drop and settling behavior in microbore tube (750 μm Y-junction, $D_T = 800 \mu\text{m}$, $O/A = 1/1$, $\tau = 1.36 \text{ s}$)

$L_T(\text{cm})$	Q (LPH)	$\% \eta$	PE	ΔP (bar)	Settling	Acceptability
75	1	91	16	< 4	Slow	X
37.5	0.5	50	14	< 1	Quick	√
19	0.25	25	11	< 1	Instantaneous	X

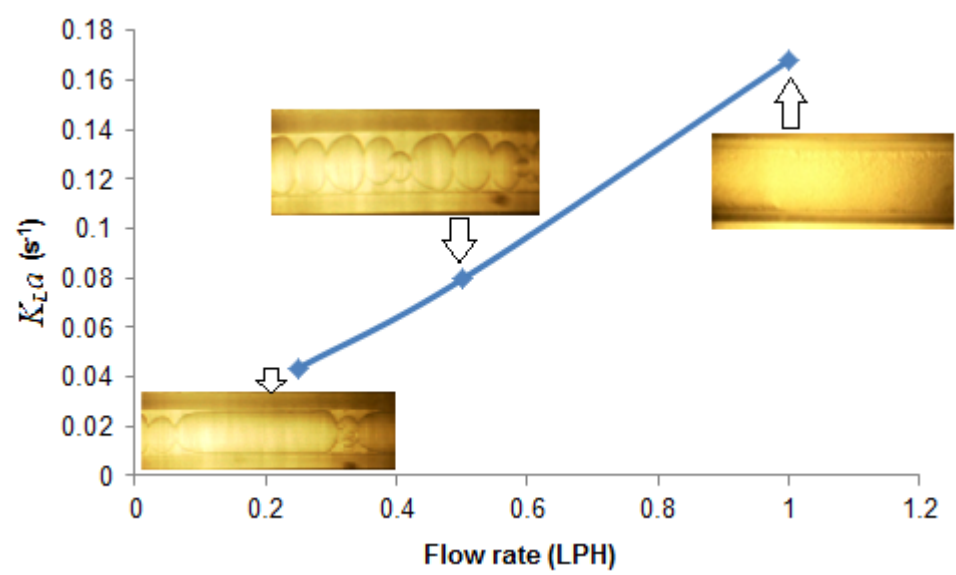


Figure 2.6: Effect of flow rate on overall volumetric mass transfer coefficient (750 μm Y-junction, $D_T = 800 \mu\text{m}$, $O/A = 1/1$, $\tau = 1.36 \text{ s}$)

2.3.2 Effect microbore tube diameter

For a given flow rate the dispersion is expected to become finer with reduction in tube diameter. Whether it becomes fine enough to cause settling problem is, however, difficult to predict without conducting experiments. Therefore, further experiments were carried out to ascertain if the maximum flow rate handled by the microbore tube of the largest available diameter ($D_T = 800 \mu\text{m}$) can also be handled by the microbore tubes of smaller diameters while still giving fast settling and low pressure drop. Experiments were conducted with 0.5 LPH total flow rate in microbore tubes of different diameters. Lengths of the tubes were different to keep the residence time same in order to attribute the difference in mass transfer solely to microbore tube diameter. Fig. 2.7 shows the variation of percentage efficiency and percentage extraction with microbore tube diameter. Fig. 2.8 shows the effect of microbore tube diameter on overall volumetric mass transfer coefficients. As expected, stage

efficiency, percentage extraction and overall volumetric mass transfer coefficient are found to increase with reduction in microbore tube diameter.

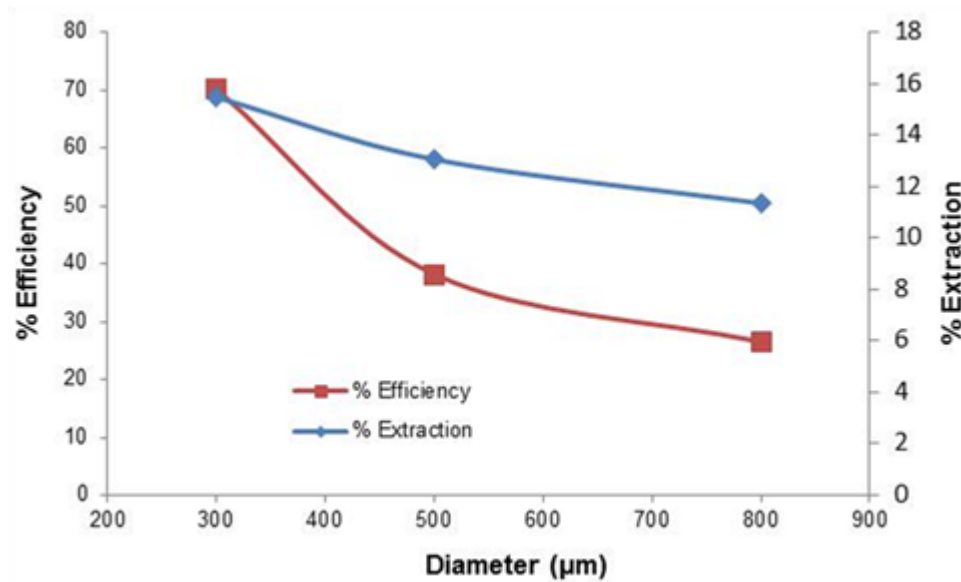


Figure 2.7: Effect of diameter of microbore tube on stage efficiency and percentage extraction(750 μm Y-junction, $O/A = 1/1$, $Q = 0.5$ LPH, $\tau = 0.45$ s)

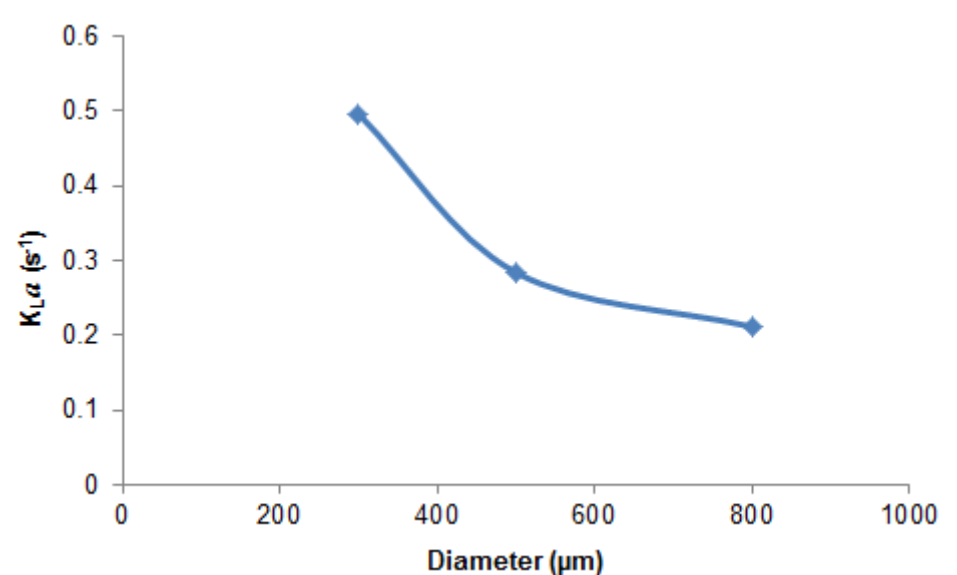


Figure 2.8: Effect of diameter of microbore tube on overall volumetric mass transfer coefficient(750 μm Y-junction, $O/A = 1/1$, $Q = 0.5$ LPH, $\tau = 0.45$ s)

Table 2.4 compiles the data obtained from the experiments with microbore tubes of different diameters. It shows that pressure drop is very high and settling is slow for 300 μm microbore tube. For these reasons, 300 μm microbore tube cannot be used despite of it giving the highest stage efficiency. Though the settling of the dispersion generated in 500 μm microbore tube is fast, pressure drop is more than 2 bar, the maximum admissible limit set by us. Thus of the three tube diameters 800 μm is found to be the one giving high throughput with quick settling and acceptable pressure drop.

Table 2.4: Effect of tube diameter on stage efficiency, pressure drop and settling behavior(750 μm Y-junction, $O/A = 1/1$, $Q = 0.5$ LPH, $\tau = 0.45$ s)

$D_T(\mu\text{m})$	$L_T(\text{cm})$	$\% \eta$	PE	ΔP (bar)	Settling	Acceptability
300	89	70	15.46	< 16	Slow	x
500	32	38	13.05	< 6	Quick	x
800	12.5	27	11.34	< 1	Quick	√

2.3.3 Effect of microbore tube length

Though 800 μm microbore tube is found to handle a flow rate of 0.5 LPH with quick settling and low pressure drop, stage efficiency observed is low. Further experiments were carried out to find out to what extent stage efficiency can be improved by increasing the length without breaching the upper limit on the pressure drop. Changing of contact time by changing length of microbore tube ensures that the quality of dispersion remains the same and thus settling is not affected due to change in length. Even if the flow pattern changes on changing the tube length it will be due to possible coalescence of slugs and drop in the region far away from the junction. But such coalescence events, if any, will enhance the size leading to better settling. Thus

increasing tube length is not expected to affect the settling behavior adversely. The only adverse effect of increasing tube length can be increased pressure drop. Fig. 2.9 shows the effect of length of microbore tube on mass transfer. As can be observed and as expected, stage efficiency increases with increase in tube length.

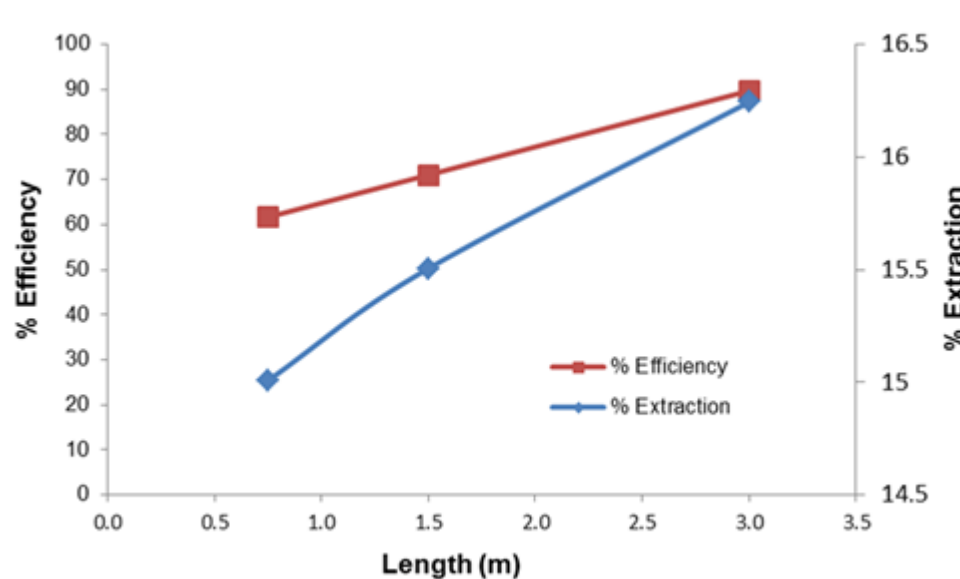


Figure 2.9: Effect of tube length on stage efficiency and percentage extraction (750 μm Y-junction, $D_T = 800 \mu\text{m}$, $O/A = 1/1$, $Q = 0.5 \text{ LPH}$)

Fig. 2.10 shows the dispersion quality inside microbore tube near the outlet for different length of tubes. It can be seen that dispersion at a distance of about 75 cm from the junction is slightly finer than the dispersion at 150 cm and 300 cm distance. Thus in a longer tube there appears to be some coalescence. Table 2.5 compiles the data resulting from this set of experiments and shows that settling continues to remain fast if flow rate is maintained constant and length of microbore tube is increased. Stage efficiency increases with increase in the length of microbore tube. Pressure drop continues to remain less than 2 bar for all the lengths explored. Thus the optimum configuration giving high stage efficiency, quick settling and low pressure drop consists of a 300 cm long microbore tube of diameter 800 μm connected to a Y-

junction of 750 μm diameter. The maximum capacity of the configuration is 0.5 LPH and stage efficiency obtained at $O/A = 1/1$ is 90% in contact time of about 10.85 s.

Table 2.5: Effect of tube length on stage efficiency, pressure drop and settling behavior(750 μm Y-junction, $D_T = 800 \mu\text{m}$, $O/A = 1/1$, $Q = 0.5$ LPH)

L_T (cm)	τ (s)	% η	PE	ΔP (bar)	Settling	Acceptability
75	2.71	62	15.01	< 1	Quick	X
150	5.42	71	15.50	< 2	Quick	X
300	10.85	90	16.24	< 2	Quick	√



Slug and droplet flow
 $L_T=75$ cm



Slug and droplet flow
 $L_T=150$ cm



Slug and droplet flow
 $L_T=300$ cm

Figure 2.10: Quality of dispersion at end of different length microbore tube
(750 μm Y-junction, $D_T = 800 \mu\text{m}$, $O/A = 1/1$, $Q = 0.5$ LPH)

2.4 METHODOLOGY FOR IDENTIFYING AN OPTIMUM CONFIGURATION OF SINGLE MICROBORE TUBES

Based on the experience gained in this study, a methodology to find out an optimum configuration for micro-scale extraction using microbore tubes is proposed. The methodology, in the form of an algorithm, is shown in Fig 2.11. Initially, one should list down all the available microbore tube diameters (D_1, D_2, \dots, D_{max}), the desired total throughput (Q_T) and O/A ratio. Maximum permissible pressure drop, a small length (L_{min} , about 10 cm or so) of each tube diameter one is able to spare should also

be decided. To begin with, number of tubes to be used in parallel (N_T) is selected to be 1. Then microbore tube of maximum diameter is selected. For $N_T = 1$, the flow rate handled by each microbore tube (Q) works out to be equal to the total flow rate. Experiment is conducted and settling of the dispersion generated in the microbore tube is observed. If settling is found to be satisfactory, one moves further as shown in [Fig. 2.11](#). If settling is found to be unsatisfactory, number of tubes to be used in parallel is increased by one and then one repeat this cycle to check, if by increasing the number of tubes in parallel and hence by reducing the flow rate handled by a single tube, satisfactory settling is achieved. Thus one moves further only when satisfactory settling is achieved in the microbore tube of maximum available diameter. The number of tubes to be used in parallel to handle the desired total flow rate is also known when one comes out of this cycle. Next cycle is basically to check if the microbore tubes having smaller diameters are also able to handle the flow rate handled by the microbore tube of maximum diameter. This check is done by starting with the microbore tube having diameter just smaller than the maximum diameter. If this microbore tube fails, further lower diameter need not be tried and one repeats the cycle. If microbore tube having second maximum diameter is also able to handle the flow rate handled by the maximum diameter tube, next smaller diameter tube is tried by going back to cycle. When one comes out of this cycle, one knows the maximum diameter which is not able to handle the flow rate handled by the largest diameter tube. The microbore tube to be used is the one which is having diameter just more than this diameter. In next cycle, one check if the pressure drop in the microbore tube is less than the permissible pressure drop and the stage efficiency is enough. If stage efficiency can be increased further, the length of the microbore tube is increased and

then one repeats the cycle. One comes out of the cycle when either stage efficiency cannot be further increased by increasing length or pressure drop does not allow for further increase in length. If one has moved of the cycle due to limitation of pressure drop, the length of the microbore tube is adjusted. Finally the configuration that can be used to ensure micro-scale extraction while giving satisfactory settling, low pressure drop and maximum possible stage efficiency is summarized.

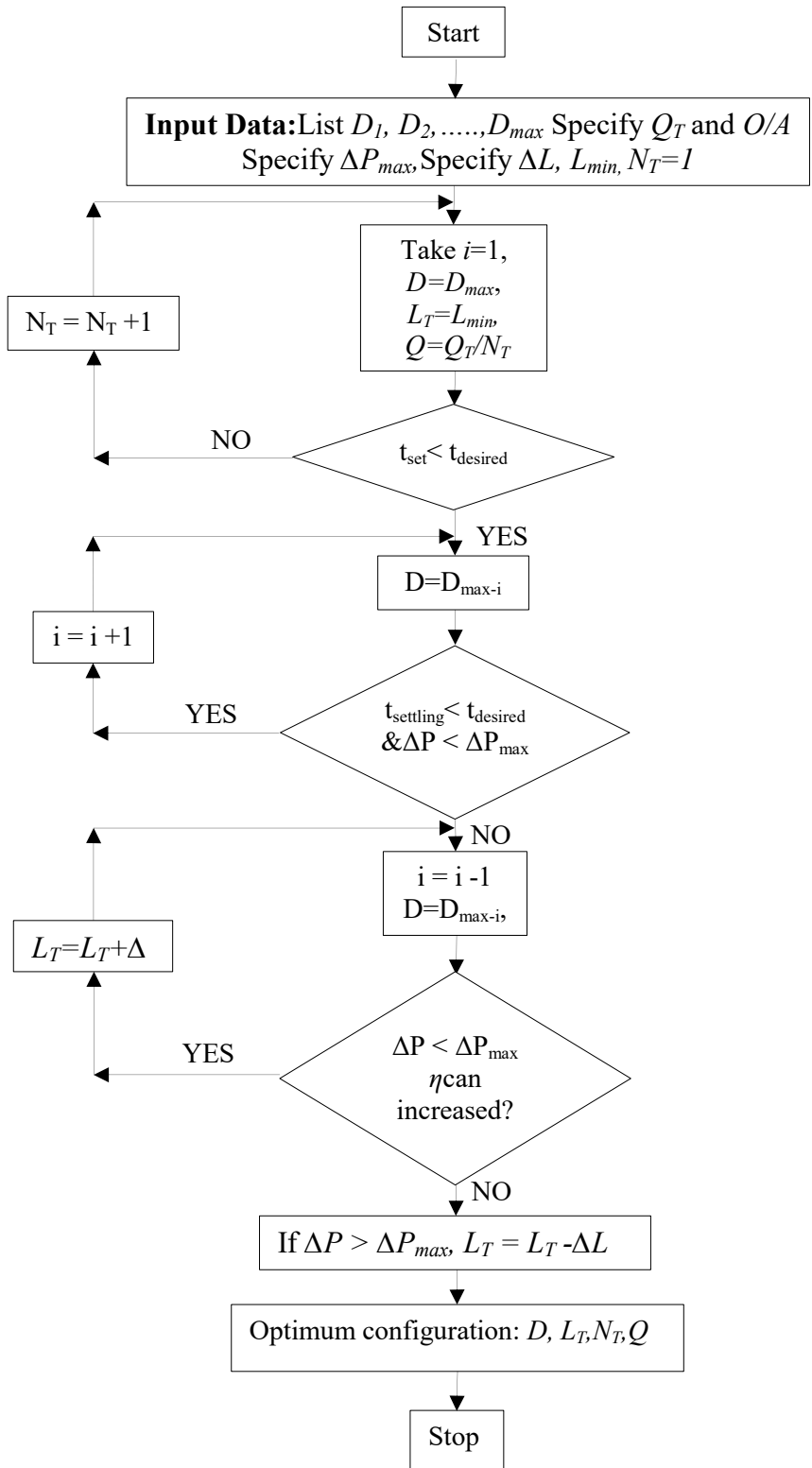


Figure 2.11: Methodology for identifying an optimum configuration for extraction in parallel microbore tubes

2.5 COMPARISON OF MICROBORE TUBE CONTACTOR WITH A MIXER-SETTLER

Table 2.6 shows the comparison of the microbore tube contactor based on microbore tubes with a mixer-settler. In Table 2.6 the data used for the microbore tube contactor are the data of the experiment conducted in single microbore tube at 0.5 LPH total throughput with $O/A = 1$ in which stage efficiency is observed to be about 90%. In this experiment nitric acid concentration in the aqueous phase is brought down from 3 M to 2.51 M. The extraction in microbore tube is very fast and takes place in contact time of about 11 seconds due to which the inventory of liquid inside the microbore tubes is very small as compared to a mixer-settler. Values used for the mixer-settler are taken from the data provided in a study on recovery of nitric acid from waste etching solution by solvent extraction using TBP (Shin et al., 2009). The authors carried out batch experiments, recommend the optimum conditions for extraction, scrubbing and stripping for continuous operation and performed pilot plant test run. Volumes of mixer, settler and feed flow rates used in Table 2.6 are the same as used by Shin et al. (2009) in their pilot test runs. O/A used by them is 3:1 and TBP is used without dilution. The feed concentration is taken as 8.143 mol/l (513 gm/l), same as used by Shin et al. (2009) in the batch experiments. A single-stage extraction is considered in which 74% extraction is considered for $O/A=3/1$ assuming percent extraction in a single-stage continuous run is the same as in a single-stage batch contact. As can be seen from Table 2.6, specific extraction rate (SER) in the microbore tube contactor is about 4 times of the same estimated for a mixer-settler. This indeed shows the scope of process intensification when microbore tube contactor is used for solvent extraction. If the comparison is done on the basis of SER per unit

power input, the microbore tube contactor turns out to be about 20 times better than the mixer-settler. For calculation of SER per unit power input for the mixer, a typical value of specific power input employed in continuous flow stirred tanks ($\sim 1000 \text{ W/m}^3$) has been used (Singh et al., 2008). It may be noted that in this comparison the data used for the mixer-settler are for $O/A = 3/1$ and 100% TBP whereas for the microbore tube contactor the data is for $O/A = 1/1$ and 30% TBP in dodecane. It is expected that for the same O/A ratio and same TBP concentration, SER for the microbore tube contactor will be still more.

Ideally the comparison of two solvent extraction contactors should be done using the same phase system (Singh et al., 2015). However, the data on extraction of nitric acid using 30% TBP in dodecane in mixer-settler is not available to the best of our knowledge. Thus the data of the mixer-settler used in the comparison shown in Table 2.6 is based on 100% TBP whereas the data of the microbore tube based contactor is for 30% TBP in dodecane. Since the percentage extraction for 30% TBP in dodecane is lower than 100% TBP (Shin et al., 2009), it is reasonable to expect that microbore tube based contactor will look still more promising compared to a mixer-settler using 30% TBP in dodecane.

In this study we have focused on single stage-extraction. However, to ensure high percentage extraction from the aqueous stream, a multi-stage cascade is indispensable especially for the systems having distribution coefficients much less than 1. Hence in near future we plan to work on and demonstrate a multi-stage cascade based on microbore tubes. The data resulting from such a cascade will help us rigorously quantify the process intensification achieved by using a cascade based on microbore tubes vis-à-vis a cascade based on conventional multi-stage extractors.

Table 2.6: Comparison of microbore tube contactor with a mixer-settler

	Microbore tube contactor (MTC)		Mixer-settler (MS)	
	Basis	Value	Basis	Value
C_A^{in} (mol lit ⁻¹)	Experiment	3	Shin et al., 2009	8.143
C_A^{out} (mol lit ⁻¹)	Experiment	2.51	Shin et al., 2009	2.12
Q (LPH)	Experiment	0.5	Shin et al., 2009	2.4
Q_A (LPH)	Experiment	0.25	Shin et al., 2009	0.6
τ (s)	Experiment	10.85	Shin et al., 2009	225
V_{mixer} (ml)	$V_{mixer} = \tau \times Q$	3.01	Shin et al., 2009	150
$V_{settler}$ (ml)	Experiment	7.5	Shin et al., 2009	900
V_{Total} (ml)	$V_{Total} = V_{mixer} + V_{settler}$	18.01	$V_{Total} = V_{mixer} + V_{settler}$	1050
SER _M (moles s ⁻¹ m ⁻³)	Eq.(2.3)	22.58	Eq.(2.3)	6.69
SER _{MS} (moles s ⁻¹ m ⁻³)	Eq.(2.4)	3.78	Eq.(2.4)	0.96
ΔP (Pa)	Experiment	200000	-	-
P (W)	$P = \Delta P \times Q$	0.028	$P = 1000(W m^{-3}) \times V_{mixer}$	0.15
SER _{MS} per unit power input (moles s ⁻¹ m ⁻³ W ⁻¹)	SER _{MS} / P	136.00	SER _{MS} / P	6.37

2.6 CONCLUSIONS

Extraction of HNO₃ from 3 M nitric acid solution using 30% TBP in dodecane as the organic phase is carried out using microbore tubes. In the first set of experiments single microbore tubes are used to identify an optimum configuration that can ensure high stage efficiency in short contact time with low pressure drop and quick phase

separation. This optimum configuration consists of a 750 μm Y-junction having microbore tube of diameter 800 μm and length 300 cm on its downstream side. This configuration can handle a total throughput of 0.5 LPH and provides 90% stage efficiency in contact time of about 11 s. In the second set of experiments, the optimum configuration is replicated in two parallel paths to demonstrate solvent extraction at total capacity of 1 LPH. Specific extraction rate in the contactor based on microbore tubes is estimated to be about 4 times of the same in a mixer-settler. Specific extraction rate per unit power input in the contactor based on microbore tubes is estimated to be about 10 times of the same estimated for a mixer-settler. The study highlights the prospect of process intensification and ease of scale-up by following numbering up approach.

In this study the focus is on intensification of mass transfer by using microbore tubes. Intensification of phase separation is also possible e.g. by using membrane separation or by using centrifugation. If intensification of phase separation is combined with intensification of mass transfer, solvent extraction in contactors based on microbore tubes is expected to be all the more attractive.

CHAPTER 3

EFFECT OF FLOW PATTERN AND LAYOUT OF MICROCHANNEL ON MASS TRANSFER AND SETTLING BEHAVIOR

3.1 INTRODUCTION

Though microchannels can be made in materials such as glass, metals, polymers etc. the microbore tubes, available commercially, are probably the cheapest microchannels that can be used for solvent extraction at room temperature and moderate pressures. Solvent extraction in a microbore tube is carried out by contacting an aqueous phase with an organic phase at a microfluidic junction which precedes a microbore tube and acts as the dispersing device. The microbore tube then provides the required residence time for mass transfer. Depending on the geometry of the microfluidic junction, physical properties of the two liquid phases and flow rates, the contact of the immiscible aqueous and organic phases at the microfluidic junction may lead to a variety of liquid-liquid two-phase flow patterns. The type of flow pattern generated at the microfluidic junction directly influences the rate of mass transfer by affecting specific interfacial area for mass transfer. Therefore, the effect of flow pattern on mass transfer need to be understood, which is studied in this chapter.

The length of microbore tubes can be changed to provide the required contact time. But microbore tubes need to be coiled if the required length is long. Coiling it in the form of a helix on a cylindrical surface is the simplest way of coiling a long microbore tube. However, the diameter of coil can affect the flow pattern and mass transfer

inside the coiled microbore tube. Therefore, understanding the effect of coiling on mass transfer is necessary, which is also the part of this chapter.

The advantages of micro-scale solvent extraction have motivated researchers to explore the possibility of using it for solvent extraction of uranium. Most of these studies focus only on mass transfer. In continuous operation settling of dispersion always follows mass transfer and can often become a bottleneck. Therefore, understanding the settling of dispersion generated in micro-scale extraction is equally important.

3.2 EXPERIMENTAL

3.2.1 Setup

The schematic diagram of the experimental setup is shown in [Fig. 3.1](#). The aqueous and organic phases are pumped at the desired flow rates by a two-channel syringe pump. Microbore tube made of PTFE having 800 μm ID has been used in the experiments. The aqueous and the organic phases are fed to the microbore tube through an opposed T-junction of 400 μm ID. This microfluidic junction serves as the dispersing device. The straight microbore tube is placed on a horizontal surface with a high-speed image acquisition camera and microscope mounted on the top of it. If not straight, the microbore tube is coiled on a cylindrical surface. The magnified microbore tube can be seen on the computer screen in real time. The camera is set to capture video at the rate of 50 to 200 fps. The images are stored in the computer memory for further analysis.

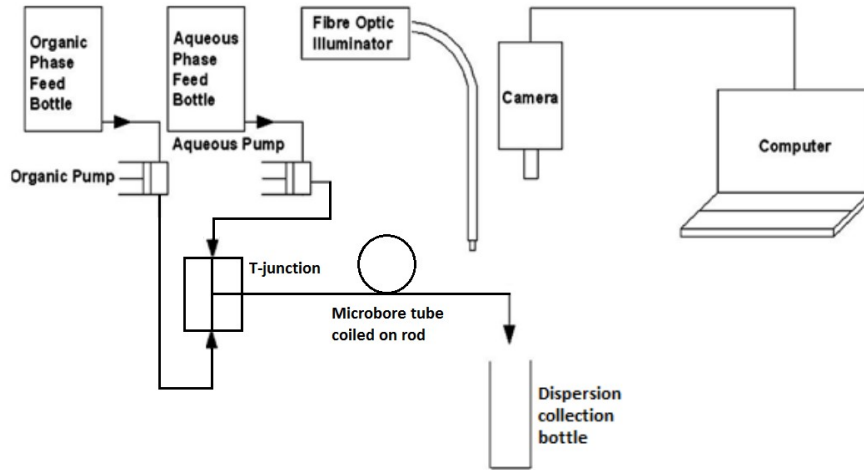


Figure 3.1: Schematic diagram of the experimental setup

3.2.2 Phases used in the experiments

Extraction of uranium from aqueous phase containing 550 ppm uranium in 1M HNO₃ is carried out by the organic phase consisting 30% (v/v) TBP in dodecane. The phases are chosen for their relevance to nuclear fuel cycle.

3.2.3 Calculations

Following equation is used to quantify the experimental results:

$$SRV = \frac{Q_D}{A_S H_D} \quad (3.1)$$

Conventionally settling behavior of liquid-liquid dispersion is quantified in terms of specific settling rate expressed as the ratio of dispersed phase flow rate and settling area. However, giving the value of specific settling rate alone, e.g. 2 (m³/h)/m² does not indicate the dispersion band thickness for which the given specific settling rate is achieved. The same specific settling rate can be achieved by a thin dispersion band which means efficient settling or with a thick dispersion band which means less efficient settling. Thus we define a new parameter which also includes dispersion band

thickness to quantify the settling behavior. This new parameter is settling rate per unit volume of the dispersion and can be abbreviated as SRV. This is nothing but conventionally used specific settling rate divided by dispersion band thickness. In this way the dispersion band thickness is also incorporated in quantification of settling. Eq. (3.1) is used to calculate settling rate per unit volume (SRV) of dispersion band. Q_D is dispersed phase flow rate (m^3/h). A_S is settling area (m^2). H_D is dispersion band height or thickness (m).

3.2.4 Experiments for measuring distribution coefficient

Experiments were conducted to find out the distribution coefficient of uranium. In these studies 550 ppm uranium in 1M HNO and 30% TBP in dodecane are taken in different volume ratios and stirred by using a magnetic stirrer for 30 minutes. The aqueous phase sample is analyzed for uranium concentration using inductively coupled plasma atomic emission spectrometer ICP-AES (Model: ULTIMA-2, Make: Jobin Horiba, France). The distribution coefficient as given in Eq. (2.5) is found to vary as shown in Table 3.1. The variation of K_D indicates that the distribution coefficient value is not constant over the range of aqueous and organic concentration concerned.

Table 3.1: Distribution coefficient of uranium

$C_{O,Batch}^{Eqb}$ (ppm)	$C_{O,Batch}^{Eqb}$ (ppm)	K_D
1180	280	4.2
750	112	6.7
419	29.5	14.2

3.3 RESULT AND DISCUSSION

3.3.1 Effect of flow rate and flow pattern on mass transfer

A change in flow rate for a given microbore tube changes the velocities with which the two liquid phases flow at the microfluidic junction and inside the microbore tube. Therefore, the shear force exerted by the continuous phase on the dispersed phase also changes with a change in flow rate. As a result, coarseness or fineness of the dispersion i.e. the quality of dispersion also changes with a change in flow rate. Thus specific interfacial area for mass transfer is directly influenced by the flow rate. Flow pattern may also change with change in flow rate e.g. slug flow may change to droplet flow. For a microbore tube of a given length, a change in flow rate changes contact time of the phases during which mass transfer occurs. Thus on changing flow rate, mass transfer is influenced both because of change in contact time and change in specific interfacial area. To study the effect of only flow pattern on mass transfer, flow rate is changed such that contact time is kept constant. This is achieved by using microbore tubes of different lengths. On changing flow rate, four different flow patterns - Droplet Flow (DF), Finely Dispersed Flow (FDF), Slug and Droplet Flow (SDF), Slug Flow (SF) – are observed. Fig. 3.2(a) shows the flow pattern (regime) map. In all the experiments aqueous phase is observed to be the dispersed phase. For $O/A = 2/1$ droplet flow and finely dispersed flow are observed indicating that when organic phase (continuous phase) flow rate is twice of the aqueous phase (dispersed phase) flow rate, the resulting dispersion is fine. As O/A reduces to $1/1$, slug flow is also observed along with droplet flow and finely dispersed flow. This shows that the coarseness of dispersion tends to increase when the ratio of continuous phase (organic phase) flow rate to dispersed phase (aqueous phase) flow rate reduces. On further

reduction of O/A to $1/2$, slug flow becomes the dominant flow pattern indicating further increase in the coarseness of the dispersion.

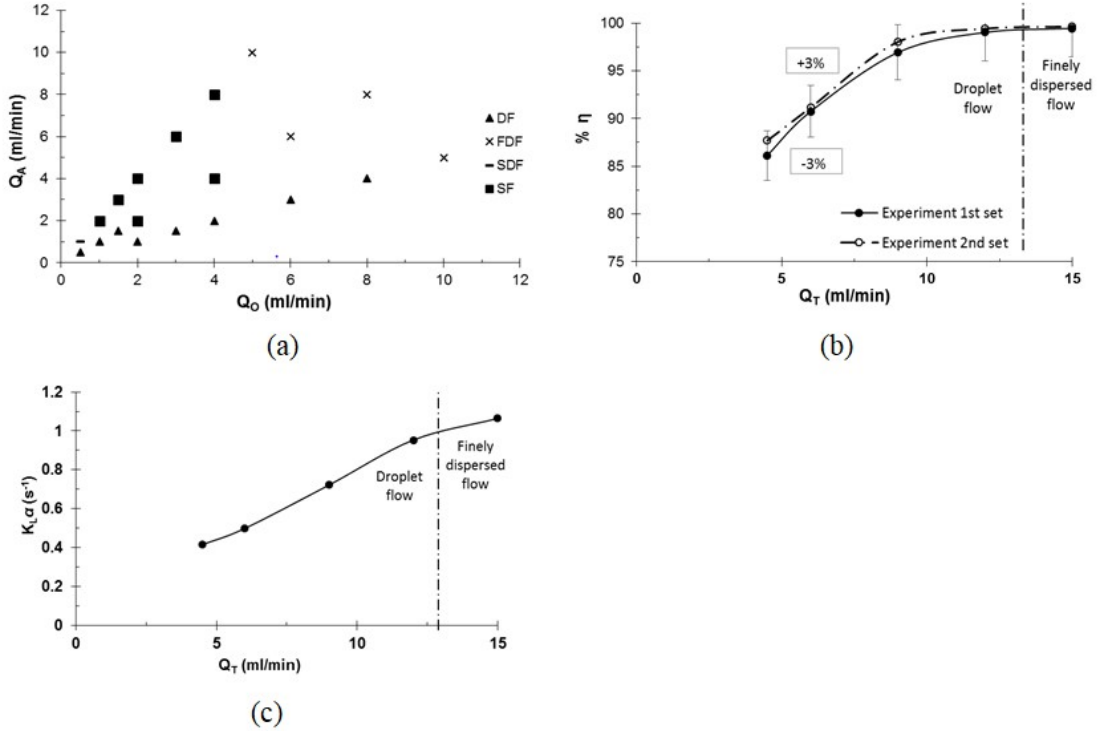


Figure 3.2: Effect of flow rates on (a) aqueous and organic phase on flow pattern flow pattern (b) percentage efficiency ($O/A=2/1$) and (c) overall volumetric mass transfer coefficient ($O/A=2/1$) at a constant residence time ($\tau_m=1.5$ s)

Fig. 3.3 shows flow patterns observed for $O/A = 2$. It can be observed that for the smallest flow rate, bigger drops are formed. As the flow rate increases, the drop size reduces causing specific interfacial area and hence stage efficiency and overall volumetric mass transfer to increase with increase in flow rate, as observed in Fig. 3.2(b) and 3.2(c). Increase in stage efficiency and overall volumetric mass transfer coefficient with increase in flow rate can also be attributed to increase in the value of film coefficients with increase in velocity. One important observation from Fig. 3.2(b) is that close to 100% stage efficiency as given by Eq. (2.1) can be obtained in a microbore tube in a contact time as small as 1.5 sec. A few experiments are repeated

to check repeatability. The results of repeated experiments are within $\pm 3\%$ of first set of experiment results, as shown in Fig. 3.2(b).

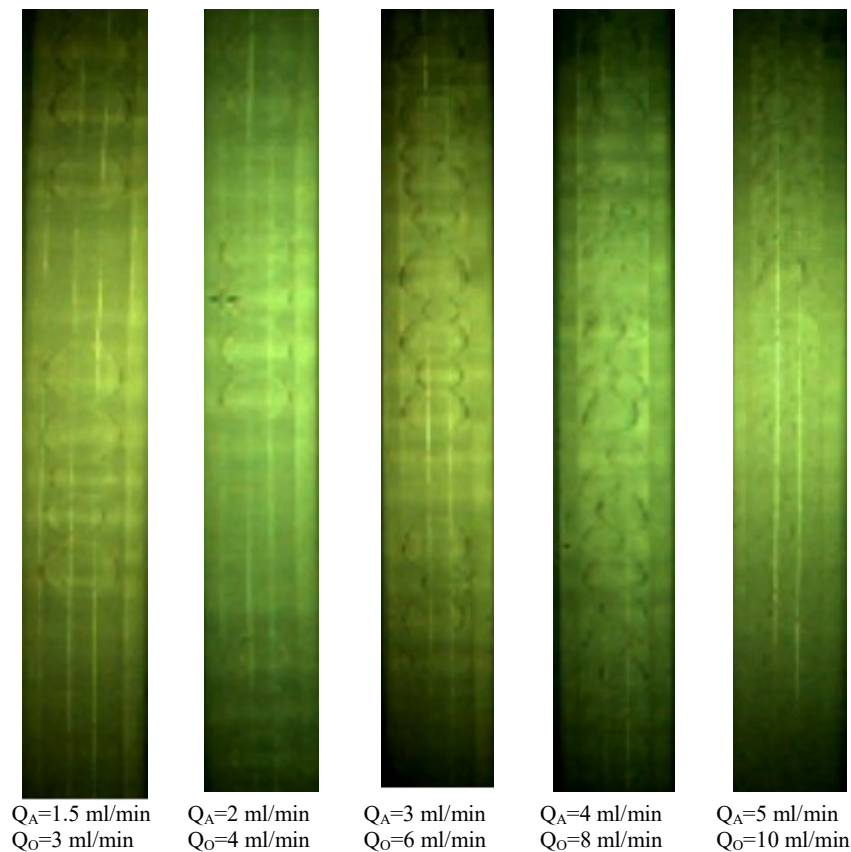


Figure 3.3: Flow patterns at different flow rates of the aqueous and organic phases
(O/A=2/1)

Since flow rate can affect mass transfer by affecting both flow patterns or quality of dispersion and contact time, another set of experiment was conducted to understand whether the change in quality of dispersion or the change in contact time has the dominant effect on mass transfer. For this, experiments were conducted by varying the flow rate but keeping the length of the microbore tube constant and thus varying the quality of dispersion as well as contact time. The results from this set of experiments are shown in Fig. 3.4. Fig. 3.4(a) shows that stage efficiency increases with increase in

flow rate. This can be attributed to increase in specific interfacial area and mass transfer coefficient with increase in flow rate. For a fixed length of the microbore tube, an increase in flow rate reduces residence time which should tend to reduce the overall mass transfer achieved in the microbore tube. The experimental observation, however, shows that stage efficiency increases with increase in flow rate. This implies that increase in specific interfacial area with an increase in flow rate overrides the reduction in residence time with an increase in flow rate. Thus, for the range of our experiments, on increasing the flow rate, the effect of increase in specific interfacial area is found to be more important than reduction in residence time. Overall volumetric mass transfer coefficient also increases with an increase in flow rate as seen in Fig. 3.4(b). This can be attributed to the combined effect of increase in specific interfacial area and increase in mass transfer coefficient due to increase in flow velocity.

Fig. 3.5 shows flow patterns at different total flow rates ($O/A=1/1$). It shows that as the flow rate increases slug size decreases. Comparison of Fig. 3.5 with Fig. 3.3 suggests that dispersion is coarser for $O/A = 1/1$ than for $O/A = 2/1$. This is because aqueous phase is the dispersed phase and hence for $O/A = 1/1$ it offers more resistance to breakup by the organic phase at the microfluidic junction. For $O/A = 1/1$ also, increase in flow rate tends to make dispersion finer by changing longer slugs to smaller slugs. Thus, specific interfacial area increases with flow rate for $O/A = 1/1$ also. Table 3.2 lists the maximum value of overall volumetric mass transfer for different flow patterns. It shows that, among all flow patterns observed in this study, the overall volumetric mass transfer coefficient (0.38 s^{-1}) is the least for slug flow. This is due to less specific interfacial area and low velocities resulting in smaller film coefficients in

slug flow. The dispersed phase flow pattern has the highest overall volumetric mass transfer coefficient (4.01 s^{-1}). This is due to high specific interfacial area and high velocities associated with finely dispersed flow.

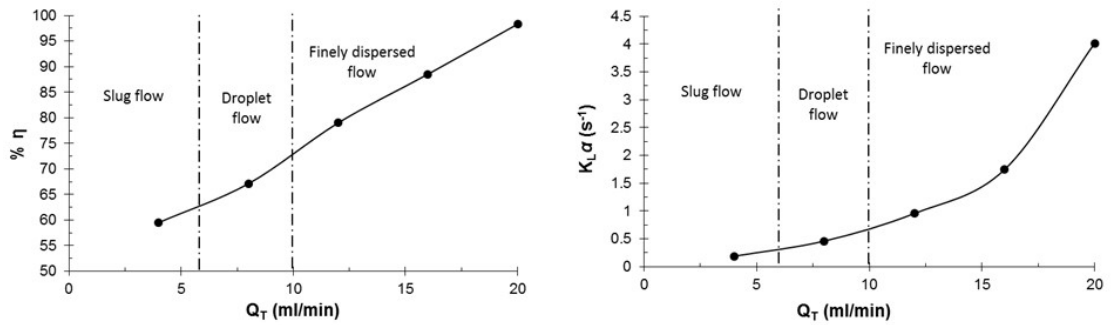


Figure 3.4: Effect of flow rate on (a) stage efficiency and (b) overall volumetric mass transfer coefficient at a constant length of microbore tube ($L= 30 \text{ cm}$, $O/A=1/1$)

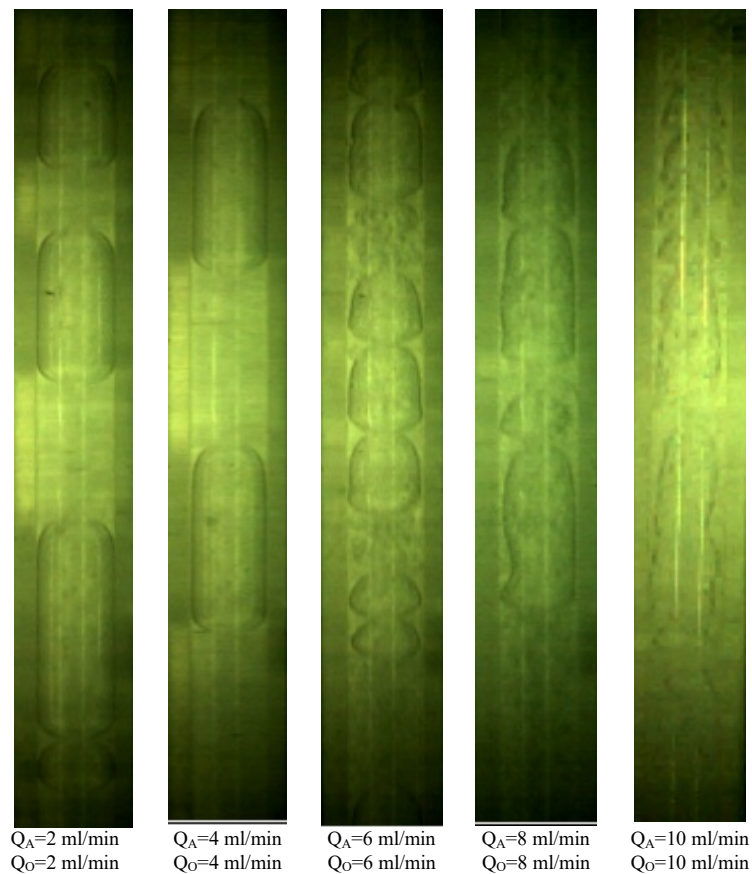


Figure 3.5: Images of flow pattern inside microbore tube at different flow rate of aqueous and organic phase ($O/A=1/1$)

Table 3.3 summarizes the range of overall volumetric mass transfer coefficient for microfluidic solvent extraction of uranium reported in previous studies and in this study. Overall volumetric mass transfer coefficients obtained in the present study are higher than reported in previous studies.

3.3.2 Effect of flow rate and flow pattern on settling

Flow rate affects mass transfer as well as the settling characteristics of the dispersion generated at the microfluidic junction. Fig. 3.6 shows the effect of total flow rate on dispersion band thickness for $O/A = 2/1$ and $1/1$. The dispersion band thickness increases with increase in total flow rate. This is attributed to reduction in drop size with increase in flow rate as smaller drops take longer time to settle. Dispersion band thickness is less for $O/A = 1/1$ than $O/A = 2/1$. The aqueous phase being the dispersed phase, flow rate of the dispersed phase is less for $O/A = 1/1$ than for $O/A = 2/1$. Thus dispersion is coarser for $O/A = 1/1$ and settles faster leading to thinner dispersion band. Table 3.2 lists the maximum value of settling rate per unit volume of dispersion band (SRV) for different flow patterns. It shows that settling is best in slug flow. This is due the large slugs which settle very fast. The finely dispersed flow pattern has the worst settling rate. Thus the flow pattern which gives the best mass transfer results in worst settling and vice versa.

Table 3.2: Overall volumetric mass transfer coefficient and observed SRV for different flow patterns

	SF	SDF	DF	FDF
K_{La} (s^{-1})	0.38	0.90	0.95	4.01
SRV (h^{-1})	118.36	78	74	30.35

Table 3.3: Overall volumetric mass transfer coefficient in different types of microchannels

Reference	Type of microchannel	Phase system	K_{La} (s^{-1})
Present work	T-junction with microbore tube	30% TBP in dodecane (uranium) nitric acid	2×10^{-1} - 4×10^0
Darekar et al., 2014c	T-junction with microbore tube	30% TBP in dodecane (uranium) nitric acid	8.2×10^{-4} - 1.5×10^{-1}
Tsaoulidis et al., 2013a	Cross T-junction and microbore tube	TBP with an ionic liquid (uranium) nitric acid	1.5×10^{-1} - 3.2×10^{-1}

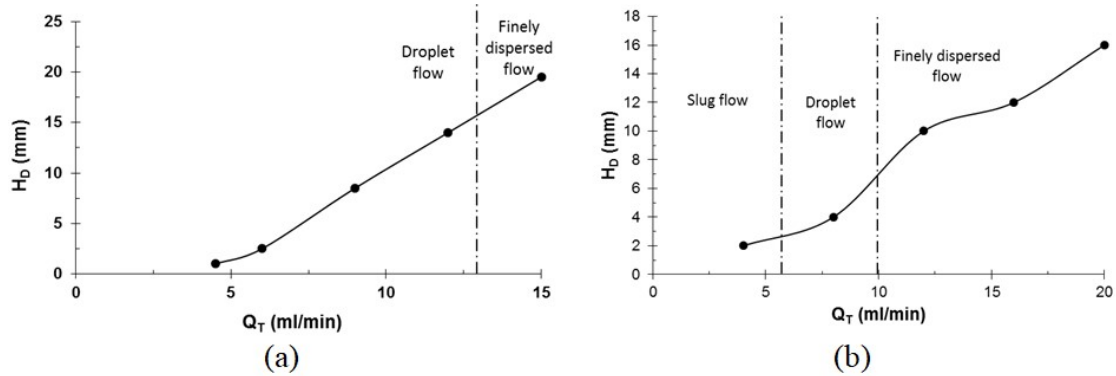


Figure 3.6: Variation of dispersion band thickness with total flow rate for (a) $O/A=2/1$ and (b) $O/A=1/1$

3.3.3 Effect of coiling on mass transfer

As mentioned earlier, a long microbore tube required to ensure sufficient contact time for extraction needs to be coiled to keep the setup compact. However, coiling may affect the quality of dispersion and as a result mass transfer and settling behavior. To study the effect of coiling, experiments were conducted with both straight and coiled microbore tubes of identical length. Fig. 3.7(a) and Fig. 3.7(b) show the effect of flow rate on stage efficiency and overall volumetric mass transfer coefficient for a straight microbore tube and a helically coiled microbore tube of the same length and the same diameter. Microbore tube of 800 μm ID has been used in the experiments. Length of

microbore tube is 30 cm. Microbore tube has coiling radius of 13 mm and pitch is 1.6 mm. As shown in Fig. 3.7(a) and 3.7(b) coiling a microbore tube causes stage efficiency and overall volumetric mass transfer coefficient to increase. Since the diameter and length of the straight and coiled tubes are the same, the change in the performance for mass transfer is solely attributed to coiling. Coiling a tube helically is known to generate secondary flow which leads to enhancement of heat and mass transfer (Mohan et al., 2010; Wu et al., 2014; Moulin et al., 1996, Prabhanjan et al., 2002, Naphon et al., 2006, Naphon et al., 2007).

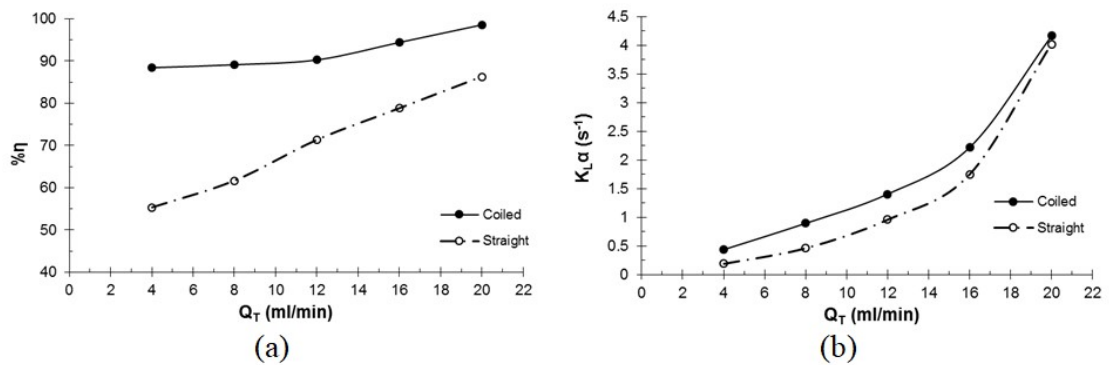


Figure 3.7: Effect of flow rate on (a) stage efficiency and (b) overall volumetric mass transfer coefficient for straight and coiled microbore tube ($O/A=1/1$, $L=30$ cm, $C_R=13$ mm)

Fig. 3.8(a) compares the stage efficiency in straight and coiled microbore tubes of different length for a constant flow rate. Stage efficiency for extraction of uranium is more in coiled microbore tube than in straight microbore tube for all lengths. Stage efficiency increases with increase in length of microbore tube for straight microbore tube as well as coiled microbore tube. Increase in stage efficiency with increase in length can be attributed to increase in residence time with increase in length of the tube. As seen from Fig. 3.8(a), coiling leads to up to 15% increase in stage efficiency.

Effect of coil radius on mass transfer was also studied and the results are shown in Fig. 3.8(b). As shown in Fig. 3.8(b), stage efficiency for extraction of uranium increases with reduction in coiling radius. As the coiling radius decreases, Dean number ($De = Re \sqrt{D_T/2r}$) increases. Dean numbers for coiling radius of 2.5, 4, 5, 8, 16 mm are 42.3, 33.4, 29.9, 23.6, 16.7 respectively. Dean number thus increases with decreasing coiling radius. Jiang et al., 2004 have carried out numerical simulations of helical flow in microchannels. They carried out simulations for $De = 10, 100$ and 200 . $De = 10$ is characterized by a weak secondary flow due to a single vortex with centre of rotation close to the middle of the cross-section of the microchannel. At $De = 100$, the strength of the secondary flow increases significantly, and centre of the vortex shifts towards the outer wall of the microchannel. At $De = 200$, an additional counter-rotating vortex appears which significantly enhances the radial mixing. In the present study, value of De is of the order of 10 and hence secondary flow is expected to be present though it may not be significantly strong. However, the experimental results suggests that, the secondary flow in the coiled microbore tubes, though may not be very strong, is able to break the stratification of concentration field inside the dispersed phase and continuous phase. Smaller is the coil radius, higher will be De and stronger will be the secondary flow and more will be radial mixing and interface stretching. Thus a smaller coiling diameter leads to better mass transfer stage efficiency and $K_L a$. However, pressure drop also increases with reduction in coil radius. This aspect should also be considered while deciding the coil radius.

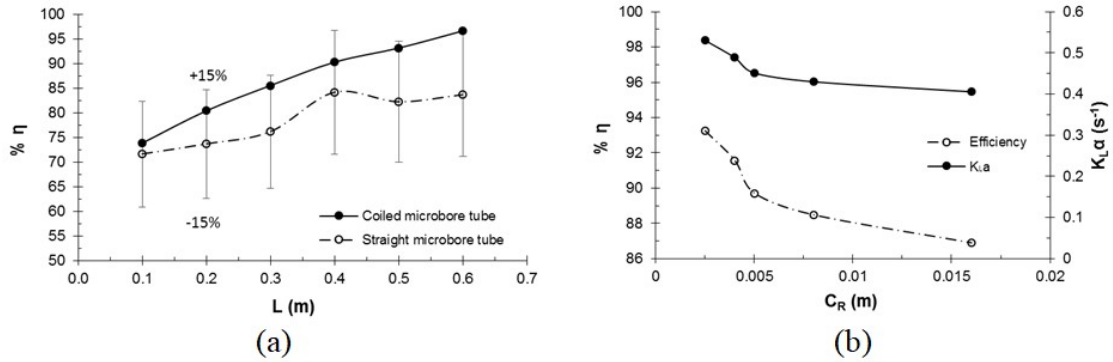


Figure 3.8: (a) Effect of microbore tube length on stage efficiency ($Q_T = 4$ ml/min, $O/A=1/1$, $C_R=5$ mm, $P=1.6$ mm) (b) Effect of coiling radius on mass transfer coefficient and stage efficiency ($Q_T = 4$ ml/min, $O/A=1/1$, $L=60$ cm, $P=1.6$ mm)

3.4 CONCLUSIONS

Micro-scale extraction of uranium from aqueous phase containing 550 ppm uranium in 1M HNO₃ using 30% (v/v) TBP in dodecane is reported. The effects of flow pattern on mass transfer and settling behavior are investigated. Four different liquid-liquid flow patterns - slug flow, slug and droplet flow, droplet flow and finely dispersed flow (FDF) - are observed. Among all observed flow patterns, maximum and minimum value of overall volumetric mass transfer coefficient were observed for finely dispersed flow ($K_L a = 4.01$ s⁻¹) and slug flow ($K_L a = 0.38$ s⁻¹), respectively. Maximum and minimum value of specific settling rate per unit volume of dispersion band were found to be for slug flow ($SRV = 118.36$ h⁻¹) and finely dispersed flow ($SRV = 30.35$ h⁻¹), respectively. Thus the flow patterns which is the best for mass transfer is the worst for settling and vice versa. Experiments conducted by varying the flow rate for constant and varying residence time suggest that the effect of flow pattern on mass transfer is more significant than the effect of residence time on mass transfer. Coiling of a microbore tube was found to increase the stage efficiency and overall volumetric mass transfer coefficient. The effect of coiling on mass transfer became more pronounced as coil diameter was reduced.

CHAPTER 4

STUDIES ON LIQUID-LIQUID TWO PHASE FLOW

PATTERNS IN Y JUNCTION MICROCHANNELS

4.1 INTRODUCTION

Knowledge of the flow pattern expected at a microfluidic junction is important to ascertain whether, for a given design of the junction and flow rates of the two liquid phases, the expected flow pattern is the desired for mass transfer and phase separation or it is not desired. The flow pattern generated at a microfluidic junction, in turn, depends on several parameters such as physical properties of the liquids (density, viscosity, interfacial tension, and wall wettability), flow rates of the liquids, and the diameter and geometry of the microfluidic junction.

This chapter is focused to understand the effects of various parameters that affect the flow pattern generated at Y-type microfluidic junctions. These parameters are physical properties of the liquids (interfacial tension, wall wettability), diameter of the microchannel and operating parameters (flow rates of the aqueous and the organic phases). Since the standard test systems for solvent extraction have already been identified by the EFCE (European Federation of Chemical Engineering) (Misek et al., 1985). In this chapter we have worked with the standard test systems and Y-junction microchannels.

We hope that in the time to come more studies will be carried out on flow patterns in other types of microchannels using the standard test systems and all such studies with standard test systems, put together will lead to a comprehensive database that can be used to predict the flow pattern expected for a given combination of test system and

microchannel without resorting to experiments provided the physical properties specially the interfacial tension of the new test system falls in the range covered by the standard test systems.

4.2 EXPERIMENTAL

4.2.1 Setup

The schematic diagram of the experimental setup is shown in [Fig. 4.1](#). The aqueous and organic phases are pumped to the microchannel etched in a glass chip at the required flow rates by a two-channel syringe pump. The microchannel is placed horizontally on a stand with a high speed camera and microscope mounted on top of it. The magnified microchannel can be seen on the computer screen in real time. The camera is set to capture video at the rate of 100 to 200 fps. The images are stored in the computer memory for further analysis. The liquids coming at the inlets of the microchannel meet at the Y-junction and dispersion is generated. The acquired images are used to determine the flow pattern prevailing inside the microchannel. The observed flow patterns are plotted in the form of flow regime maps. The glass chip having microchannels etched in it is shown in [Fig.4.2](#). The chips are procured from M/s. Dolomite Microfluidics Ltd. UK. Each chip has two microchannels, one with hydrophobic coating and one without hydrophobic coating. To make the channels hydrophobic silane coating is used. The procured microchannels were used as such without any further characterization. A chip holder holds the glass chip. This chip distributor ensures connection of the microchannel with the pump with the help of PTFE tubings of 1/16" OD. The other components of the setup are high speed imaging and illumination system.

Microchannels of two different diameters (260 μm and 760 μm) are used to study the effect of diameter on flow pattern. For each diameter, microchannels with and without hydrophobic coating are used to study the effect of wall wettability on the flow pattern. Silane coating is used to make the microchannel hydrophobic.

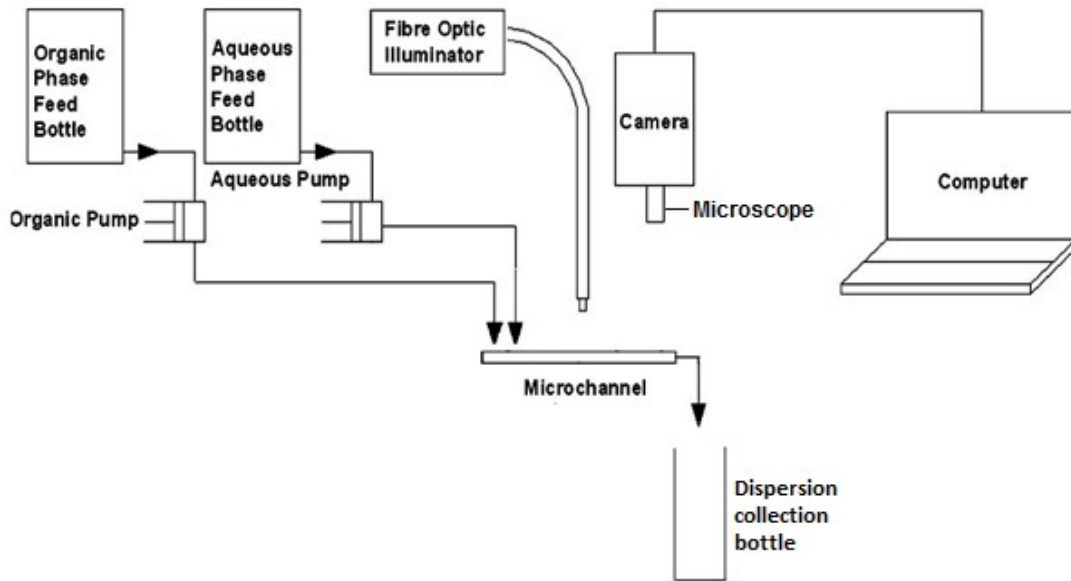


Figure 4.1: Schematic diagram of the experimental setup

4.2.2 Phases used in the experiments

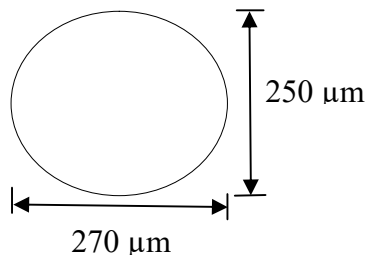
The test systems used in the experiments are the standard test systems recommended by EFCE. Water-butanol test system has a very low interfacial tension. Water-butyl acetate test has a medium interfacial tension while water-toluene has a high interfacial tension. The physical properties of the three test systems are given in [Table 4.1](#). Aqueous and organic phases are mutually equilibrated before conducting the experiments.

Table 4.1: Physical properties of the test systems used in the experiments at 20⁰ C

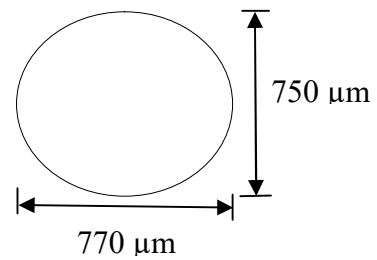
Test System		ρ (kg/m ³)	μ (mPa·s)	σ (mN/m)
aqueous	water	985.6	1.426	1.75
organic	n-butanol	846	3.364	
aqueous	water	997.6	1.0274	14.1
organic	n-butyl acetate	880.9	0.734	
aqueous	water	998.2	0.963	36
organic	toluene	865.2	0.584	



(a)



(b)



(c)

Figure 4.2: (a) Microchannel chip with holder for microbore tubing (b) Cross-section of the microchannel having $D_H = 260 \mu\text{m}$ (c) Cross-section of the microchannel having $D_H = 760 \mu\text{m}$

4.3. RESULTS AND DISCUSSION

4.3.1 Typical flow patterns

Four different types of flow patterns such as Slug flow (SF), Slug and droplet flow (SDF), Droplet flow (DF) and Parallel flow (PF) are observed in the experiments. Typical images of these flow patterns are shown in Fig.4.3.

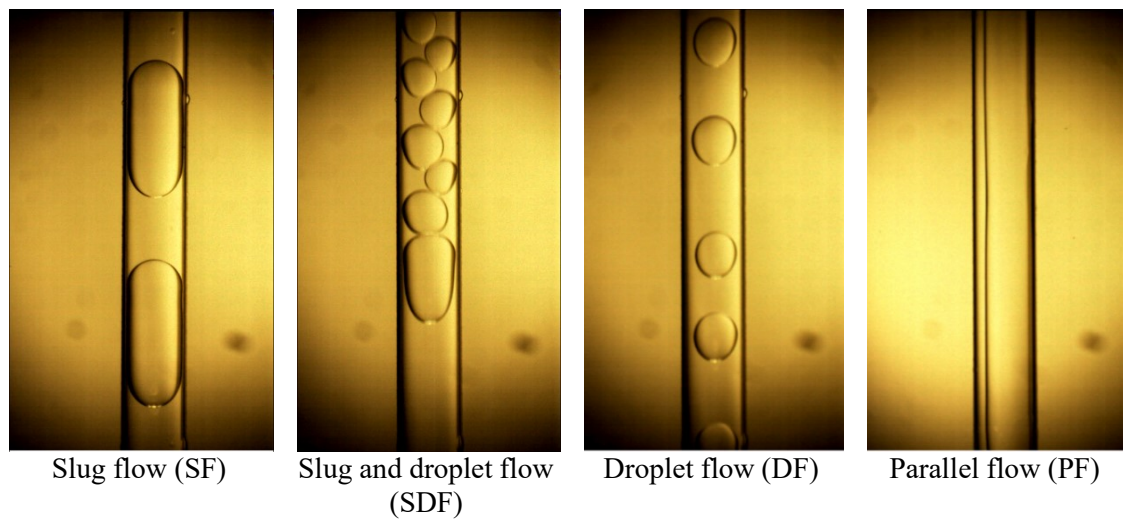


Figure 4.3: Different liquid-liquid two-phase flow patterns observed in the experiments (images from uncoated microchannel, $D_H = 760 \mu\text{m}$)

Slug Flow: Slug flow regime is observed at low flow rates of the aqueous and organic phases. The flow regime responsible for generation of slugs is the squeezing flow regime (De Menech et al., 2008; Sarkar et al., 2012). In this regime, shear stress is not important and breakage of dispersed phase into slugs is governed by the interfacial tension and pressure gradient due to the obstruction to the flow of the continuous phase caused by the growing slug. The slug occupies almost the whole cross-section of the microchannel with a very thin layer of the continuous phase between the slug and the wall of the microchannel. In all the experiments, the aqueous phase was the

dispersed phase and the organic phase was the continuous phase. At constant dispersed phase flow rate increase in the flow rate of the continuous phase was observed to cause reduction in slug size, as shown in Fig.4.4. Further increase in continuous phase flow rate led to transition of flow pattern from slug flow to slug and droplet flow, droplet flow and parallel flow depending upon the dispersed phase flow rate.

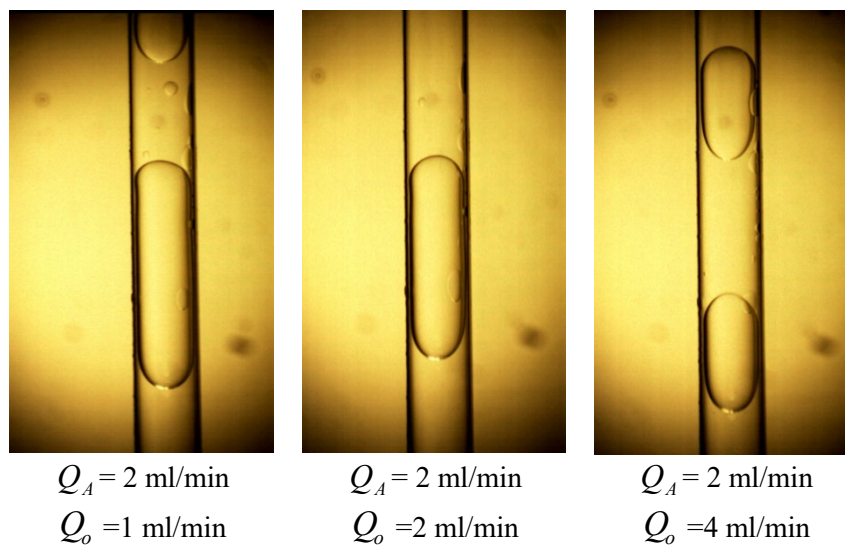


Figure 4.4: Slugs formed for different continuous phase (organic phase) flow rates at a constant dispersed phase (aqueous phase) flow rate (phase system: water– butyl acetate, $D_H = 760 \mu\text{m}$, uncoated microchannel)

Increase in dispersed phase flow rate at constant continuous phase flow rate caused transition from slug flow to parallel flow. There is no significant change in slug size with change in continuous phase flow rate at a constant dispersed phase flow rate as shown in Fig.4.5.

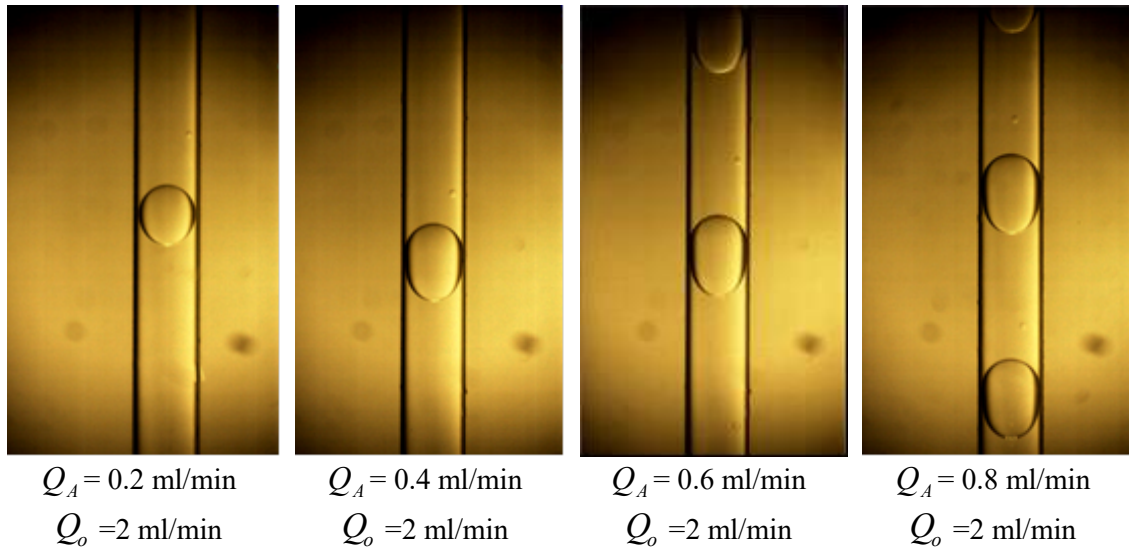


Figure 4.5: Slugs formed for different dispersed phase (aqueous phase) flow rate at a constant continuous phase (organic phase) flow rate (phase system: water– butyl acetate, $D_H = 760 \mu\text{m}$, uncoated microchannel)

Slug and Droplet Flow: This type of flow regime is observed at flow rates which are just higher than the flow rates at which slug flow is observed. This flow pattern marks the transition of squeezing flow regime to dripping flow regime (Sarkar et al., 2012). A typical image of slug and droplet flow pattern is shown in Fig.4.3.

Droplet Flow: A typical image of the droplet flow pattern is shown in Fig.4.3. This flow pattern is observed after complete transition from squeezing regime to dripping regime (De Menech et al., 2008; Sarkar et al., 2012). It is characterized by the drops having diameters less than the diameter of the microchannel. This flow pattern typically occurs at relatively high continuous phase flow rates and low dispersed phase flow rates i.e. the condition when the inertial force associated with higher flow rate of the continuous phase is high enough to knock down the dispersed phase into small droplets and the resistance offered by the dispersed phase is small due to its

lower flow rate. As the flow rate of the continuous phase increases for a constant dispersed phase flow rate, the size of the droplets reduces, as shown in Fig.4.6.

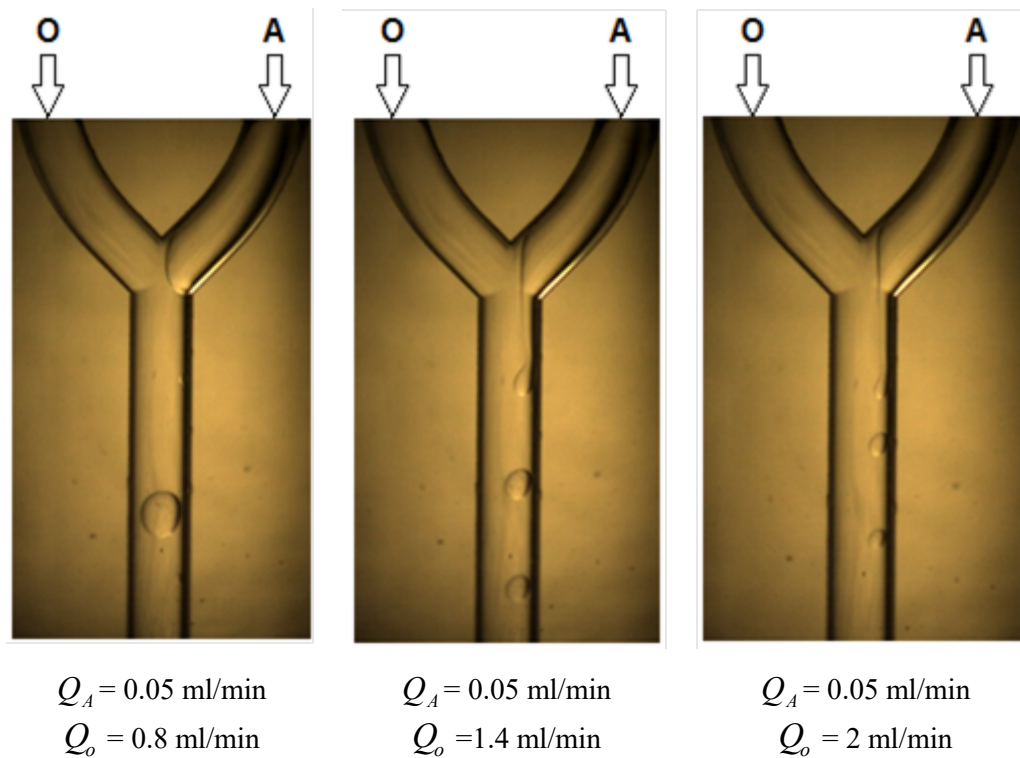


Figure 4.6: Effect of the continuous phase (organic phase) flow rate on the size of the droplet in droplet flow regime. (phase system: water – butanol, $D_H=760 \mu\text{m}$, coated microchannel)

Parallel Flow: This flow pattern is the result of jetting flow regime in microchannel. At higher flow rates of both the phases, the inertial force dominates over the interfacial tension force and the two phases flow past each other without generation of dispersion. Typical images of parallel flow are shown in Fig.4.3 and Fig.4.7.

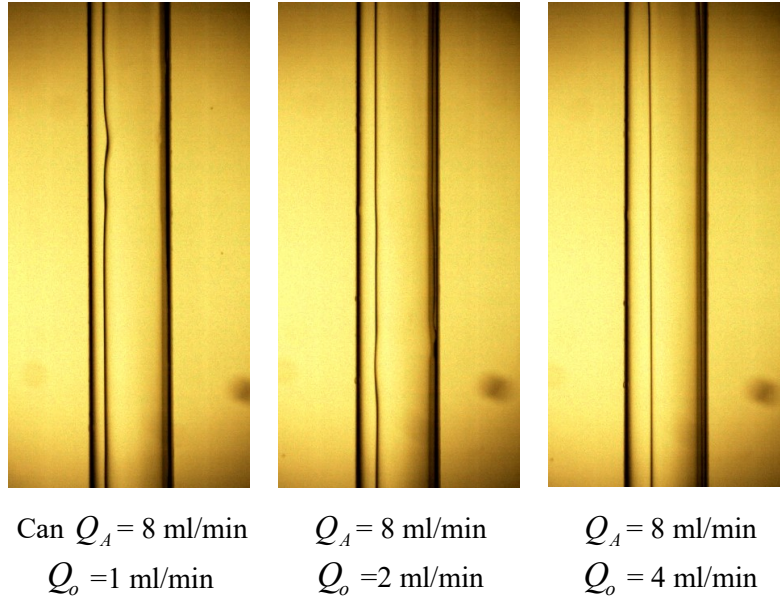


Figure 4.7: Effect of the continuous phase (organic phase) flow rate on the position of the interface between the two liquids in parallel flow. (phase system: water – butyl acetate, $D_H = 760 \mu\text{m}$, uncoated microchannel).

Fig.4.7 shows that the position of the interface shifts inside the microchannel as the relative flow rates of the continuous and dispersed phase change.

4.3.2 Effect of flow rate on the flow regime map

To illustrate the typical effect of flow rate on the flow pattern, the flow regime maps for the intermediate interfacial tension system (water - butyl acetate) and high interfacial tension system (water -toluene) are shown in Fig.4.8. These flow patterns are completely repeatable. Fig.4.8 shows that slug flow is obtained for very small values of the flow rates of the aqueous phase and the organic phase. When the dispersed phase (aqueous phase) flow rate is kept constant and the continuous phase flow rate is increased, slug flow changes to slug and droplet flow or droplet flow. This is because, for a constant flow rate of the dispersed phase, an increase in the flow rate

of the continuous phase increases its inertial force leading to enhancement in its tendency to break down the dispersed phase in smaller fragments causing transition from slug flow to slug and droplet flow or to droplet flow. Flow regime for high flow rate of the continuous phase and low flow rate of the dispersed phase is the droplet flow. On continued increase in continuous phase flow rate, flow regime does not change further but size of the droplets keeps reducing.

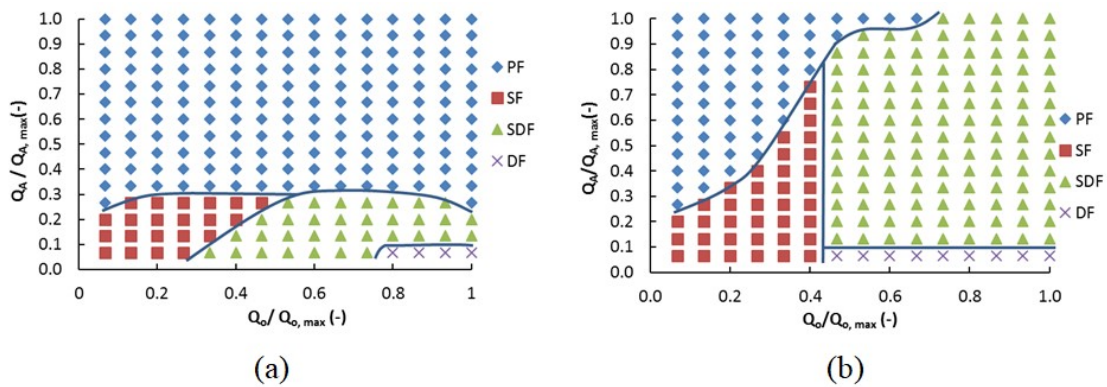


Figure 4.8: Effect of flow rate on flow pattern in coated microchannel. $D_H=260\mu\text{m}$, $Q_{A,max}=3\text{ ml/min}$, $Q_{O,max}=3\text{ ml/min}$ (a) water – butyl acetate (b) water – toluene

When the dispersed phase (aqueous phase) flow rate is increased keeping the continuous phase (organic phase) flow rate constant, dispersion tends to become coarser with shorter slugs changing to longer slugs or droplet flow changing to slug and droplet flow or slug flow. On continued increase in the dispersed phase flow rate, continuous phase is eventually not able to break down the dispersed phase and the two phases flow side by side in parallel flow.

4.3.3 Effect of microchannel diameter on flow regime map

Fig. 4.9 illustrates the effect of microchannel diameter on the flow pattern for two test systems (water- butyl acetate and water - toluene). Fig. 4.9(a) is compared with Fig.

4.9(b) and Fig. 4.9(c) is compared with Fig. 4.9(d). The comparison of the flow regime map for the larger diameter and smaller diameter microchannels suggests that all the flow regime transitions occur at lower flow rates in 260 μm diameter microchannel compared to 760 μm diameter microchannel. For example, for water-butyl acetate system the organic phase flow rate at which transition from slug flow to droplet flow occurs at the smallest flow rate of the aqueous phase is about 3.3 ml/min in 760 μm compared to 0.75 ml/min in 260 μm . Dominance of the parallel flow regime over other flow regimes can also be observed in smaller diameter microchannel.

In previous studies on liquid-liquid two-phase flow patterns in microchannels, different researchers have used different coordinates numbers to present flow regime maps (Fu et al., 2015). For example, Dessimoz et al. (2008) used Capillary number ($Ca = \mu U/\sigma$) and Reynolds number ($Re = D_H \rho U/\mu$). Kashid et al. (2011), Salim et al.(2008) and Sarkar et al. (2012) used velocities or flow rates. Cherlo et al. (2010) and Zhao et al. (2006) used Weber number ($We = \rho U^2 D_H/\sigma$). The data of Fig.4.9 can be used to identify which dimensionless number is most appropriate to present the generalized flow regime maps. The relations between the flow rates in the microchannels of two different diameter for keeping Ca or Re or We same for a given test system (constant physical properties) are expressed by Eq. 4.1:

$$Q_2 = \begin{cases} \left(\frac{D_{H2}}{D_{H1}}\right)^2 Q_1 & \forall Ca_2 = Ca_1 \\ \left(\frac{D_{H2}}{D_{H1}}\right)^1 Q_1 & \forall Re_2 = Re_1 \\ \left(\frac{D_{H2}}{D_{H1}}\right)^{1.5} Q_1 & \forall We_2 = We_1 \end{cases} \quad (4.1)$$

Using Eq. 4.1, the flow rate (Q_2) of the organic phase in 260 μm diameter (D_{H2}) microchannel at which transition from slug flow to the droplet flow occurs at the minimum flow rate of the aqueous phase is evaluated using the experimental values of the organic phase flow rate (Q_1) at which this transition occurs in 760 μm diameter (D_{H1}) microchannel. The evaluated value of Q_2 can be compared with the experimental value of Q_2 . The evaluation is done both for water – butyl acetate and water – toluene system. The results are shown in Table 4.2. For water-butyl acetate as well as water-toluene system, equivalence of We gives the best estimate of Q_2 followed by equivalence of capillary number. This suggests that among the three dimensionless numbers mentioned above, We is the most appropriate to present the flow regime maps using dimensionless numbers.

Table 4.2: Comparison of the experimental and estimated values of the organic phase flow rate (Q_2) at which transition from slug flow to droplet flow occurs at the lowest flow rate of the aqueous phase in 260 μm (D_{H2}) microchannel ($Q_1 = 3.5$ ml/min for water – butyl acetate system, $Q_1 = 6.5$ ml/min for water – toluene system, $D_{H1} = 760$ μm)

		Q_2 (ml/min)			
		Experimental	$Ca_2 = Ca_1$	$Re_2 = Re_1$	$We_2 = We_1$
Water	– butyl acetate	0.69	0.41	1.20	0.70
Water	- toluene	1.05	0.76	2.22	1.30

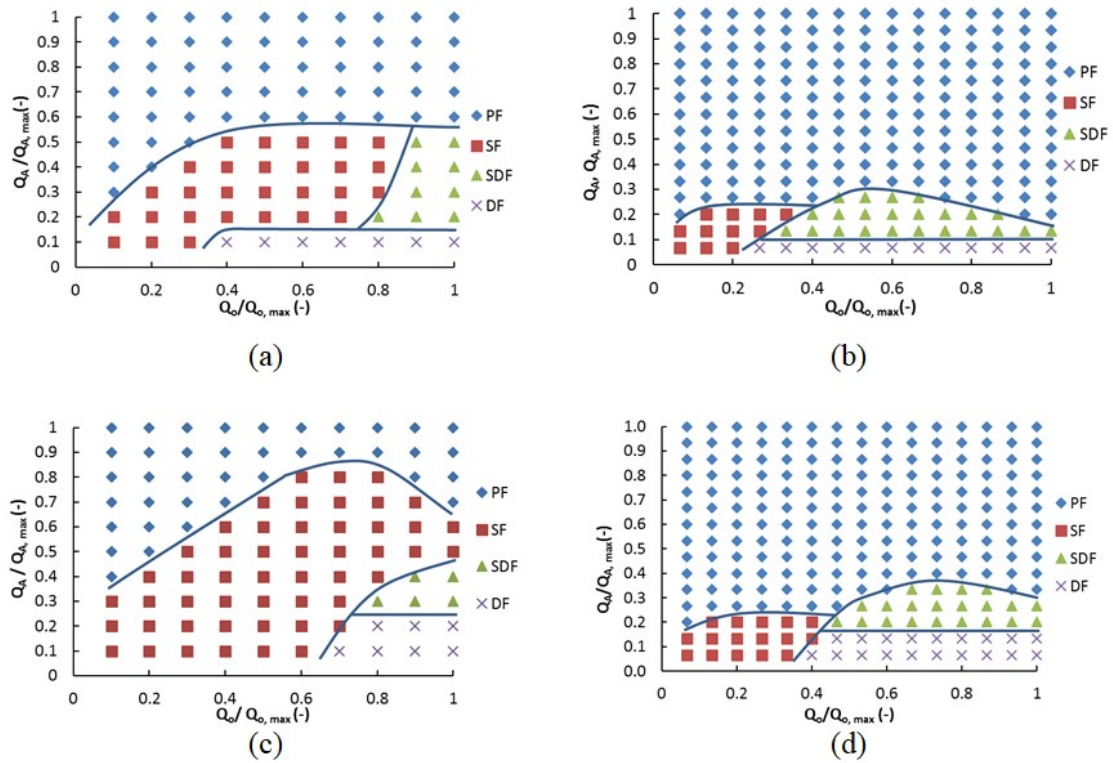


Figure 4.9: Effect of microchannel diameter on flow regime map. (a) phase system: water – butyl acetate, $D_H = 760 \mu\text{m}$, uncoated microchannel, $Q_{A, \max} = 10 \text{ ml/min}$, $Q_{O, \max} = 10 \text{ ml/min}$ (b) phase system: water – butyl acetate, $D_H = 260 \mu\text{m}$, uncoated microchannel, $Q_{A, \max} = 3 \text{ ml/min}$, $Q_{O, \max} = 3 \text{ ml/min}$ (c) phase system: water – toluene, $D_H = 760 \mu\text{m}$, uncoated microchannel, $Q_{A, \max} = 10 \text{ ml/min}$, $Q_{O, \max} = 10 \text{ ml/min}$ (d) phase system: water – toluene, $D_H = 260 \mu\text{m}$, uncoated microchannel, $Q_{A, \max} = 3 \text{ ml/min}$, $Q_{O, \max} = 3 \text{ ml/min}$.

4.3.4 Effect of interfacial tension on flow regime map

The effect of interfacial tension on the flow regime map is illustrated through Fig.4.10 which shows flow regime maps of the three test systems in $760 \mu\text{m}$ diameter microchannel. Fig. 4.10 shows that for water-toluene system which has the maximum interfacial tension, slug flow dominates the flow regime map. As interfacial tension reduces, prominence of slug flow in flow regime map diminishes and for the water – butanol system which has a low interfacial tension, slug flow regime is observed in

only a few experiments. On the contrary, with an increase in interfacial tension, prominence of parallel flow in flow regime map reduces. While parallel flow is observed for many experimental points in the flow regime map for water-butanol system, parallel flow is obtained for less number of points in the flow regime map for water – toluene system.

The data of Fig.4.10 can be once again used to identify which of the important dimensionless numbers is most appropriate to present the flow regime maps. For the same microchannel, the equivalence of the three dimensionless numbers requires the following relations between the flow rates of two different test systems.

$$Q_2 = \begin{cases} \left(\frac{\sigma_2}{\sigma_1} \right) \left(\frac{\mu_1}{\mu_2} \right) Q_1 & \forall Ca_2 = Ca_1 \\ \left(\frac{\mu_2}{\mu_1} \right) \left(\frac{\rho_1}{\rho_2} \right) Q_1 & \forall Re_2 = Re_1 \\ \left(\frac{\sigma_2}{\sigma_1} \right)^{0.5} \left(\frac{\rho_1}{\rho_2} \right)^{0.5} Q_1 & \forall We_2 = We_1 \end{cases} \quad (4.2)$$

Using Eq. 4.2, the flow rate (Q_2) of the organic phase for water-butanol and water – acetone test systems at which transition from slug flow to the droplet flow occurs at the minimum flow rate of the aqueous phase can be estimated using the experimental value of the organic flow rate (Q_1) at which this transition occurs for water – butyl acetate system. The experimental value of Q_2 and its estimate based on equivalence of the three relevant dimensionless numbers are listed in Table 4.3. For water-butanol system, the equivalence of Ca gives the best estimate followed by equivalence of We. For water- toluene system equivalence of We gives the best prediction followed by equivalence of Ca. Thus, the data listed in Table 4.2 and Table 4.3 suggest that in majority of the cases We is the best dimensionless number to represent flow regime maps.

Table 4.3: Comparison of estimated and experimental value of organic flow rate (Q_2) at which transition from slug flow to droplet flow occurs for the lowest flow rate of the aqueous phase ($Q_1 = 3.5$ ml/min for water – butyl acetate system, $D_H = 760$ μ m)

	Q_2 (ml/min)			
	Experimental	$Ca_2 = Ca_1$	$Re_2 = Re_1$	$We_2 = We_1$
Water - butanol	0.30	0.09	16.61	1.26
Water - toluene	6.50	11.23	2.83	5.64

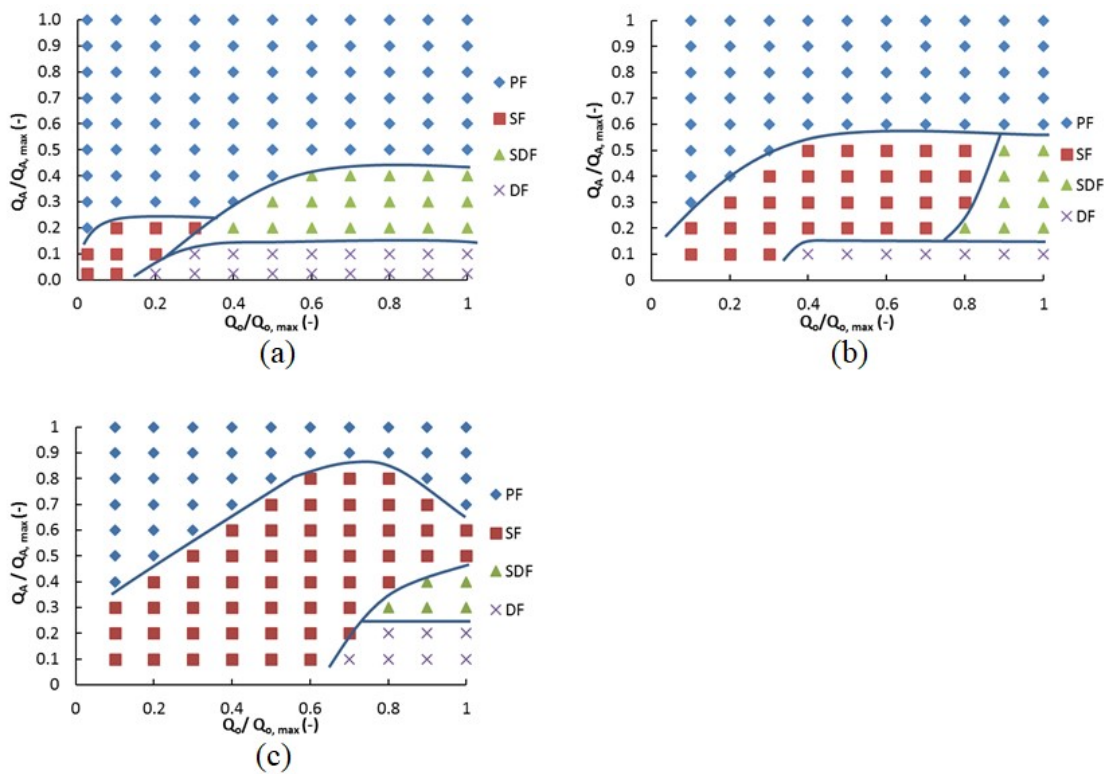


Figure 4.10: Effect of interfacial tension between the two liquids on the flow regime maps in uncoated microchannels of 760 μ m diameter (a) phase system: water – butanol, $Q_{A, \max} = 2$ ml/min, $Q_{O, \max} = 2$ ml/min (b) phase system: water – butyl acetate, $Q_{A, \max} = 10$ ml/min, $Q_{O, \max} = 10$ ml/min (c) phase system: water – toluene system, $Q_{A, \max} = 10$ ml/min, $Q_{O, \max} = 10$ ml/min).

4.3.5 Effect of hydrophobicity of channel on flow regime map

Fig.4.11 shows the effect of hydrophobicity of channel wall on the flow regime map.

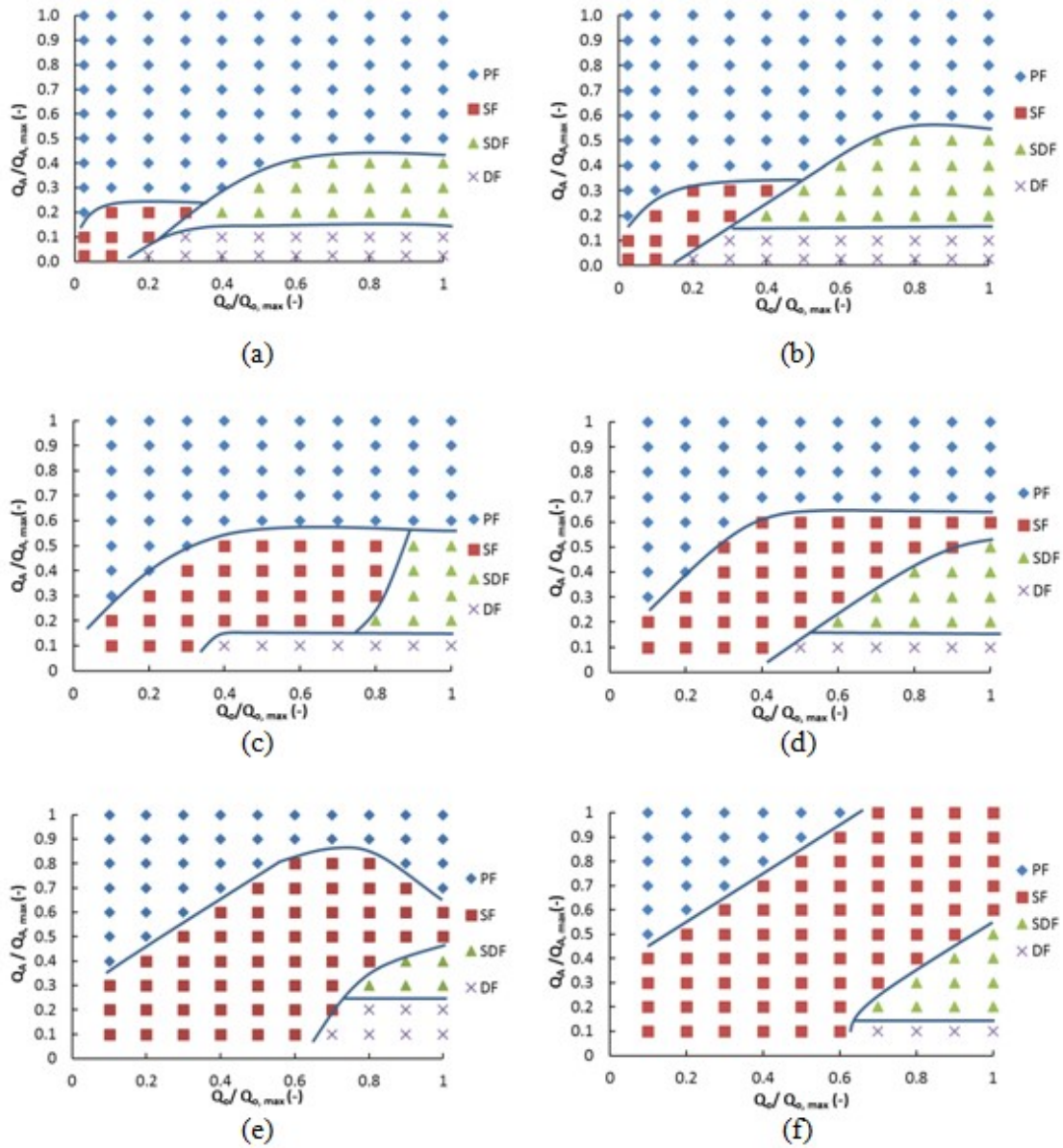


Figure 4.11. Flow regime map for uncoated microchannel and coated microchannel of 760 μm diameter (a) phase system: water – butanol, uncoated microchannel, $Q_{A, \max} = 2$ ml/min, $Q_{O, \max} = 2$ ml/min. (b) phase system: water – butanol, coated microchannel, $Q_{A, \max} = 2$ ml/min, $Q_{O, \max} = 2$ ml/min (c) phase system: water – butyl acetate, uncoated microchannel, $Q_{A, \max} = 10$ ml/min, $Q_{O, \max} = 10$ ml/min. (d) phase system: water – butyl acetate, coated microchannel, $Q_{A, \max} = 10$ ml/min, $Q_{O, \max} = 10$ ml/min. (e) phase system: water – toluene, uncoated microchannel, $Q_{A, \max} = 10$ ml/min, $Q_{O, \max} = 10$ ml/min. (f) phase system: water – toluene, coated microchannel, $Q_{A, \max} = 10$ ml/min, $Q_{O, \max} = 10$ ml/min.

Flow regime maps for water – toluene system in 760 μm diameter microchannel show that dispersed flow (slug flow and slug and droplet flow) is more prominent than parallel flow in the microchannel having hydrophobic coating. As the water is dispersed phase, the hydrophobic coating promotes dispersed flow than parallel flow in which the aqueous phase must wet the wall of the microchannel. Similar observation can be made from the flow regime maps of water – butanol and water – butyl acetate, as shown in [Fig.4.11](#).

4.3.6 Generalized flow regime map

In this study diameter of microchannel, physical properties as well as flow rates have been varied. The resulting experimental data offer an opportunity to check if the data is plotted using appropriate dimensionless number a generalized flow regime map emerges or not. In the previous section, suitability of various dimensionless numbers in prescribing flow regime map in dimensionless form was evaluated and We was found to be the most appropriate dimensionless number. Weber number ($We = \rho U^2 D_H / \sigma$) is also recommended to present flow regime map by [Cherlo et al. \(2010\)](#) and [Zhao et al. \(2006\)](#). As mentioned previously different researchers have used different combinations of dimensionless numbers as coordinates to present flow regime maps for liquid-liquid two phase flow in microchannel. Therefore, in [Fig.4.12](#) we have additionally plotted our experimental data in different ways to identify the best combination of dimensionless numbers as coordinates for flow regime map. One of the way to present the generalized flow regime map is by using Capillary number ($Ca = \mu U / \sigma$) and Reynolds number ($Re = D_H \rho U / \mu$) as the coordinates as done by [Dessimoz et al. \(2008\)](#) Similarly data has also been plotted using velocities or flow

rates as coordinate as done by [Kashid et al. \(2011\)](#), [Salim et al.\(2008\)](#) and [Sarkar et al. \(2012\)](#). $We \cdot Oh$ is also used as coordinates as prescribed by [Yagodnitsyna et al. \(2016\)](#) for generalized flow regime maps for a T-junction microchannel. Here Oh represents Ohnesorge number ($Oh = \mu/(\rho\sigma D_H)^{1/2}$).

Flow regime map given in [Fig.4.12\(c\)](#) which is based on velocity as the coordinates shows that points corresponding to slug flow are scattered at two different regions separated by points corresponding to other flow patterns. The same is true for slug and droplet flow regime. Similar observation holds when flow regime map is presented using capillary numbers and Reynolds number as seen in [Fig.4.12\(e\)](#). Flow regime map given in [Fig.4.12\(a\)](#) which is based on Weber number as the coordinates and flow regime map given in [Fig.4.12\(d\)](#) which is based on capillary number as the coordinates shows that points corresponding to a particular flow pattern do cluster together. Thus there are separate zone on flow regime map for each flow pattern. But the size of the zone in which overlapping of points corresponding to different flow patterns occurs is minimum when $We \cdot Oh$ is used as the coordinates, as shown in [Fig.4.12\(b\)](#). Thus, as was reported for T-junction microchannels, for Y-junction microchannels also, $We \cdot Oh$ is found to be good for presenting generalized liquid-liquid flow regime map.

The type of flow pattern generated in liquid-liquid two-phase flow in microchannels is dictated by the interfacial tension force, inertial force and viscous force as elucidated by [De Menech et al. \(2008\)](#). who proposed squeezing, dripping and jetting regimes of dispersion at T-type microfluidic junction. Weber number (We) takes into account inertial force and interfacial tension force but does not account for the viscous force. The combination $We \cdot Oh$ accounts for viscous force also and, therefore, is more

suitable than We alone for presenting the generalize flow regime map which has flow patterns belonging to squeezing, dripping as well as jetting regime.

Whether the generalized flow regime map proposed for liquid-liquid dispersion at Y-junction microchannel as given by Fig.4.12 (b) of this study holds good for the data reported previously is also checked. For this data of Kashid et al. (2011) flow regime map have been plotted in Fig.4.12 (f) which has the same demarcation lines or curves as used in Fig.4.12 (b). The data of Kashid et al. (2011) are for a Y-junction microchanel having a square cross-section and 269 μm hydraulic diameter. The phase system used by Kashid et al. (2011) is water-acetone-toluene system. Fig.4.12 (f) shows that slug flow and parallel flow data of Kashid et al. (2011) fit well in the generalized flow regime map. Kashid et al. (2011) did not differentiate between slug and droplet flow and droplet flow. Their data points for slug and droplet flow when put in the generalized flow regime map are spread in the region of slug flow, droplet flow, parallel flow and common region in the generalized flow regime map. Our generalized flow regime map also has some data points of SDF in the overlapping region as that of Kashid et al. (2011) Thus Only 5 data points of Kashid et al. (2011) out of 69 violate our generalized flow regime map. The violation is not significant as the data points violating the generalize flow regime map are not deep inside the regions representing different flow patterns but close to the demarcation lines or curves. A good match with the data of Kashid et al. (2011) suggests the utility of the generalized flow regime maps for liquid-liquid dispersion at Y-junction microchannels presented in this study.

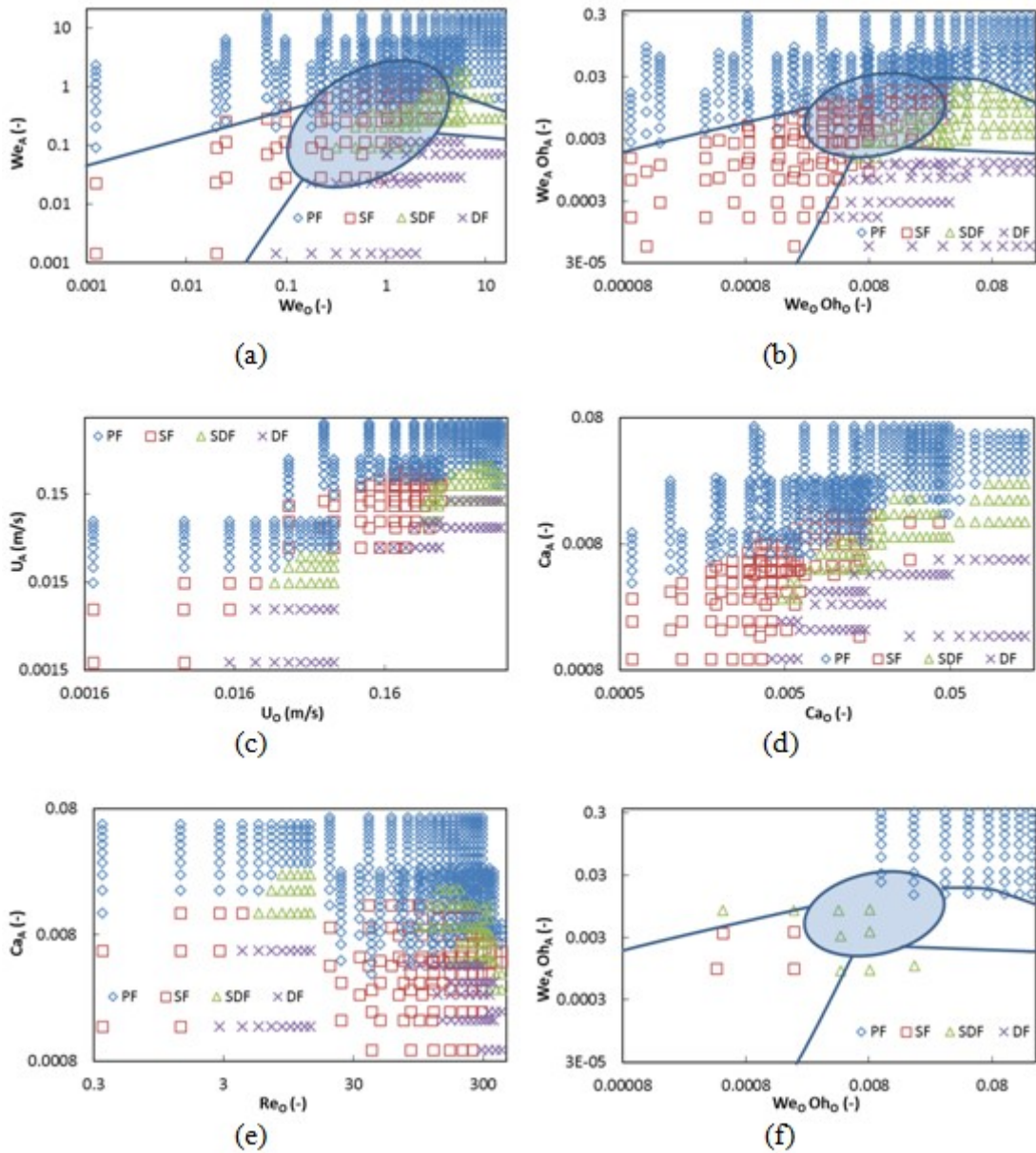


Figure 4.12: Generalized flow regime map for (a) uncoated microchannels with We as the dimensionless number (b) uncoated microchannels with $We \cdot Oh$ as the dimensionless number (c) uncoated microchannels with velocity as the dimensionless number (d) uncoated microchannels with Ca as the dimensionless number (e) uncoated microchannels with Ca and Re as the dimensionless number (f) data of [Kashid et al. \(2011\)](#)

4.4 CONCLUSIONS

Experiments are performed to study the effects of diameter, flow rate, interfacial tension and wall wettability on the liquid-liquid two-phase flow patterns generated at Y-junction microchannels. The experiments are conducted using the standard test systems prescribed by the EFCE. Four different types of flow patterns - slug flow, slug and droplet flow, droplet flow and parallel flow – are observed. Aqueous phase is found to be the dispersed phase. Slug flow is observed for low flow rates of dispersed and continuous phases. Slug flow changes to slug and droplet flow and then to droplet flow when continuous phase flow rate is increased keeping dispersed phase flow rate constant at a low value. Slug flow changes to parallel flow when dispersed phase flow rate is increased keeping the continuous phase flow rate constant at a low value. Parallel flow is observed for high flow rates of both dispersed phase and continuous phase. As microchannel diameter is reduced, flow pattern transitions are observed to occur at lower flow rates. With increase in interfacial tension, slug flow and other dispersed flow patterns (slug and droplet flow and droplet flow) become more prominent. Similarly, with hydrophobic coating which reduces wetting of the wall by the dispersed phase, slug flow and other dispersed flow pattern become more prominent at the cost of parallel flow. Different dimensionless numbers are evaluated for their suitability for presenting the generalized flow regime map. For this purpose, We is found to be a better candidate than Ca and Re. Thus the generalize flow regime map are presented using We and $We \cdot Oh$ and the latter is found to be better. These generalized flow regime map will be useful for estimating flow pattern in a Y-junction microchannel.

CHAPTER 5

SCALE-UP FOR ACHIEVING LARGER THROUGHPUT

5.1 INTRODUCTION

Single microbore tubes can handle a very low flow rate as reported in chapter 2. For realizing high throughput several microbore tubes need to be stacked in parallel. Therefore, a distributor is required to equally distribute the flow into parallel microbore tubes. The distributor should not only equally distribute the aqueous and the organic flow into parallel microbore tubes but also generate liquid-liquid dispersion.

This chapter reports scale-up by using conventional structural bifurcations and a novel compact distributor having in-built microfluidic junctions to generate dispersion to feed parallel microbore tubes. Microbore tubes connected to the novel distributor can be shorter or longer to suit to the kinetics of extraction of the phase system at hand. It is named as Monoblock Distributor with In-built Microfluidic Junctions (MDIMJ). It does flow distribution as well as generates liquid-liquid dispersion for carrying out solvent extraction in parallel microbore tubes. The experiments are conducted in two different types of MDIMJ. First type of MDIMJ has 6 outlet. 6 parallel microbore tubes are connected to the 6 outlets of the MDIMJ to achieve maximum throughput of 3LPH in extraction experiments. The second type of MDIMJs have 20 outlets. These MDIMJs along with 20 parallel microbore tubes are used to achieve maximum throughput of 10 LPH in multistage extraction and stripping experiments. Such distributors can also be used for other processes involving contact and/or reaction between two streams e.g. synthesis of ionic liquids which have potential applications in nuclear fuel cycle ([Sen et al., 2016](#))

5.2 SCALE-UP BY USING STRUCTURAL BIFURCATION

5.2.1 Experimental setup

Fig. 5.1 shows the photograph and Fig. 5.2 shows the schematic diagram of the experimental setup used in the experiments carried out at 1 LPH total throughput using two parallel microbore tubes. The setup consists of two 2 mm diameter Y-junction distributors drilled in separate polytetrafluoroethylene (PTFE) blocks for splitting the incoming aqueous and organic streams into two streams each. The microfluidic junctions used are Y-junction of 750 μm diameter drilled in polytetrafluoroethylene (PTFE) disks. The included angle between the two inlets of the Y-junctions is 120° . PTFE microbore tubes are connected to the disks housing the microfluidic Y-junctions by using a threaded connector. Dispersion generated at the Y-junctions passes through the microbore tubes. The microbore tubes are coiled on 1 inch diameter rod to make the system compact. The microbore tubes are then connected to an acrylic pipe settler which is used for continuous phase disengagement. Separated phases are then collected in respective sample bottles.

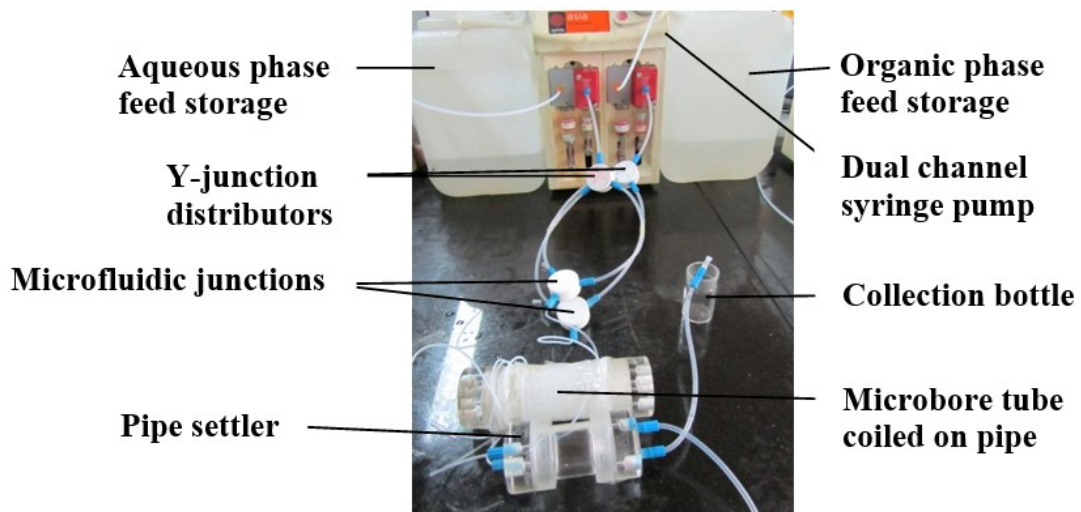


Figure 5.1: Experimental setup for conducting experiments at 1 LPH total throughput by using two microbore tubes connected in parallel

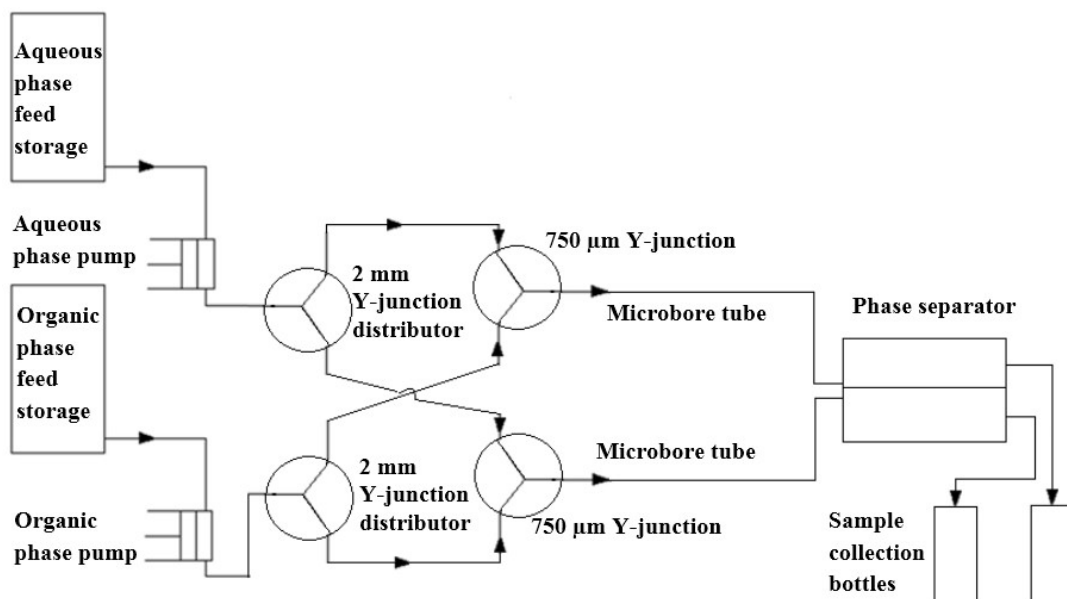


Figure 5.2: Schematic diagram of experimental setup used for conducting experiments at 1 LPH total throughput by using two microbore tubes connected in parallel

The pipe settler is separately shown in Fig. 5.3. It is made of 1 inch inner diameter acrylic pipe to ensure visual observation. The length of the pipe settler is 3 cm. The pipe is threaded at both the ends. The end cap on one side has two inlets to receive the dispersion coming from the two microbore tubes. The end cap on the other side has two outlets, one each for the clear aqueous phase and the clear organic phases.

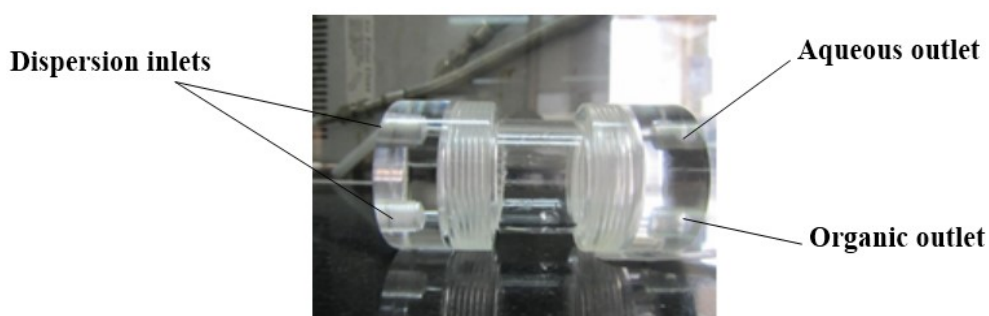


Figure 5.3: Pipe settler used in the experiments conducted with two parallel microbore tubes

In chapter 2, the focus was on finding an optimum configuration (flow rate, diameter and length of microbore tube) which can provide high stage efficiency with low pressure drop and quick settling. In this section, experiments are focused on demonstrating solvent extraction at a total throughput of 1 LPH by replicating the optimum configuration in parallel.

5.2.2 Phases used in the experiments

The aqueous phase is 3 M nitric acid and the organic phase is 30% (v/v) TBP in dodecane. Demineralized water and organic phases are equilibrated with each other to rule out mass transfer due to mutual solubility. Solute (nitric acid) is added to the equilibrated demineralized water to prepare the feed. The system is chosen for its relevance to nuclear fuel cycle wherein metal ions are typically extracted from nitrate media (Darekar et al., 2014c; Desigan et al., 2012; Hotokezaka et al., 2005; Kumar et al., 2012). Physical properties of the phases are given in Table 2.1.

5.2.3 Scale-up for 1 LPH total throughput

The experiments reported in the chapter 2 were aimed at finding an optimum configuration of microbore tube and maximum flow rate handled by it while providing high stage efficiency with low pressure drop and quick phase disengagement. Based on the experiments reported in the chapter 2, this configuration was found to consist of a 300 cm long microbore tube of 800 μm diameter connected to a 750 μm Y-junction. The maximum throughput this configuration can handle was found to be 0.5 LPH. If higher throughputs are to be achieved then this configuration must be replicated in parallel. Number of parallel paths can be decided considering that flow through each

path does not exceed 0.5 LPH. Since the target demonstration capacity was 1 LPH total throughput, experiments were conducted with two parallel microbore tubes of the optimum configuration. The setup used in this experiment has already been described in a previous section and is shown in [Fig. 5.2](#).

[Table 5.1](#) summarizes the results of the experiments conducted with parallel microbore tubes. Unlike the experiments with single microbore tubes reported in chapter 2, experiments were done for $O/A = 1/2$ and $2/1$ also to check the versatility of the setup for handling O/A ratios other than $1/1$. The results show that high stage efficiency in the range of 90-100% can be achieved with a short contact time of about 11 seconds for O/A ratio $1/2$, $1/1$ and $2/1$ at total throughput of 1 LPH. [Table 5.1](#) shows that by putting two parallel tubes, the benefits of optimum configuration are retained while achieving larger throughput. With an increase in O/A ratio, the concentration of nitric acid extracted in the organic phase reduces. Thus with an increase in O/A ratio, driving force for mass transfer of nitric acid from the aqueous phase to the organic phase increases. This leads to a reduction in concentration of nitric acid in the outlet aqueous stream with an increase in O/A ratio.

Table 5.1: Results of the experiments conducted at 1 LPH total throughput with two microbore tubes of optimum configuration connected in parallel (750 μm Y-junction, $D_T = 800 \mu\text{m}$, $L_T = 300 \text{ cm}$, $Q_T = 1 \text{ LPH}$, $\tau_m = 10.85 \text{ s}$)

O/A	$\% \eta$	PE	ΔP (bar)	Settling
1/2	99	8.00	< 2	Quick
1/1	90	16.24	< 2	Quick
2/1	95	28.27	< 2	Quick

5.3 SCALE-UP BY USING MDIMJ

5.3.1 CFD modeling of MDIMJ

To begin with the flow paths of the distributor (MDIMJ) were conceptualized. Schematic of the conceptualized flow paths inside the MDIMJ is shown in [Fig. 5.5](#). The flow paths consist of two inlet channels (one each for organic and aqueous phase) and six microfluidic cross T-junctions. The microfluidic cross T-junctions are fed by the inlet channels. In the geometry of MDIMJ, there are several parameters that can affect the flow distribution. These are diameter of the inlet channels, diameter of the microchannels, distance between the outlets, flow rate and pressure imbalance at the outlets. Considering relatively large number of parameters, CFD simulations were carried out to have insights into how these parameters affect the flow distribution. These insights were required to freeze the design for fabrication. Since the distributor is to be used for two-phase flow distribution, ideally two-phase CFD simulations should be carried out. However, such two-phase CFD simulations would involve tracking of the interface between two-liquids and would require methods like VoF (Volume of Fluid) which are computationally very expensive. Considering this, only single-phase CFD simulations were carried out to evaluate various geometries of MDIMJ for flow distribution. Since the diameters of the channels inside MDIMJ are small, the flow is laminar and hence the CFD model involved numerical solution of Navier-Stokes equations. The governing equations are well known and omitted here for brevity. A commercial solver CFD-ACE+ was used for carrying out numerical simulations. The incompressible fluid used in the simulations is water. In the CFD model, the inlets of the distributor are defined as the velocity inlets and the outlets are defined as the pressure outlets. No slip condition is used at the walls of the channels

housed in MDIMJ. A typical computational domain along with the mesh is shown in Fig. 5.4.

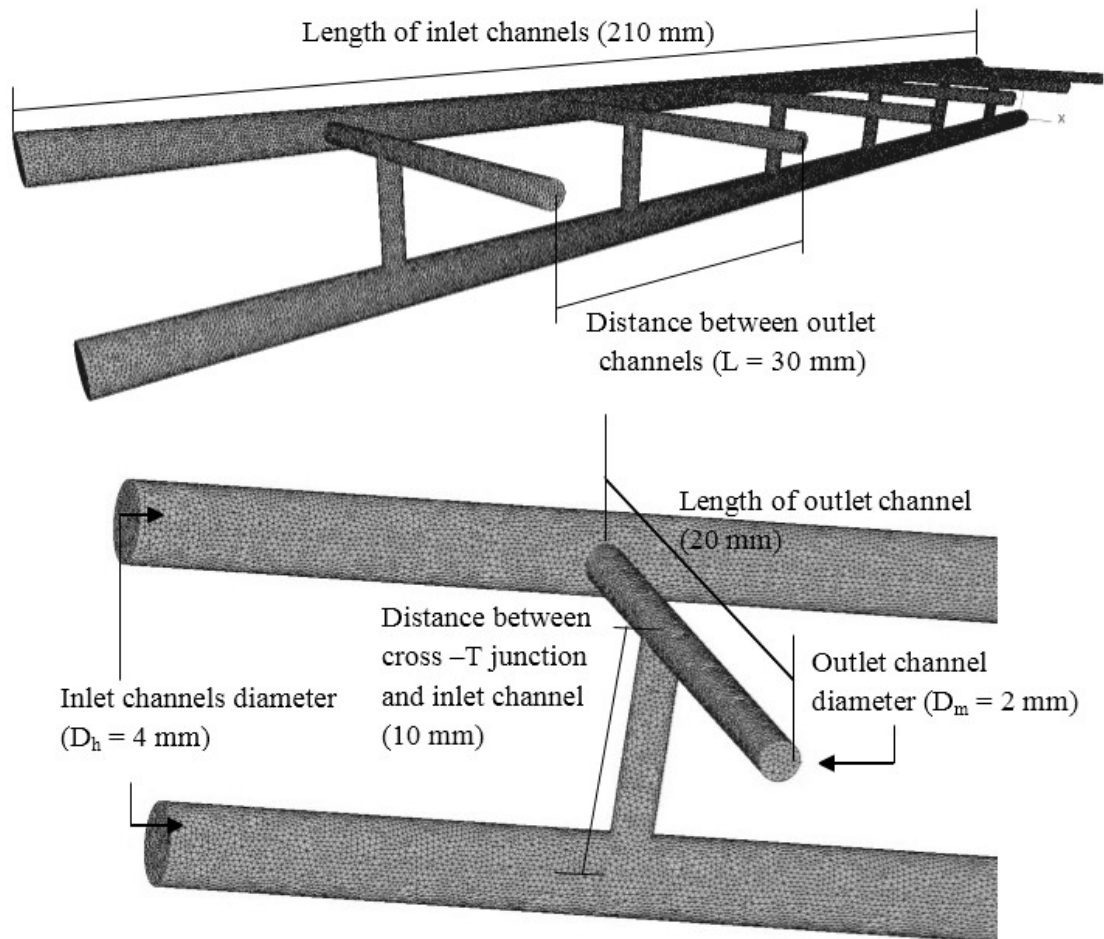


Figure 5.4: Meshed computational domain representing MDIMJ (top) and a closer view of the mesh near one of the junctions (shown in bottom. The dimensions shown are some typical dimensions used in the CFD simulations)

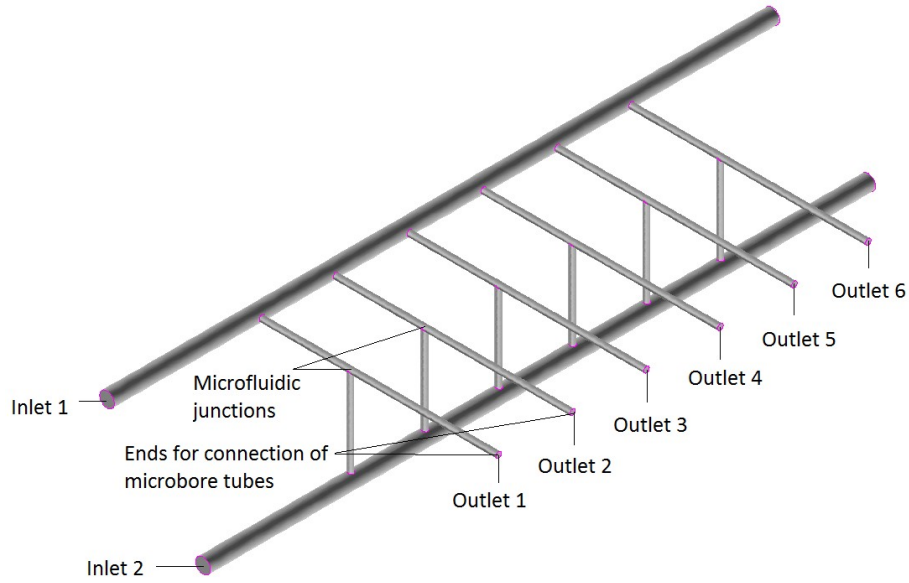


Figure 5.5: Schematic of the flow path of MDIMJ

As the geometry is complex, unstructured tetrahedral grids are used for meshing. Grid independence test is carried. For this, simulations are carried out for different grid densities and the grid density for which flow rate at one of the outlets becomes almost independent of grid density is identified. Using the flow rate obtained at each outlet from CFD simulation, % flow non-uniformity at each outlet can be defined by using Eq. (5.1).

$$\Delta_i = \frac{Q_i - Q_{avg}}{Q_{avg}} \times 100 \quad (5.1)$$

Where, Q_i is the volumetric flow rate at the i^{th} outlet and Q_{avg} is the average volumetric flow rate at each outlet calculated as total flow rate divided by the number of outlets.

5.3.2 Effect of flow rate

Fig. 5.7 shows the effect of flow rate on % flow non-uniformity for MDIMJ as predicted from numerical simulations. For a fixed total flow rate, % flow non-uniformity for the outlet nearest to the inlet is maximum, flow non-uniformity then reduces as the distance of the outlet from the inlet increases. Flow rate at first three outlets is more than the average flow rate. While next three outlets have flow rate less than average flow rate. Thus, the first three outlets have surplus flow, the next three outlets are starved. This trend of variation of flow non-uniformity at different outlets is also evident from Fig. 5.6 which shows the spatial variation of velocity in a vertical cross-section of MDIMJ. As observed from Fig. 5.6, the velocity in the inlet is maximum at the end at which the flow enters. The velocity down the inlet channel keeps reducing as part of the inlet flow keeps leaving the inlet channel through the outlets connected to the inlet channel. The variation of the velocity (or flow rate) at the outlets follows the variation of velocity in the inlet channel with the first outlet having the maximum velocity (receiving the maximum flow rate) and the last outlet having the least velocity (receiving the least flow rate).

Fig. 5.7 also shows that an increase in the inlet flow rate reduces flow non-uniformity across all the outlets. The non-uniformity depends on the ratio of the pressure drop in the inlet channel and the outlet channels. The higher this ratio, the more will be non-uniformity. For low flow rates, the pressure drop in the outlet channels is low due to low velocity. These results in higher ratio of pressure drop in the inlet channel to the outlet channels and leads to higher flow non-uniformity. For high flow rate, the pressure drop in the outlet channels is high due to high velocity. This results in low

ratio of the pressure drop in the inlet channel to the outlet channels leading to reduced flow non-uniformity.

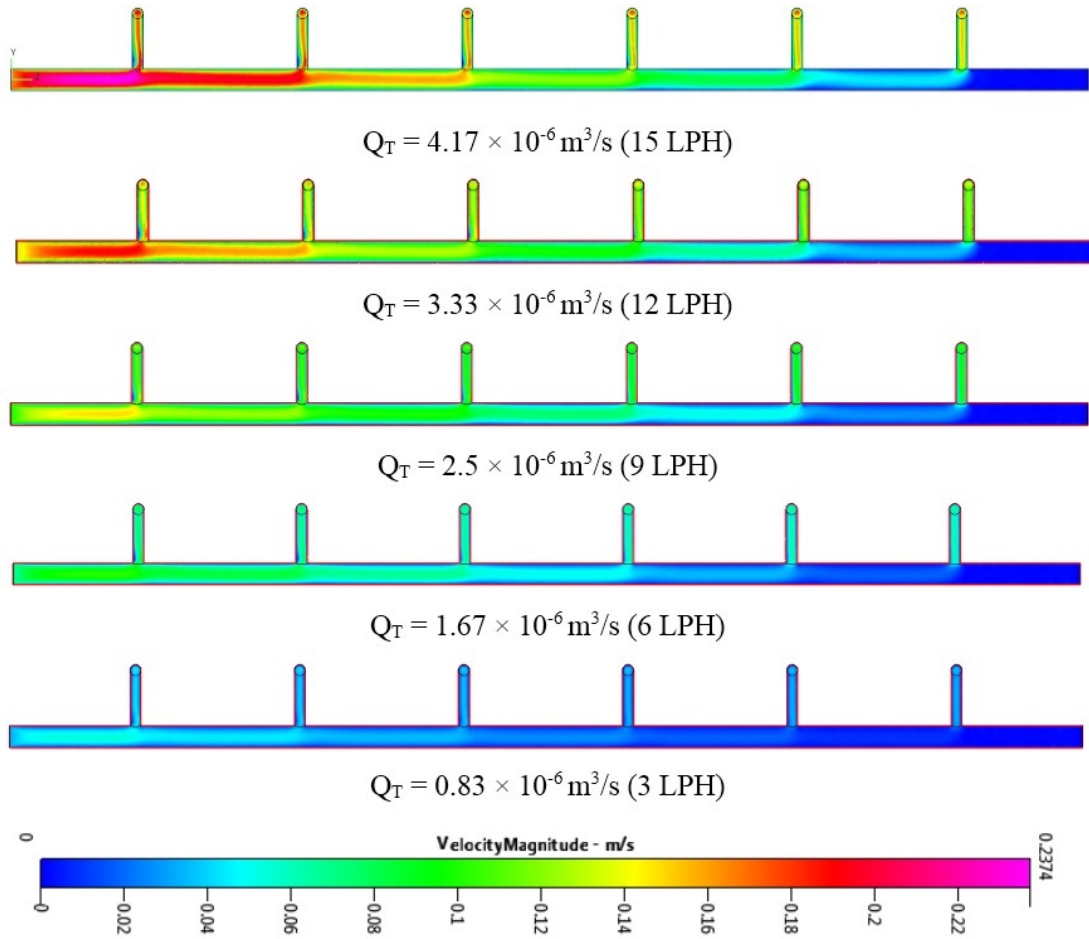


Figure 5.6: Spatial variation of velocity in the inlet channel and the outlet channels of MDIMJ contour for different flow rates. Direction of flow in the inlet channel is from left to right. ($D_h = 4 \text{ mm}$, $D_m = 2 \text{ mm}$, $L = 30 \text{ mm}$)

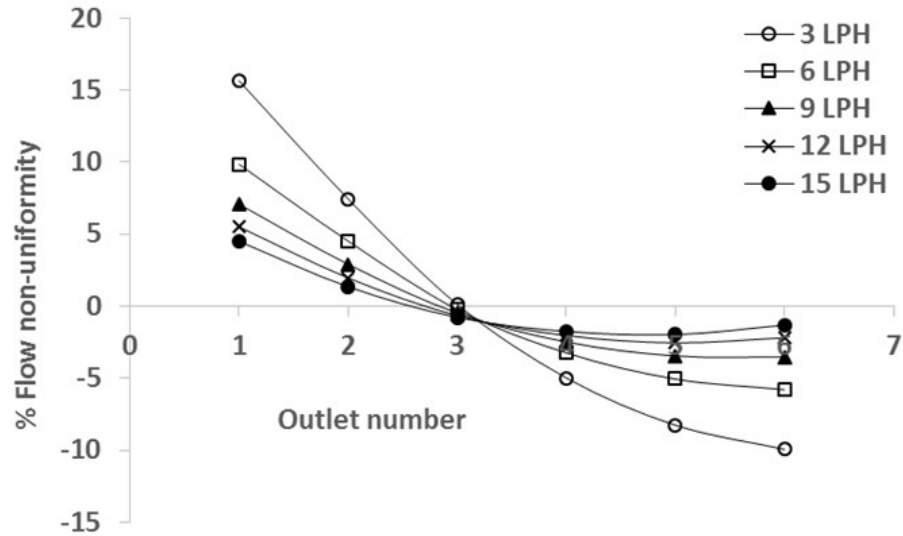


Figure 5.7: Effect of flow rate on % flow non-uniformity
 ($D_h = 4$ mm, $D_m = 2$ mm, $L = 30$ mm)

5.3.3 Effect of inlet channel diameter

Fig. 5.8 shows the effect of inlet channel diameter on % flow non-uniformity for MDIMJ. For a constant flow rate, % flow non-uniformity for all the outlets increases as diameter of the inlet channels reduces. For laminar flow, the pressure drop in a channel is directly proportional to velocity and inversely proportional to the square of diameter. When the inlet channel diameter is reduced at fixed flow rate, pressure drop in the inlet channel increases due to smaller diameter and increase in the velocity. At the same time the pressure drop in the outlet channels remains constant as the diameter of the outlet channels remains constant and, for a fixed flow rate, there is only slight change in the velocities in the outlet channels. A smaller diameter inlet channel thus results in higher ratio of the pressure drop in the inlet channel to the outlet channels leading to higher flow non-uniformity.

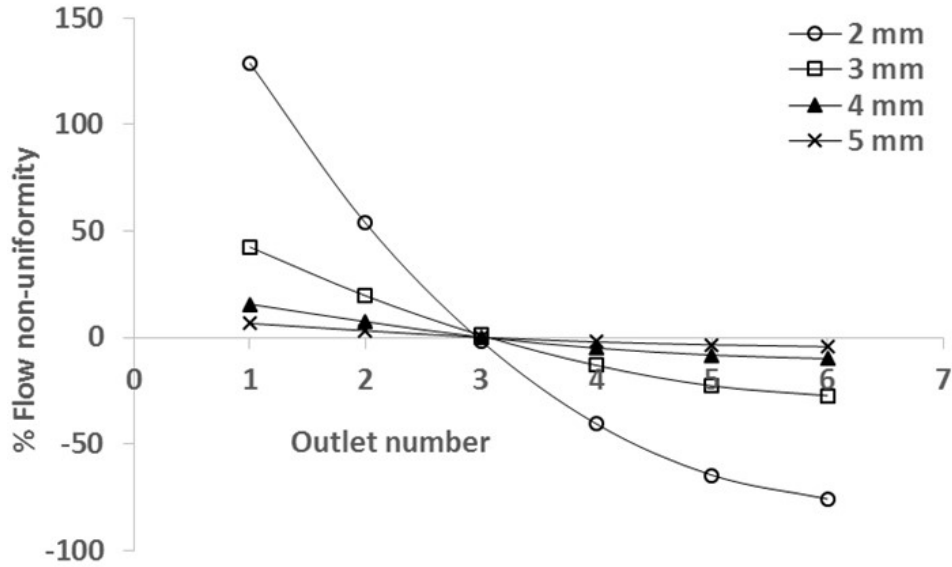


Figure 5.8: Effect of inlet channel diameter on % flow non-uniformity
 ($D_m = 2 \text{ mm}$, $Q_T = 3 \text{ LPH}$, $L = 30 \text{ mm}$)

5.3.4 Effect of the outlet channel diameter

Simulations were carried out to study the effect of the diameter of the outlets on flow distribution. Fig.5.9 shows the results of these simulations. It shows that as the diameter of the outlets is reduced, flow distribution becomes more uniform.

For a fixed total flow rate, a reduction in the diameter of the outlet channels increases the pressure drop in the outlet channels due to increase in the velocity and reduction in diameter. The pressure drop in the inlet channel remains constant as there is no change in the inlet flow rate and inlet channel diameter. A reduction in the outlet channels diameter for a constant total flow rate thus results in lower ratio of the pressure drop in the inlet channel to the outlet channels and thus leads to lower flow non-uniformity.

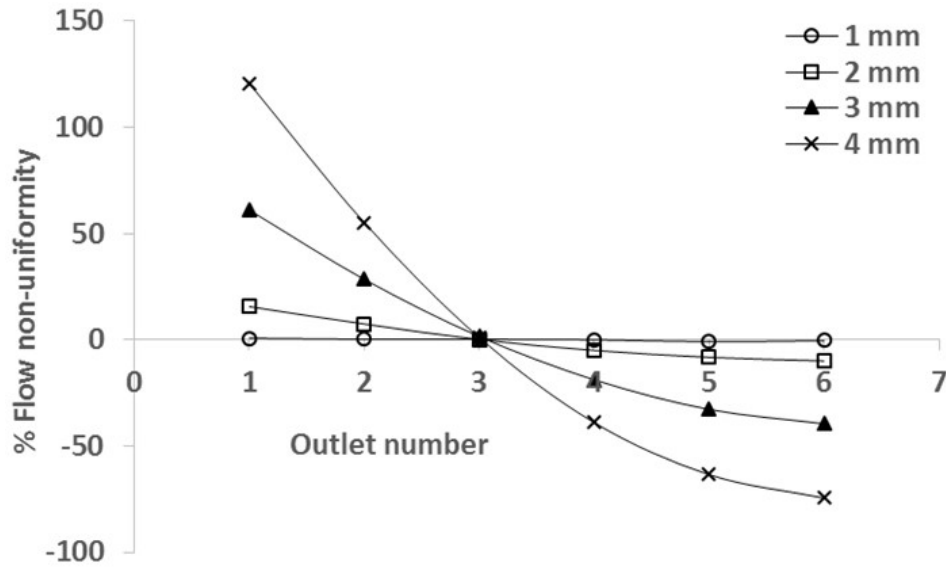


Figure 5.9: Effect of outlet channel diameter on % flow non-uniformity
 ($D_h = 4$ mm, $Q_T = 3$ LPH, $L = 30$ mm)

5.3.5 Effect of distance between outlet channels

Fig. 5.10 shows the effect of the distance between the outlet channels of MDIMJ on % flow non-uniformity. As the distance between the outlets increases, % flow non-uniformity increases. As the distance between the outlet channels increases, the total length of the inlet channel also increases. Assuming that the pressure gradient in the inlet channel remains constant, an increase in the distance between the outlet channels increases the difference of the pressure at the roots of two consecutive outlet channels. This leads to higher flow non-uniformity.

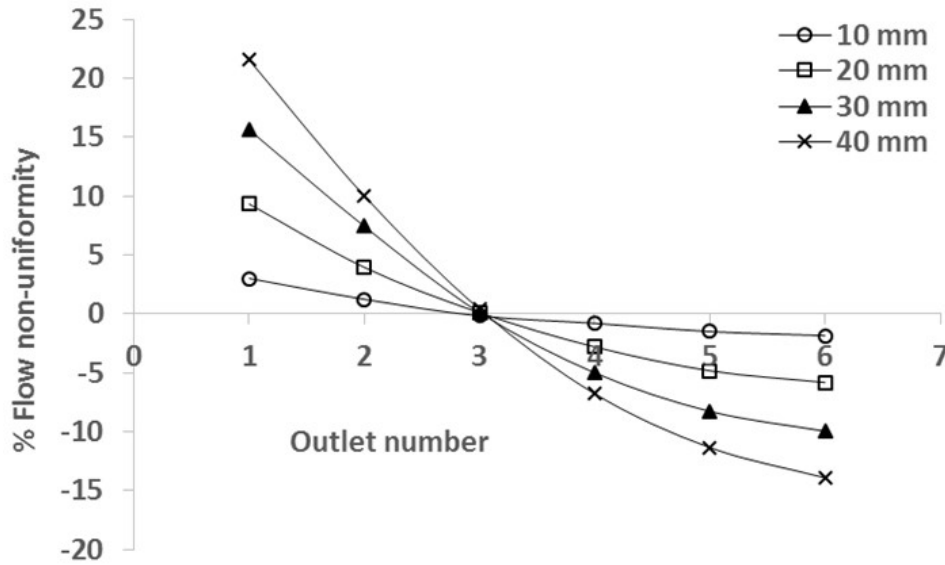


Figure 5.10: Effect of the distance between the outlet channels on % flow non-uniformity ($D_h = 4$ mm, $D_m = 2$ mm, $Q_T = 3$ LPH)

5.3.6 Effect of pressure imbalance at the outlets

Usually the microbore tubes connected to a MDIMJ will be identical (the same length and the same diameter). However, after prolonged operation, one or more tubes may get partially or fully choked leading to pressure imbalance at the outlets. This possible condition of pressure imbalance is modeled by assigning different pressure values at the outlets of the MDIMJ. Two simulations are carried out, one for outlet diameter of 1 mm and the other for outlet diameter of 2 mm. The outlet number and corresponding pressure values at the outlets are listed in [Table 5.2](#). [Fig. 5.11](#) and [5.12](#) show the results for the case of 1 mm outlet diameter and 2 mm outlet diameter, respectively. [Fig. 5.11](#) shows that for the MDIMJ having 1 mm outlet diameter, % flow non-uniformity due to pressure imbalance at the outlet increases up to $\pm 5\%$. But the same pressure imbalance for the MDIMJ having 2 mm outlet diameter causes % flow non-uniformity to increase up to $\pm 60\%$, as shown in [Fig. 5.12](#). This shows that pressure

imbalance has minor effect on flow non-uniformity for an MDIMJ with smaller outlet diameter than an MDIMJ with larger outlet diameter.

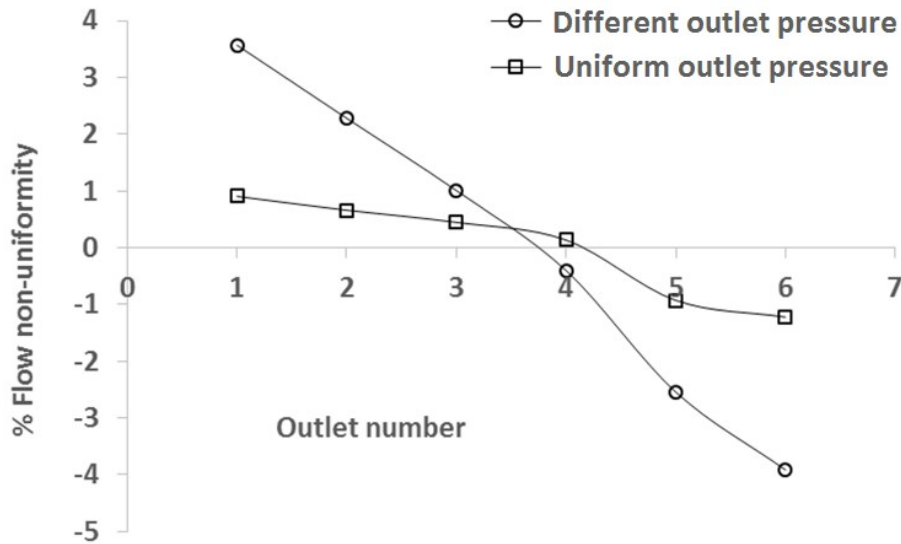


Figure 5.11: Effect of outlet pressure imbalance on % flow non-uniformity
($D_h = 4$ mm, $D_m = 1$ mm, $Q_T = 3$ LPH, $L = 30$ mm)

Table 5.2: Outlet pressures used in the simulations to study the effect of pressure imbalance at the outlets on flow distribution by an MDIMJ

Outlet number	1	2	3	4	5	6
Pressure (Pa)	0	3.07	6.13	9.2	12.27	15.33

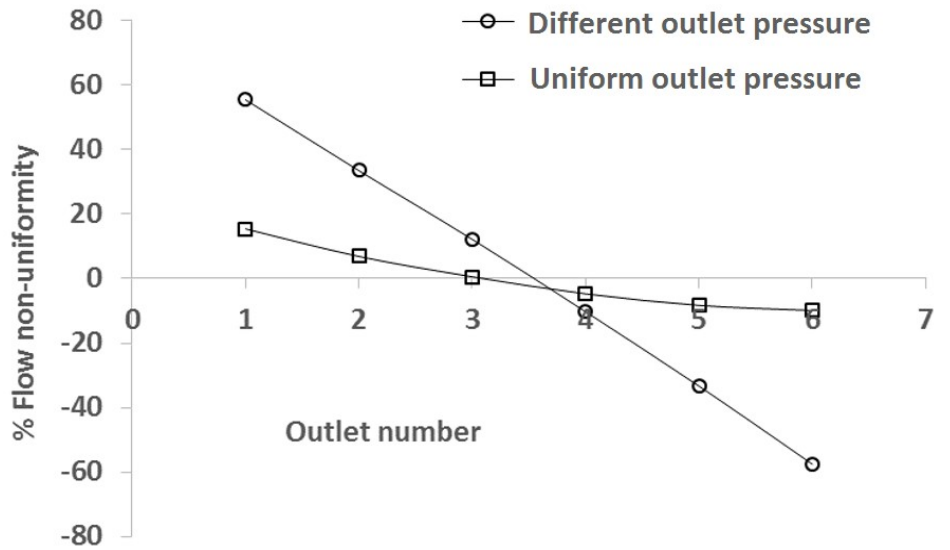


Figure 5.12: Effect of outlet pressure imbalance on % flow non-uniformity
 ($D_h = 4$ mm, $D_m = 2$ mm, $Q_T = 3$ LPH, $L = 30$ mm)

5.3.7 Selection of final design

The simulations of the MDIMJ show the effects of various geometrical and operating parameters on flow non-uniformity. This knowledge can be used as a guideline for design of the MDIMJ. For this study, the target throughput is 3 LPH. Inlet channel diameter is selected as 4 mm, as Fig. 5.8 shows that at 3 LPH good flow distribution is achieved up to 4 mm inlet diameter. Inlet channel diameter more than 4 mm increases the inventory of the liquid in the distributor which is not desirable. Inlet channel diameter less than 4 mm adversely affects the flow distribution, as observed in Fig. 5.8. Fig. 5.9 shows that as the outlet channel diameter is reduced, flow becomes more uniform. For 1 mm or lesser diameter of the outlet channels, flow distribution is very good. Thus 750 μm (0.75 mm) is chosen as the outlet channel diameter as it is less than 1 mm and it allows us to have microfluidic junctions for generating the dispersion. Fig. 5.10 shows that as the distance between the outlet channels reduces, the flow distribution becomes more uniform. Therefore, in the MDIMJ the distance

between the outlet channels has been kept 10 mm which is minimum among the designs evaluated by CFD. It is not possible to further reduce the distance, as it will create difficulty in putting the threaded connectors which are required to join the microbore tubes to the microfluidic junctions. Thus, the conceptualized and fabricated design of MDIMJ has 4 mm inlet channel diameter, 0.75 mm outlet channel diameter and 10 mm distance between the outlets. The CFD simulation of the final design was also carried out and validated with the experimental data for flow distribution obtained from the actual fabricated MDIMJ. Flow rate at each outlet and hence % flow uniformity at each outlet is experimentally measured. As shown in Fig. 5.13, the simulation results shows uniform flow across the outlets with % flow non-uniformity at each outlet less than 1%. The experimental results show that flow non-uniformity at each outlet is within $\pm 2\%$ which is very close to the predictions of the simulation.

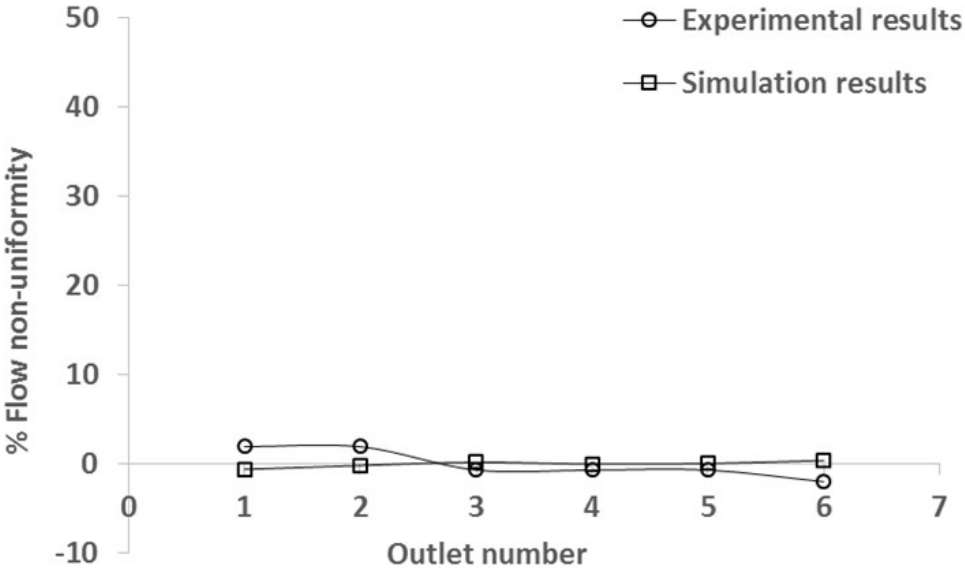


Figure 5.13: Comparison of experimentally measured flow non-uniformity with predicted flow non-uniformity ($D_h = 4$ mm, $D_m = 0.75$ mm, $Q_T = 3$ LPH, $L = 10$ mm)

5.4 SOLVENT EXTRACTION USING MDIMJ AT 3 LPH

5.4.1 Experimental setup

The fabricated MDIMJ is used for solvent extraction in parallel microbore tubes. The schematic diagram of the experimental setup is shown in Fig. 5.14. The aqueous phase containing 720 ppm of uranium and the organic phase containing 30% TBP in dodecane are pumped using precision piston pumps. Flow distribution and dispersion is achieved at microfluidic cross T-junction housed in the MDIMJ. Residence time for mass transfer is provided by the microbore tubes connected to the outlets of the MDIMJ. The other ends of the microbore tubes are connected to a settler made of acrylic. The MDIMJ and the settler are shown in Fig. 5.15. Settler is 1 cm wide, 4 cm high and 7 cm long. The settling area is thus 7 cm². The aqueous phase sample is analyzed for uranium concentration using inductively coupled plasma atomic emission spectrometer ICP-AES (Model: ULTIMA-2, Make: Jobin Horiba, France).

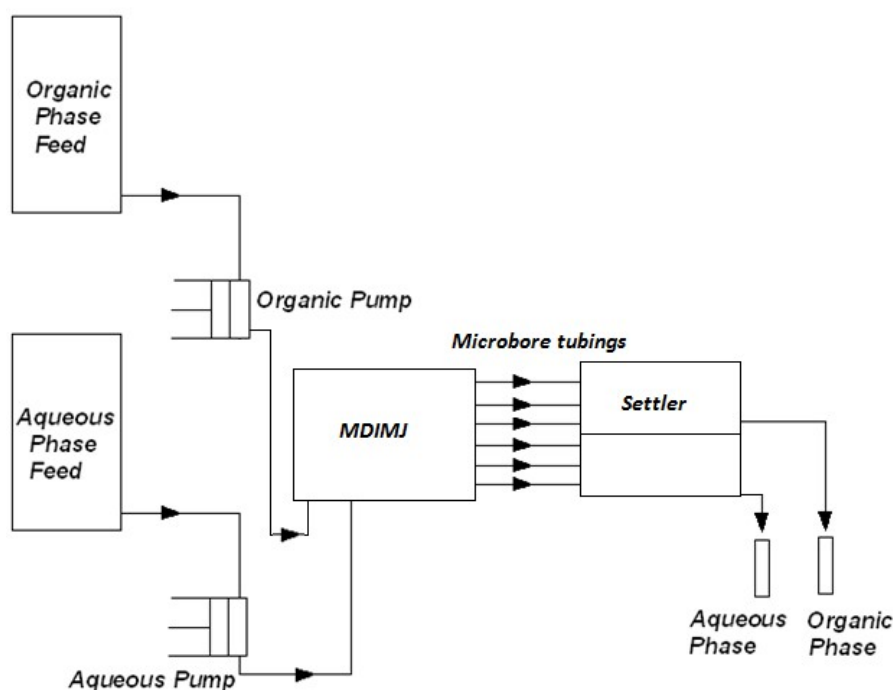


Figure 5.14: Schematic diagram of the experimental setup used for solvent extraction at total throughput of 3 LPH by using MDIMJ

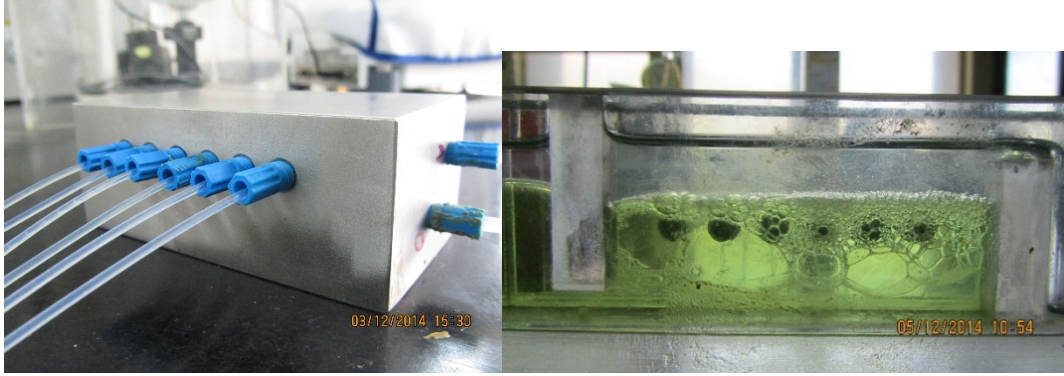


Figure 5.15:The MDIMJ (left) and the settler (right)

5.4.2 Calculations

Eqs. (5.2 – 5.8) are used to quantify the experimental results. Eq. (5.2) is used for calculating specific settling rate (SSR). Here Q_D is the dispersed phase flow rate and A_S is the settling area. Eqs. (5.3-5.5) are used for calculating average total flow rate, average aqueous phase flow rate and average organic flow rate in each microbore tube, respectively. Here Q_T is total flow rate, Q_T^{Avg} is the average total flow rate, Q_A^{Avg} is the average aqueous phase flow rate, Q_O^{Avg} is the average organic phase flow rate. Eqs. (5.6-5.8) represent percentage aqueous flow non-uniformity (AFNi), percentage organic flow non-uniformity (OFNi) and percentage total flow non-uniformity (TFNi) for individual outlet. Here $Q_{A,i}$ is aqueous phase flow rate in i^{th} outlet of the MDIMJ, $Q_{O,i}$ is organic phase flow rate in the i^{th} outlet of the MDIMJ, $Q_{T,i}$ is the total flow rate in the i^{th} outlet of the MDIMJ.

$$SSR = \frac{Q_D}{A_S} \quad (5.2)$$

$$Q_T^{Avg} = \frac{Q_T}{6} \quad (5.3)$$

$$Q_A^{Avg} = \frac{Q_T^{Avg}}{\left(1 + \frac{O}{A}\right)} \quad (5.4)$$

$$Q_O^{Avg} = \frac{Q_T^{Avg}}{\left(1 + \frac{A}{O}\right)} \quad (5.5)$$

$$AFNi = \frac{Q_{A,i} - Q_A^{Avg}}{Q_A^{Avg}} \times 100 \quad (5.6)$$

$$OFNi = \frac{Q_{O,i} - Q_O^{Avg}}{Q_O^{Avg}} \times 100 \quad (5.7)$$

$$TFNi = \frac{Q_{T,i} - Q_T^{Avg}}{Q_T^{Avg}} \times 100 \quad (5.8)$$

5.4.3 Flow distribution

Initial experiments were conducted to study performance of the MDIMJ for flow distribution for 3 LPH inlet total flow rate. In these experiments dispersion coming from 6 outlets is collected in sample bottles for a fixed interval of time as shown in [Fig. 5.16](#). The dispersion is then allowed to disengage into two clear phases. The sample volumes are then measured. [Table 5.3](#) summarizes the results of the experiments conducted to check the flow distribution. As can be observed, the total non-uniformity in flow distribution is less than $\pm 5\%$ which is acceptable.

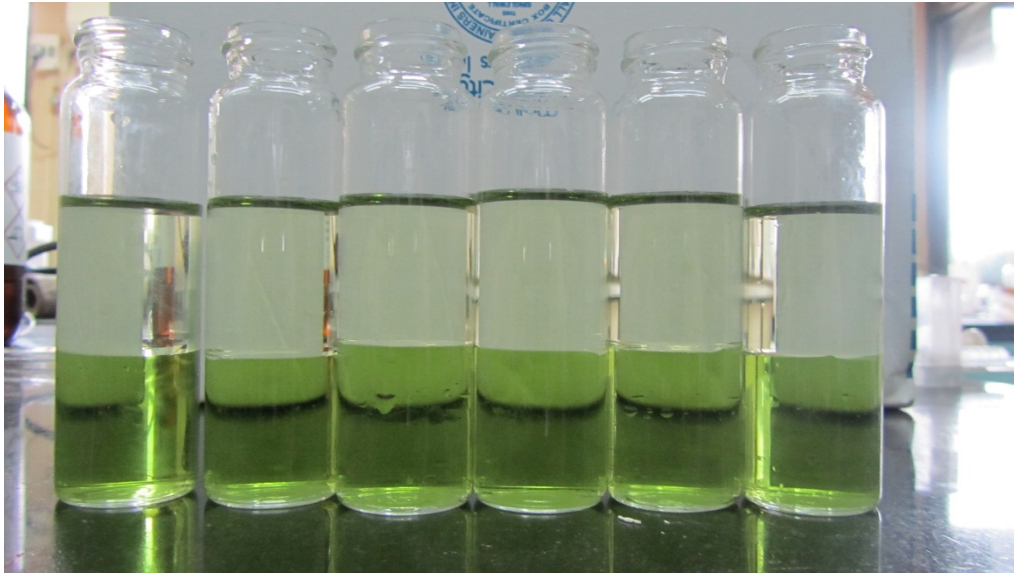


Figure 5.16: Samples collected at each outlet during a fixed interval of time to check the flow distribution by the MDIMJ

Table 5.3: Flow non-uniformity in the MDIMJ at O/A=1/1

Outlet No.	1	2	3	4	5	6
AFNi	-2.19	-4.57	4.97	0.20	0.20	1.39
OFNi	-2.19	2.58	-4.57	4.97	4.97	-5.77
TFNi	-2.19	-0.99	0.20	2.58	2.58	-2.19
O/A	1.00	1.08	0.91	1.05	1.05	0.93

5.4.4 Solvent extraction experiments

[Fig. 5.17](#) shows the effect of flow rate on percentage efficiency and percentage extraction. As observed from [Fig. 5.17](#), at O/A=1/1, for all flow rates percentage extraction is between 75 – 85% and percentage efficiency is between 80 to 95%. The MDIMJ thus ensures fast mass transfer. Besides fast mass transfer, fast settling was also observed for all flow rates covered in [Fig. 5.17](#).

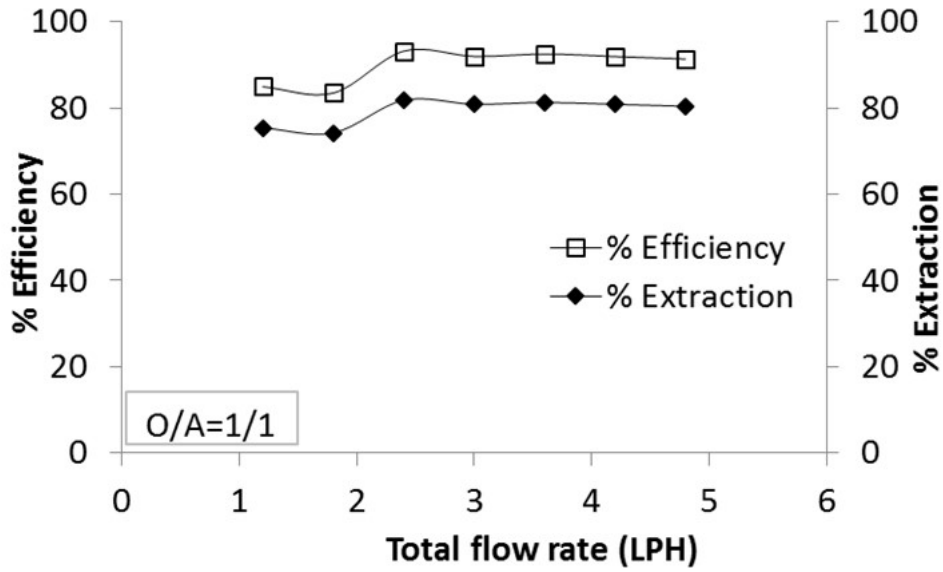


Figure 5.17: Effect of flow rate on percentage efficiency and percentage extraction (O/A=1/1)

Table 5.4 shows that at 4.8 LPH total flow rate percentage extraction is 80.4% and percentage efficiency is 91.3%. Residence time in microchannels is less than 3 s and total residence time (including the residence time in the settler) is about 16 s. The SSR at $3.4 \text{ m}^3 \text{ h}^{-1} \text{ m}^{-2}$ is also high at this flow rate.

Table 5.4: Effect of flow rate on percentage efficiency and percentage extraction at O/A=1/1

Q_T (LPH)	τ_m (s)	τ_s (s)	τ (s)	PE	% η	SSR ($\text{m}^3 \text{ h}^{-1} \text{ m}^{-2}$)
1.2	11.30	52.50	63.80	75.4	84.9	0.9
1.8	7.54	35.00	42.54	74.2	83.4	1.3
2.4	5.65	26.25	31.90	81.8	93.2	1.7
3.0	4.52	21.00	25.52	80.9	91.9	2.1
3.6	3.77	17.50	21.27	81.3	92.5	2.6
4.2	3.23	15.00	18.23	82.3	93.8	3.0
4.8	2.83	13.13	15.95	80.4	91.3	3.4

Fig. 5.18 shows the effect of total flow rate on overall volumetric mass transfer coefficient in MDIMJ. Overall volumetric mass transfer coefficient increases with increase in flow rate. This increase in $K_L a$ with increase in flow rate can be attributed to increase in specific interfacial area due to generation of fine dispersion due to increase in flow rate. Also due to increase in velocity, mass transfer coefficients also increase. These two factors cause the overall volumetric mass transfer coefficient, which is product of mass transfer coefficient and specific interfacial area, to increase with increase in flow rate. Overall volumetric mass transfer coefficient obtained in the MDIMJ based setup is an order of magnitude higher than in conventional solvent extraction equipment such as mixer-settler (1×10^{-2} to 2×10^{-2}), packed column (3×10^{-4} to 6×10^{-3}), tray column (5×10^{-3} to 7×10^{-2}), liquid-liquid-solid fluidized bed (7×10^{-3} to 1×10^{-2}), and spray and packed columns (5×10^{-4} to 1×10^{-2}) (Darekar et al., 2014c).

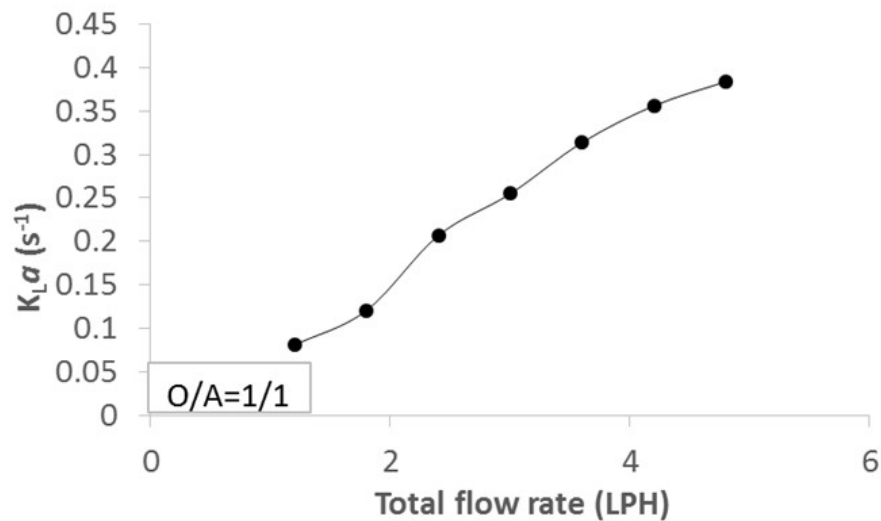


Figure 5.18: The effect of flow rate on overall volumetric mass transfer coefficient

5.5 TWO-STAGE SOLVENT EXTRACTION AT 10 LPH USING MDIMJ

5.5.1 Experimental setup

The schematic of the MDIMJ used for solvent extraction at 20 LPH total throughput in parallel microbore tubes is shown in Fig. 5.19. The diameter of the inlet channels is 4 mm. Each inlet channel feeds 20 microchannels having 500 μm diameter each. The microchannels fed by the two inlet channels are connected perpendicularly to form microfluidic opposed T-junctions. The dispersion is generated at these microfluidic T-junctions of 500 μm diameter. Microbore tubes are connected at the outlets of the opposed T-junctions. Various dimensions of the MDIMJ are shown in Fig. 5.19. Fig. 5.20 shows the actual photographs of the MDIMJ used in the experiments.

Schematic diagram of the setup for two-stage micro-scale solvent extraction is shown in Fig. 5.21. Each stage consists of two peristaltic pumps, a monoblock distributor with in-built microfluidic junction (MDIMJ), twenty parallel microbore tubes connected to MDIMJ and a gravity settler. The aqueous and the organic phases are fed to the MDIMJ. Dispersion generated at the outlets of the MDIMJ is passed through 20 PTFE microbore tubes (800 μm ID and 70 cm long) the other ends of which are connected to a gravity settler where phase separation takes place. As shown in Fig. 5.19, the aqueous phase is fed to the MDIMJ by inlet2 and the fresh organic phase is fed to the MDIMJ by inlet 1. The aqueous and the organic phases coming out of the settler are fed to the next MDIMJ using peristaltic pumps. As shown in Fig. 5.21, overall counter-current contact of the aqueous and the organic phase is achieved.

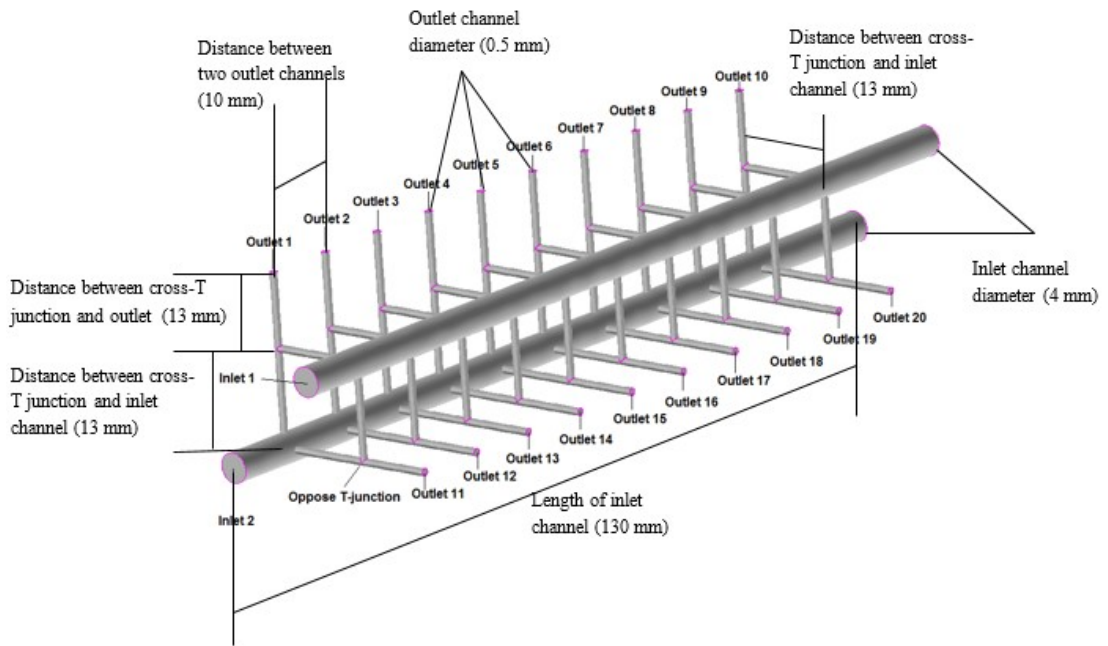


Figure 5.19: Schematic diagram of a MDIMJ

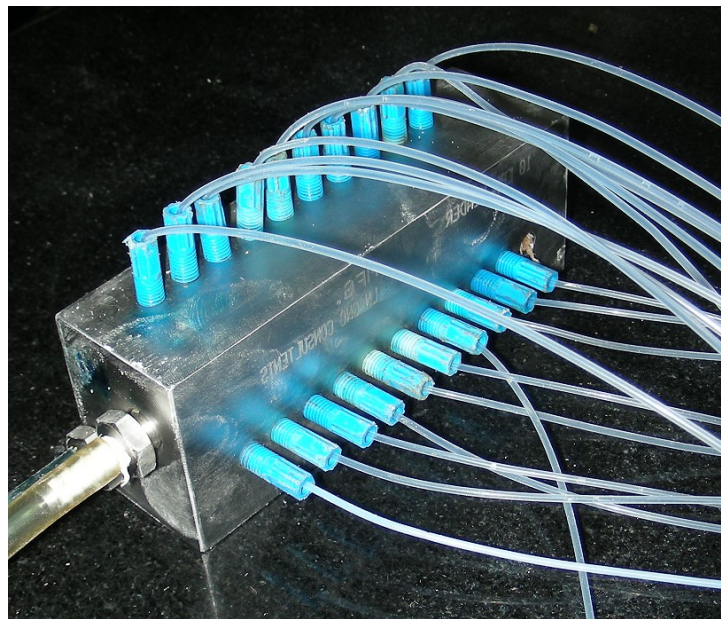


Figure 5.20: The MDIMJ with 20 microbore tubes connected to it

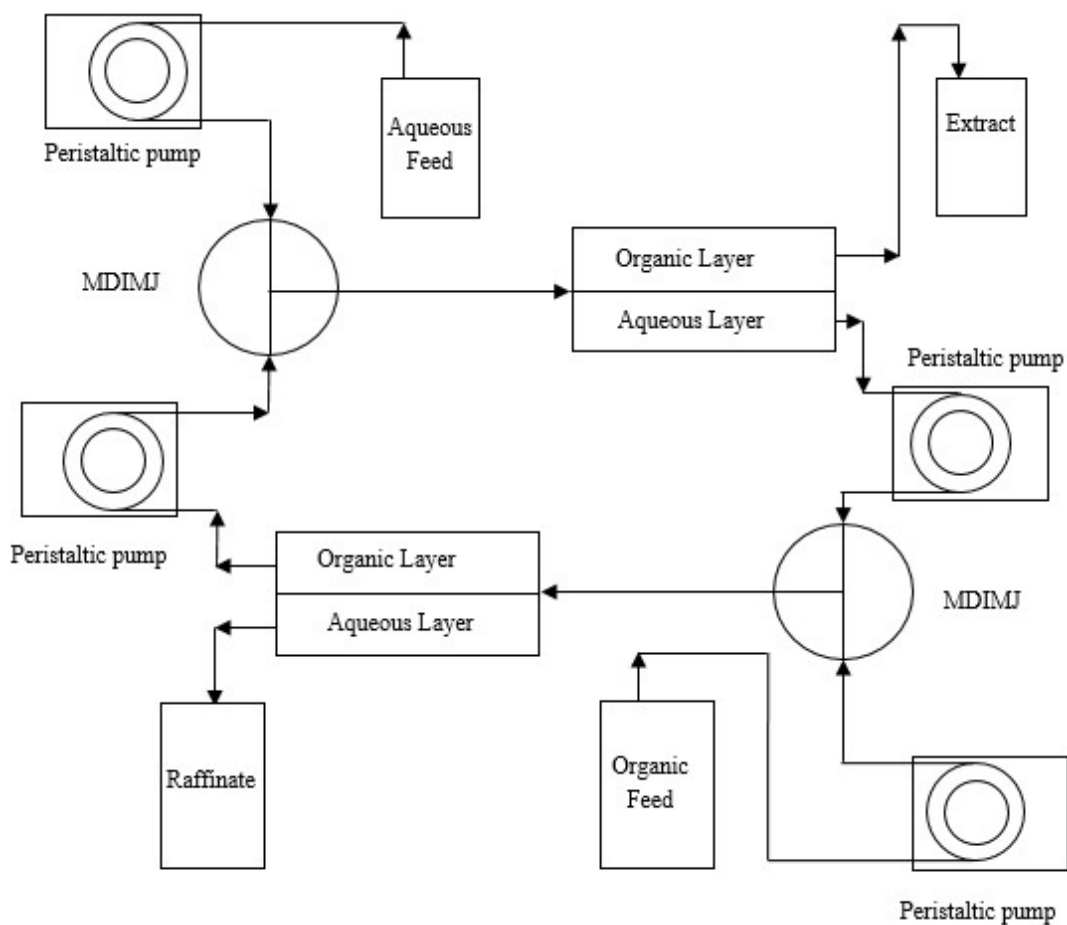


Figure 5.21: The schematic of two-stage microfluidic solvent extraction

5.5.2 Solvent extraction experiments

The target total flow rate is 10 LPH which is achieved by using 20 parallel microbore tubes such that each tube handles 0.5 LPH. To distribute organic and aqueous phases equally into 20 parallel microbore tubes, a monoblock distributor with in-built microfluidic junctions (MDIMJ), which has been reported in previous section, is used. The microfluidic junctions of the MDIMJ generate liquid-liquid dispersion to feed 20 parallel microbore tubes. Extraction of uranium takes place inside the microbore tubes. Both single-stage and two-stage micro-scale extraction and stripping at 10 LPH are demonstrated. Extraction of uranium from the aqueous phase containing 550 ppm uranium in 1 M HNO_3 is carried out by the organic phase consisting 30% (v/v) TBP in

dodecane. The extract phase consisting of 330 ppm uranium resulting from the extraction experiments is used as the feed for the stripping experiments. Stripping is carried out by DM water. Peristaltic pumps are used for pumping the liquid phases. The schematic diagram of the setup for two-stage extraction is already shown in Fig. 5.21. Table 5.5 summarizes the results of single-stage and two-stage extraction and stripping at 10 LPH. Table 5.5 shows that by using two stages instead of a single stage, percentage extraction as high as 90% can be achieved. Similarly two-stage stripping is found to be more effective than single-stage stripping. It may be noted that the contact time in the mixer (microbore tubes) is less than 3 s. For conventional single stage mixer-settler, residence time is of the order of 2- 3 minutes in mixer. Thus contact time required in microbore tube is much smaller than the conventional mixer-settler.

Table 5.5:Extraction and stripping studies in parallel microbore tubes at 10 LPH
($\tau_m=2.23$ s, $\tau_s=129$ s)

	C_A^{in} (ppm)	C_O^{in} (ppm)	O/A	C_A^{out} (ppm)	C_O^{out} (ppm)	PE	PS
Two-stage extraction	550	0	1.4	52.58	355	90	-
Single-stage extraction	550	0	1.4	205.6	246	63	-
Two-stage stripping	0	330	1	263.7	66.3	-	80
Single-stage stripping	0	330	1	142.3	188	-	43

5.6 CONCLUSIONS

Following are the conclusions emanating from this study.

- 1) In the first set of experiments scale-up has been achieved using Y-junction flow distributors using structural bifurcation. Microbore tube having the optimum configuration has been replicated in two parallel paths to demonstrate solvent extraction at total capacity of 1 LPH. This configuration can handle a total throughput of 1 LPH and provides 90% stage efficiency in contact time of about 11 seconds for O/A=1/1 in microbore tube.
- 2) A compact distributor with 6 outlets, which also houses microfluidic cross T-junctions has been conceptualized and designed using the insights obtained from CFD simulations. This distributor named as Monoblock Distributor with In-built Microfluidic Junctions (MDIMJ) is found to give very good two-phase flow distribution among 6 parallel microbore tubes with flow non-uniformity less than $\pm 5\%$.
- 3) In the second set of experiments carried out using the MDIMJ with 6 outlets at throughput of 3 LPH, simulated lean stream having 720 ppm of U(VI) concentration has been used as the aqueous phase. High stage efficiency (above 90% in most cases) in short contact times (in most cases less than 10 seconds) could be achieved for O/A ratio 2/1 and 1/1 and 1/2. The contact time required for high stage efficiency is much shorter than typically provided in conventional contactors such as mixer-settlers. Maximum value of $K_L a$ obtained is 0.4 s^{-1} which is at least an order of magnitude higher than $K_L a$ values obtained in conventional contactors. This shows the process intensification achieved by using micro-scale

extraction. SSR as high as $3.4 \text{ m}^3 \text{ h}^{-1} \text{ m}^{-2}$ has been realized which shows fast settling of dispersion generated at the microfluidic junctions of the MDIMJ.

- 4) In the third set of experiments carried out using MDIMJ with 20 outlets, higher throughput (total 10 LPH) counter-current micro-scale solvent extraction was demonstrated by using 20 parallel microbore tubes. About 90% extraction of uranium was achieved in two-stage micro-scale extraction with contact time in microbore tube of about less than 3 s which is much smaller than provided in conventional mixer (2 – 3 minutes).
- 5) These experiments demonstrate the possibility and ease of scale-up of microscale solvent extraction by following numbering up approach and using novel design of compact distributors. MDIMJ used in this study are compact and better than distributors with structural bifurcations for numbering up.

CHAPTER 6

METALLIC MESH BASED DEVICES FOR IN-LINE PHASE SEPARATION OF MICROFLUIDIC DISPERSION

6.1 INTRODUCTION

The prerequisite for a solvent extraction equipment to be suitable for deployment in the back-end of the nuclear fuel cycle is that it should not have moving parts as maintenance is difficult in high radiation environment. Another requirement which assumes importance during recovery of value material from high burn-up nuclear fuels is that the contact time in the solvent extraction equipment should be as small as possible to avoid the degradation of solvent which is used for extraction. None of the available types of contactors can meet both the requirements (Wang et al., 2019). For example, centrifugal extractor, which can significantly reduce the contact time and thus avoids solvent degradation, is considered suitable for high burn-up fuels (Natarajan and Raj, 2007). But it suffers from the disadvantage of having the parts rotating at very high speeds. Air pulsed columns which do not have moving parts typically involve large contact time and thus may be suitable for low burn-up fuels but not suitable for high burn-up fuels. Thus the quest for having an extractor which can meet both the requirements is still relevant.

Liquid-liquid dispersion coming out from a microfluidic contactor needs to be separated into clear phases. Different methods can be used for separation of dispersion such as gravity settler which working on the principle of density difference (Kumar et al., 2017), separation based on difference in wettability (Bannock et al., 2013; Castell et al., 2009; Cervera-Padrell et al., 2012; Holbach and Kockman, 2013; Kralj et al.,

2007; Weeranoppanant et al., 2017) and retardation of flow (Bremond et al., 2008).

Typically the residence time in such phase separators is either very high or the flow rates handled are much less ($\sim 10^{-2}$ mL/min). Thus, a phase separator that can work for larger flow rates (total flow rates of the order of 20 mL/min) and can separate phases in very short contact time need to be designed for use along with a microfluidic contactor. The earlier chapters focused on intensification of mass transfer by using a microfluidic contactor. However, the settler used was gravity settler. This chapter focuses on intensification of settling process. In this chapter, a metallic mesh based device has been used as in-line phase separator for separating the dispersion generated in a microfluidic contactor.

The separator comprises of two flow channels. A metallic mesh of 5 μm pore size separates the two flow channels. The upper flow channel receives the dispersion from the microcontactor. Dispersion generated in microchannel is nearly of uniform size higher than pore size of mesh. The metallic mesh is hydrophobic in nature which is reported by Willersinn and Bart (2015) also. In the microchannel that precedes the phase separator, the organic phase is continuous phase. Thus metallic mesh preferentially allows the organic phase to pass through it preventing dispersed phase (aqueous phase) droplets which have size larger than the mesh pore size to pass through. The continuous phase permeates to the lower flow channel through the mesh as the dispersion flows from the inlet to the outlet of the upper channel. Due to draining of continuous phase dispersed phase droplets come close to each other. They coalesce and become bigger in size. At the end of upper channel all continuous phase is drained out and only dispersed phase is remaining. Dispersed phase in upper channel is prevented to flow from upper channel to lower channel due to capillary

pressure higher than pressure difference across two channel due to small pore size of mesh and wettability factor. Thus the clear continuous phase and clear dispersed phase are obtained from the outlets of the lower flow channel and upper channel, respectively. Thus phase separation depends on wetting properties of fluids. Polymeric membrane are subjected to degradation when radiation is present hence metallic mesh is selected in this study

The experiments have been conducted to understand the effects of operating parameters (flow rates of the aqueous and the organic phases), flow channel geometry and mesh properties (pore size and thickness) on the performance of the in-line phase separator. After identifying the operating window in which good phase separation is observed, mass transfer experiments are also performed after connecting the microcontactor with the in-line phase separator.

The focus of this study is in-line phase separation of microfluidically generated liquid-liquid dispersion. That is the reason most of the chapter deals with understating the effects of different variables on the performance of in-line phase separator. However, in actual practice the inline phase separator will always be used along with a microfluidic contactor (microbore tube) that will ensure mass transfer. Considering this, the mass transfer part is included in this chapter just to demonstrate the working of inline phase separator along with the microfluidic contactor. The mass transfer study is thus not comprehensive. The mass transfer in microbore tubes has been reported extensively in our previous chapters.

6.2 EXPERIMENTAL STUDY

6.2.1 Metallic mesh based device

The metallic mesh based device is similar to the one reported in a previous study (Willersinn and Bart, 2015). The exploded view of the device is shown in Fig. 6.1. The device has two identical flow channels cut in PTFE sheets named as upper channel plate and lower channel plate. A mesh of stainless steel (named as mesh structure in Fig. 6.1) is sandwiched between these flow channels. The flow channels along with the metallic mesh are kept between two acrylic plates. The device is made leak tight when this assembly along with a metallic upper base plate and lower base plate are fastened together. The inlet and the outlet of the flow channel in the upper channel plate are provided by drilling holes in the acrylic plate fitted in the upper base plate. Similarly the inlet the and outlet of the flow channel in the lower channel plate are provided by drilling hole in the acrylic plate fitted in the lower base plate. The length of the flow channels was varied by varying the number of bends (straight channel of 90 mm length, 2-bend channel of 355 mm length and 6-bend channel of 535 mm length) in the flow channel. The metallic mesh and three different flow channels used in the experiments are shown in Fig. 6.2.

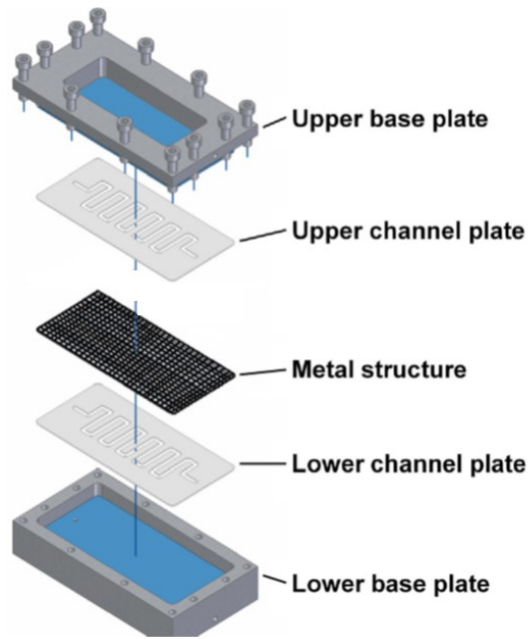


Figure 6.1: Metallic mesh based device ([Willersinn and Bart, 2015](#))

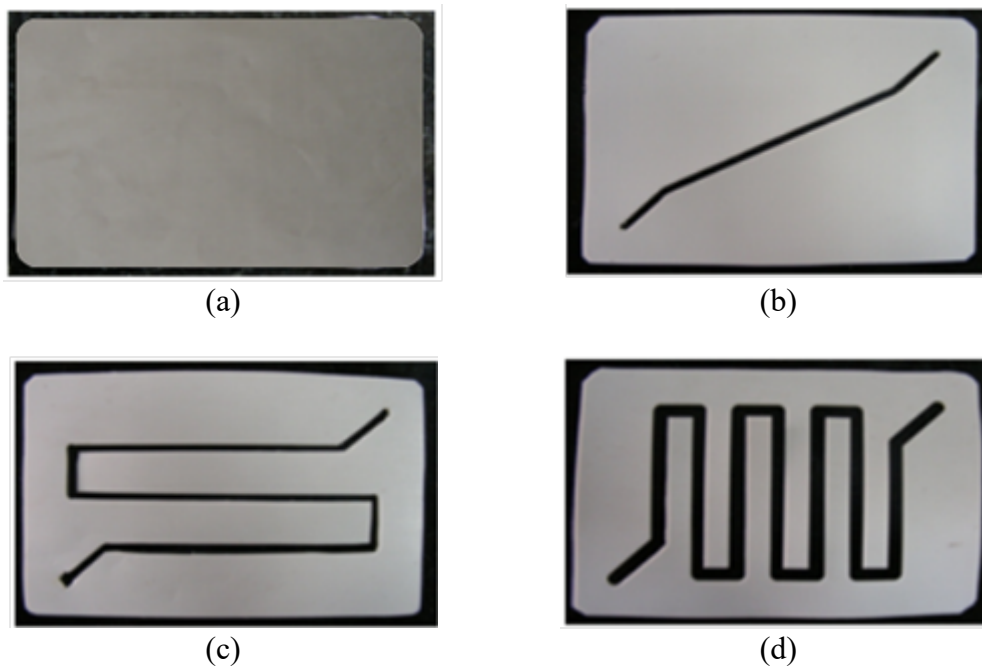


Figure 6.2: (a) Metallic mesh, (b) straight flow channel, (c) flow channel with two-bends and (d) flow channel with 6 bends

6.2.2 Setup for in-line phase separation

The experiments for in-line phase separation were conducted in two parts. The first part comprised of the experiments on hydrodynamics with the objective of identifying the operating window of complete phase separation for different operating conditions and configurations of the in-line phase separator as reported in [section 6.3](#). The second part of the mass transfer experiments within the operating window in which complete phase separation is observed. Mass transfer experiments are reported in [section 6.4](#). The schematic diagram of the in-line phase separator and the experimental setup are shown in [Fig. 6.3](#). The setup comprises of a microfluidic T-junction (diameter 400 μm) having a microbore tube (diameter 800 μm , length 7 m) connected to it on the downstream side. The other end of the microbore tube is connected to the in-line phase separator. In all the experiments, the organic phase comprised 30% (v/v) TBP in n-dodecane. In the first part of the experiments, the aqueous phase was 1 M nitric acid. In the second part of the experiments the aqueous phase comprised 700 ppm uranyl nitrate solution of 1 M acidity. The aqueous phase used in the second part of the experiments was prepared from the aqueous phase used in the first part of the experiments which had been equilibrated with the organic phase during the course of the experiments. The aqueous phase and the organic phase were fed to the microfluidic junction at the desired flow rates using syringe pumps. Since the microfluidic junction was made of PTFE, it was preferentially wetted by the organic phase and thus the aqueous phase was the dispersed phase. The microbore tube connected to the microfluidic junction provided the residence time for mass transfer in the mass transfer experiments. Phase separation occurred when the dispersion flowed through the in-line phase separator.

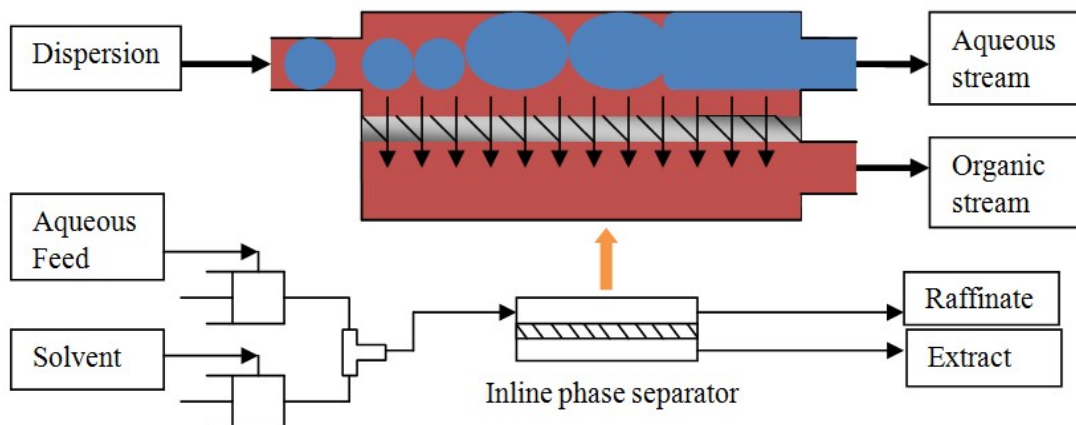


Figure 6.3: Schematic diagram of the in-line phase separator (top) and the experimental setup (below)

6.3 HYDRODYNAMICS STUDIES WITH IN-LINE PHASE SEPARATOR

6.3.1 Flow regimes

In the experiments conducted to study the in-line phase separation, flow rates were varied along with other parameters. The aqueous phase and the organic phase were contacted at microfluidic T-junction. Different flow patterns resulted at different flow rates in the microbore tube connected to the T-junction. The flow patterns were observed using a microscope mounted on a high speed camera kept above the microbore tube. Different types of flow patterns observed are shown in [Fig.6.4](#).

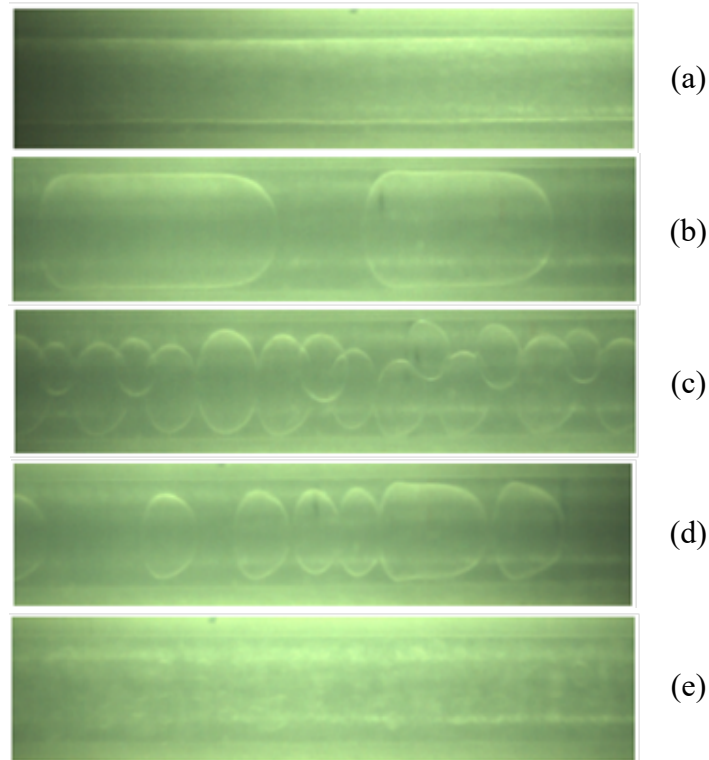


Figure 6.4: Different flow patterns observed in the experiments (a) annular flow at $Q_A = 4$ ml/min & $Q_O = 10$ ml/min, (b) slug flow at $Q_A = 4$ ml/min & $Q_O = 1$ ml/min, (c) droplet flow at $Q_A = 3$ ml/min & $Q_O = 3$ ml/min, (d) slug-droplet flow at $Q_A = 4$ ml/min & $Q_O = 5$ ml/min, (e) dispersed flow at $Q_A = 7$ ml/min & $Q_O = 10$ ml/min.

In the in-line phase separator, the dispersed phase is separated from the continuous phase with the help of metallic mesh. The dispersion is fed to the upper flow channel. The continuous phase passes through the pores of the mesh while the pores of the mesh do not allow the dispersed phase droplets, size of which is larger than the mesh size, to pass through the mesh. The droplets coalesce in the upper channel of the separator as they travel from the inlet to the outlet of the upper channel. The clear dispersed phase is obtained from the end of the upper channel. The clear continuous phase is obtained from the end of the lower channel. The working of the in-line phase separator is schematically shown in [Fig.6.3](#).

6.3.2 Effect of volumetric flow rate

The effect of flow rates on separation behavior was studied by varying the flow rates of the aqueous phase and the organic phase. The effect of flow rate on phase separation efficiency is shown in Fig. 6.5. If the total flow rate is very high, then a part of the continuous phase and all of dispersed phase are obtained from the upper channel and a part of the continuous phase is obtained from the lower channel. Thus at high total flow rates phase separation is not complete. If we compare the two cases i.e. high dispersed phase (aqueous phase) flow rate, low continuous phase (organic phase) flow rate, and low dispersed phase (aqueous phase) flow rate, and high continuous phase (organic phase) flow rate, window of complete phase separation is wider in the former case. Thus it can be concluded that the phase separator can handle higher dispersed flow rate better than higher continuous phase flow rate. As shown in Fig. 6.5 the zone of complete phase separation is below and/or on the left side the line and the zone of incomplete flow separation is above and/or on the right side of the line.

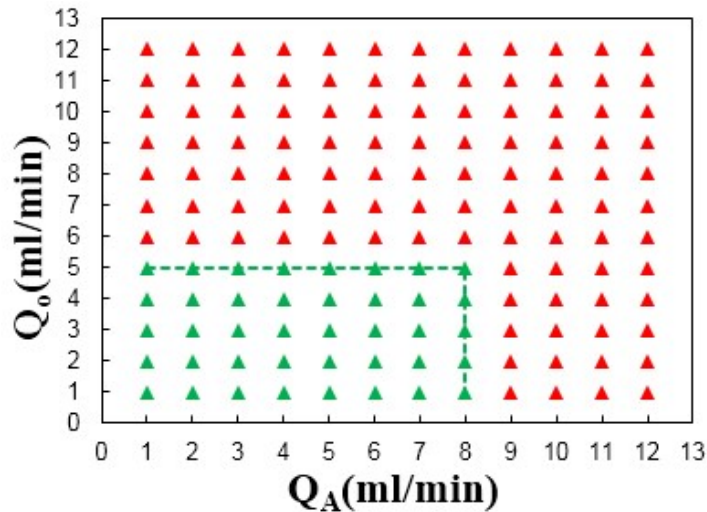


Figure 6.5: Effect of volumetric flow rate on phase separation characteristics with 100 μm thick mesh with 5 μm pore size, straight, 3 mm width and 1 mm height flow channels. (Partial separation ▲, complete separation ▲, transition line — —)

6.3.3 Effect of design of flow channels

The effect of the design of the flow channels (length and width) on in-line phase separation was also studied. For this, three different flow channel layouts, shown in Fig. 6.2, were used. The length of the flow channels was increased by altering the number of bends in the flow channel. The width of the channels was also varied. The results of the experiments conducted with the flow channels of different lengths are shown in Fig. 6.6. Fig. 6.6 shows the comparison of straight flow channels and flow channels having 2 and 6 bends for 100 μm thick metallic mesh having 5 μm pore size. Fig. 6.6 shows that with straight channels, complete phase separation could be achieved only at lower volumetric flow rates ($Q_o = 1-5$, $Q_A=1-8$ ml/min). Whereas, with the 6-bend channels the zone of complete phase separation is quite wide ($Q_o =1-10$, $Q_A =1-11$ ml/min). The zone of complete phase separation for 6-bend channels almost covered the entire range of flow rates explored in the experiments. The performance of the 2-bend flow channels for phase separation was in between that of the straight channels and 6-bend channels. This observation holds for thin (100 μm) as well as thicker (200 μm) mesh. With increase in length of the flow channels, the time as well as the area available for the continuous phase to cross the mesh increase. Thus, the zone of complete phase separation increases with increase in the length of flow channels. Also, for the same flow rate and same channel height and width, the pressure drop is more in a longer channel. Thus the pressure difference across the mesh is more for longer channels. This also helps the continuous phase to cross from the upper flow channel to the lower flow channel resulting in a wider zone of complete phase separation.

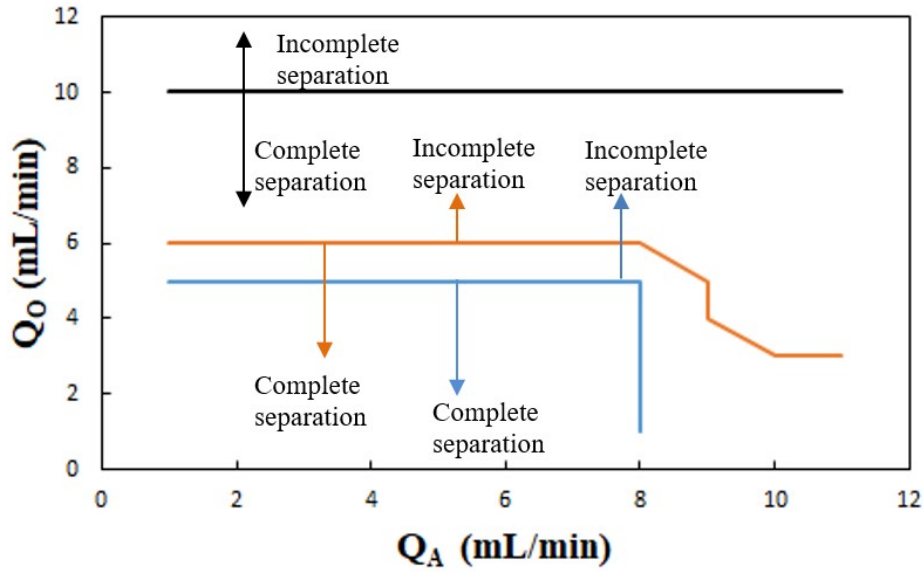


Figure 6.6: Effect of layout of the channels on phase separation characteristics. —straight channels, — 2-bend channels, — 6-bend channels. Flow channels are 3 mm wide, 1 mm in height and mesh is 100 μm thick having 5 μm pore size.

Fig.6.7 shows the effect of width of the flow channels on the zone of complete phase separation. For 200 μm thick mesh, 6-bend and 5 mm width flow channels configuration, the window of complete phase separation was not as wide as for 200 μm thick mesh, 6-bend, 3 mm width flow channels configuration. Thus despite longer residence time provided by 5 mm width channels, the zone of complete phase separation is larger in 3 mm width channels. For the same flow rate, the pressure drop in the 3 mm width channel will be more than the pressure drop in 5 mm width channel. This results in higher cross-mesh pressure in the case of 3 mm width channels than in the case of 5 mm width channels. The higher cross-mesh pressure for 3 mm width channels will help the continuous phase to pass through the mesh easily resulting in better phase separation in 3 mm width channels than in 5 mm width channels. Thus it is concluded that not only the residence time available for continuous phase to cross

the mesh, pressure drop across the mesh is also important in determining the zone of complete phase separation.

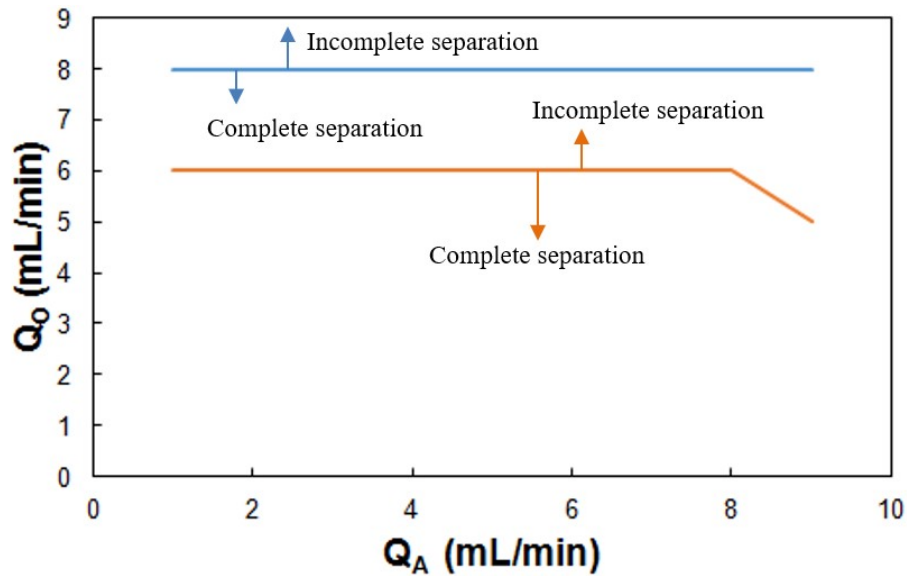


Figure 6.7: Effect of width of flow channels on phase separation characteristics- — 3 mm width channel, — 5 mm width channel. Flow channels are 6-bend channels. Height

of flow channels is 1 mm, mesh is 200 μm thick with 5 μm pore size.

It may be noted that though, for the same flow rate, the residence time and mesh area available for the continuous phase are more for 5 mm width channels than 3 mm width channels, the separation performance is better with 3 mm width channels. Thus the width of the channels is a parameter to be optimized. It is expected that on continued reduction in the width of the channels, a stage may reach in which despite rise in cross-mesh pressure with reduction in width of the channels, the effect of reduction in residence time and area of the mesh will become more important. Thus, on continued reduction in width of the channels, the zone of complete phase separation may eventually start shrinking.

6.3.4 Effect of mesh thickness

The effect of mesh thickness on phase separation was also studied. It was observed that the zone of complete phase separation reduced with increase in mesh thickness, as shown in Fig.6.8. This can be explained in terms of the resistance offered by the mesh to the continuous phase passing through it from the upper flow channel to the lower flow channel. On increasing the mesh thickness, this resistance increases and as a result it becomes difficult for the continuous phase to pass through the mesh.

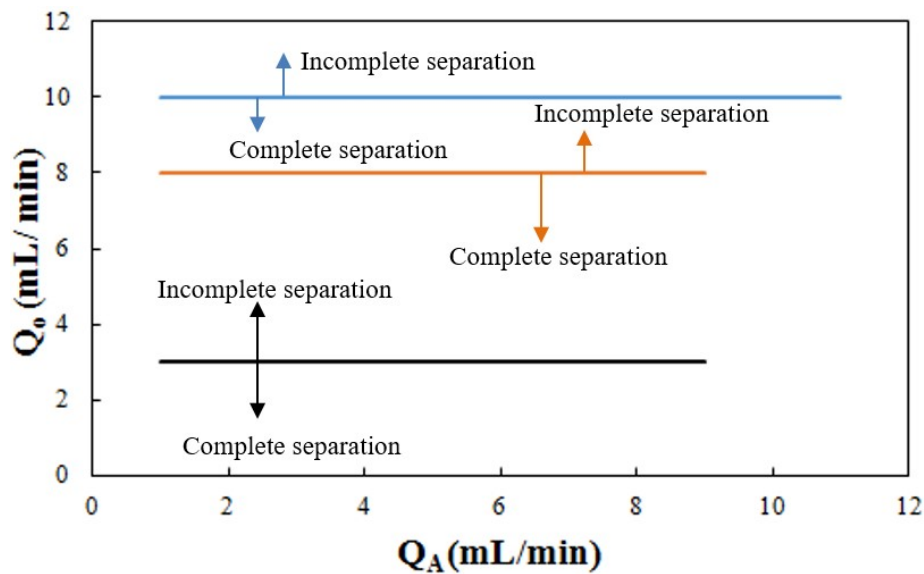


Figure 6.8: Effect of mesh thickness on phase separation——100 μm thick mesh, —200 μm thick mesh, —300 μm thick mesh. Flow channels are 3 mm wide 6-bend channels and mesh has 5 μm pore size.

6.3.5 Effect of mesh pore size

Effect of mesh pore size on phase separation was also studied and the results are shown in Fig. 6.9. For this, two different meshes having pore size of 5 μm and 500 μm were used. For larger pore size, complete phase separation was not observed at all, as continuous phase as well as dispersed phase both could cross the mesh through the larger pores. Whereas, for smaller pore size, a finite window of complete phase separation was observed. No complete phase separation for the case of larger pore size is shown by the horizontal line along the x-axis in Fig.6.9. A smaller pore size offers a larger pressure drop to the continuous phase to permeate through the mesh. A larger pore size offers less resistance. When the resistance is too high, continuous phase cannot pass through the mesh. When the resistance is too small, both continuous and dispersed phase can pass through the mesh. Thus it can be concluded that complete phase separation is achieved when the pore size is such that it neither offers too much pressure drop nor too less pressure drop across the mesh.

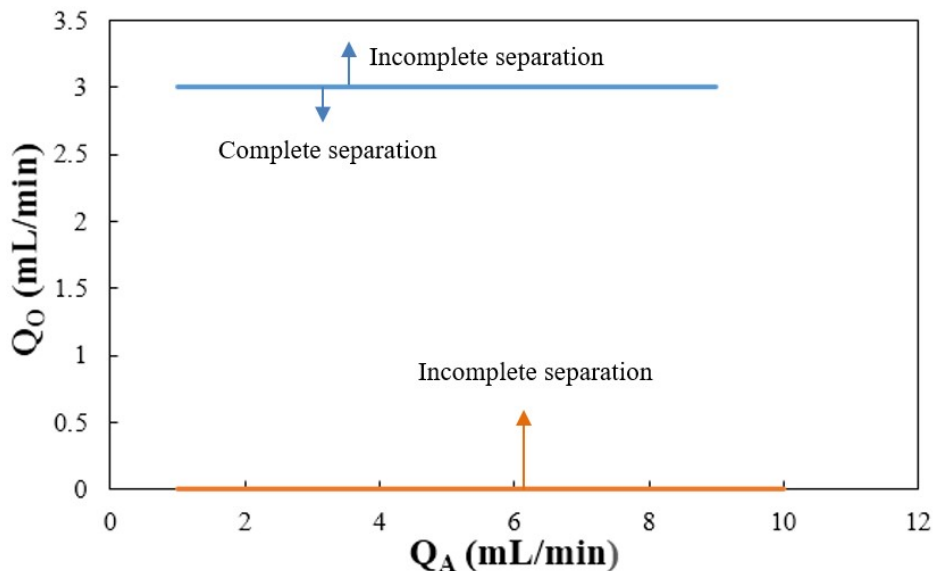


Figure 6.9: Effect of mesh pore size on phase separation— $5 \mu\text{m}$ pore size, $500 \mu\text{m}$ pore size. Flow channels are 3 mm wide 6-bend channels and mesh is 300 μm thick.

6.3.6 Effect of back pressure

The experimental results on the effects of mesh thickness and mesh pore size clearly suggest that the pressure drop across the mesh determines the ease of phase separation. Thus it should be possible to get clear phase separation by altering the pressure in one of the two flow channels separated by the mesh. To check this, the experiments were conducted with the flow channel having 6 bends along with 300 μm thick mesh. In normal configuration, the phase separation was observed in a small zone of the flow rates. However, when the height of the tip of the tube connected to the outlet of the upper flow channel was increased, complete phase separation could be achieved. This is shown in [Fig. 6.10](#). This is because, on increasing the height of the tip of the outlet tube of the upper flow channel, the pressure in the upper flow channel increases. This, in turn, increases the pressure drop across the mesh which facilitates passage of the continuous phase through the mesh even at higher flow rates. Thus the phase separation can be achieved by altering the back pressure by altering the height of the outlets. [Bannock et al. \(2013\)](#) also studied the effect of back pressure on the separation of immiscible liquids. They also observed that the dispersed phase is forced through the pores of mesh at higher back pressure and continuous phase is carried along with dispersed phase if back pressure is low. Thus, back pressure plays an important role for complete phase separation. In principle, non-intrusive sensors can be mounted on the outlet tubes of the in-line phase separator to detect the entrainment and then a mechanism can be provided to affect the pressure drop in one of the channels. Thus the in-line phase separator can be made to work continuously.

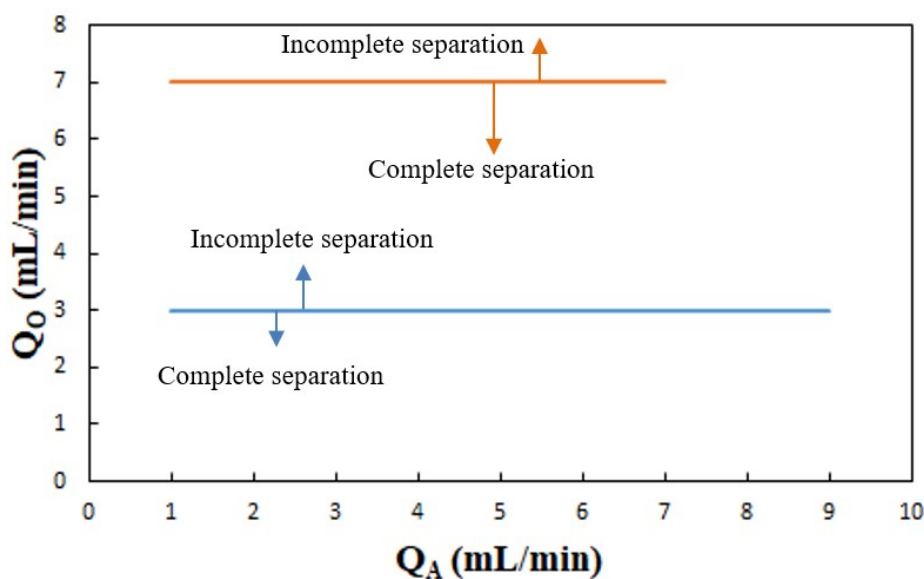


Figure 6.10: Effect of back pressure on phase separation- —without back pressure, —with back pressure. Flow channels are 3 mm wide 6-bend channels and mesh is 300 μm thick.

6.4 MICROCONTACTOR WITH IN-LINE PHASE SEPARATOR

Having obtained the operating window in which complete phase separation is observed, mass transfer experiments were performed. For this extraction of uranium from the aqueous phase to the organic phase was studied. Aqueous uranyl nitrate stream was contacted with 30% TBP in dodecane stream at the T-microfluidic junction. Dispersion was generated at the junction and flowed through the microbore tube connected to it where mass transfer took place. The dispersion flowed into the in-line phase separator where phase separation occurred. The effect of residence time (or flow rate) on percentage extraction of uranium was studied. The results of these experiments are shown in Fig.6.11 and Fig.6.12. In-line phase separator in mass transfer experiments comprised of 6-bend flow channels and 200 μm thick mesh having 5 μm pore size. The range of the aqueous phase flow rate and organic phase flow rate was 3-6 mL/min. The residence time shown in Fig.6.11 and Fig. 6.12 is

based on total volume i.e. volume of the micromixer and the upper channel of the in-line phase separator. The residence time based on just micromixer is in the range from 1.5 – 3.4 sec which is very small compared to a conventional contactor.

Stage Efficiency (SE) is defined by Eq. (2.1) and Percentage Extraction (PE) is defined by Eq. (2.2). Distribution coefficient is 6.7. The feed concentration is 700 ppm. Feed acidity is 1 M.

Percentage extraction is found to reduce with increase in residence time. Longer residence time corresponds to a lower flow rate. If the flow rate is less, the dispersion is expected to be coarser leading to smaller specific interfacial area. Lower flow rate will also lead to reduced value of mass transfer coefficients. Thus, a less flow rate may lead to lower overall volumetric mass transfer coefficient leading to reduced percentage extraction, as observed in the experiments. It may be noted that a lower low rate leads to longer residence time also which should promote mass transfer. But the experimental data suggest that in the range of the experiments, on reducing flow rate, the effect of reduction in overall volumetric mass transfer coefficient is more prominent than the effect of increased residence time.

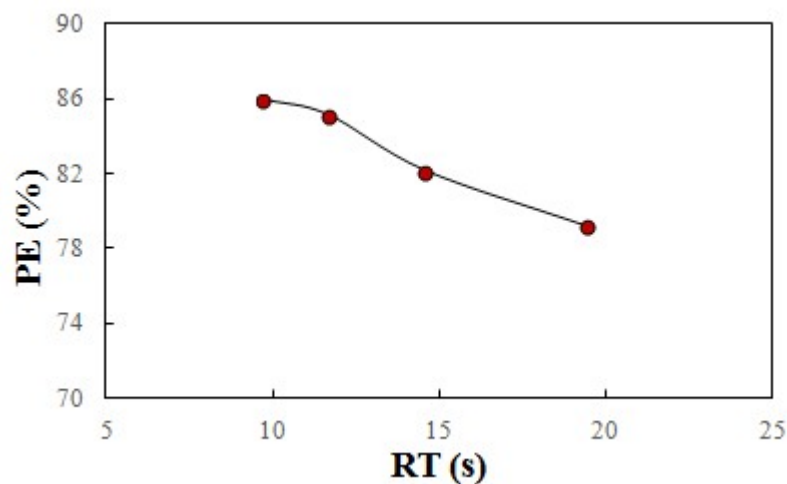


Figure 6.11: Effect of residence time on percentage extraction

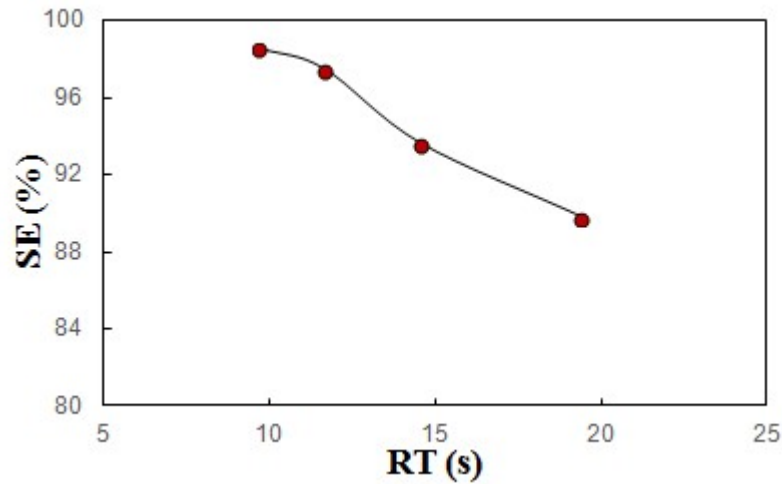


Figure 6.12: Effect of residence time on stage efficiency.

The range of settling rate per unit volume of dispersion band for these experiments is worked out to be $112 - 224 \text{ h}^{-1}$. Whereas, the same for gravity settler is $30 - 120 \text{ h}^{-1}$ as mentioned in chapter 3. In the mass transfer experiments, 6-bend flow channels have been used. However, for the range of flow rate used in the mass transfer experiments, the in-line phase separator comprising 2-bend flow channels are also good. Use of 2-bend channel can further increase the specific settling rate per unit volume of dispersion band by a factor of 1.5. Clearly, the use of in-line phase separator instead of gravity settler can provide significant intensification of settling process.

6.5 CONCLUSIONS

Experiments have been carried out to evaluate metallic mesh based devices for in-line phase separation of liquid-liquid dispersion generated at microfluidic junctions. The effects of flow rates of the aqueous and the organic phases, length of the flow channels, mesh thickness, mesh pore size and back-pressure on the zone of complete phase separation are studied. More number of bends in flow channels (longer flow channels) led to wider phase separation window due to larger residence time in the in-

line phase separator. The window of complete phase separation is found to depend on the width of the flow channel also. The experimental data suggest that the width of the flow channel should be optimum as both very small width and a very large width are expected to affect the window of complete phase separation adversely. An increase in mesh thickness increases the fluidic resistance for the continuous phase passing through the mesh and thus adversely affects the phase separation. Mesh pore size also affects the phase separation window, too small a pore size or too large a pore size adversely affects the complete phase separation window. Phase separation characteristics can be improved by modifying the pressure drop across the metallic mesh by altering the back pressure. Mass transfer experiments on uranium extraction is performed at the conditions for which complete phase separation occurred. Percentage uranium extraction is found to reduce with increase in residence time which indicated that the effect of reduced flow rate on specific interfacial area and mass transfer coefficients is more significant than the effect of reduced flow rate on the residence time. Specific settling rate per unit volume of dispersion band is compared for the in-line phase separator and the gravity settler. It is observed that the use of in-line phase separator leads to intensification of the settling process.

CHAPTER 7

RECOVERY OF URANIUM FROM LEAN STREAMS BY EXTRACTION AND DIRECT PRECIPITATION IN MICROCHANNELS

7.1 INTRODUCTION

The work reported in previous chapters pertains to either extraction or stripping in co-current flow which essentially represents a single-stage mass transfer. The process of recovery of the value material from the strip phase typically involves precipitation process. Thus precipitation is an integral part of a solvent extraction flow sheet. The work reported in this chapter focuses on solvent extraction as well as precipitation of the value material, uranium in this case. Precipitation is attempted directly from the loaded organic thereby combining conventionally two separate stripping and precipitation steps in a single reactive stripping step. Combining two steps into a single step leads to process intensification. This leads to process intensification. The process is implemented in microchannels. Briefly, a continuous processing route for direct precipitation of ammonium diuranate (ADU) from loaded organic using microchannels is explored. Uranium is first extracted from a lean aqueous stream into the organic phase by using a microbore tube such that majority of uranium is picked up by the organic phase. Subsequently, the loaded organic is contacted in another microbore tube with ammonium hydroxide to remove almost entire uranium from the organic phase in the form of ADU. The effects of different operating parameters (residence time, O/A ratio and concentration of ammonium hydroxide) are studied. Reusability of the organic phase after repeated contact with ammonium hydroxide is

also studied. This work specifically addresses the issue of processing of lean streams which are otherwise difficult to process using conventional techniques.

7.2 EXPERIMENTS

7.2.1 Materials

Tributyl phosphate and dodecane were of analytical grade. A solution of uranium of concentration 860 ppm and 1N acidity was used as the aqueous feed. Commercial grade of ammonium hydroxide (specific gravity of 0.91) was used as the strippant.

7.2.2 Setup and procedure

[Fig. 7.1](#) shows the schematic diagram of the experimental setup. The organic phase (30% TBP in dodecane) and the aqueous phase were first contacted in a microchannel comprising a microfluidic T-junction (750 μm diameter, fabricated in SS). A 750 μm diameter PTFE microbore tube followed the T-junction. Syringe pumps were used to pump the liquids at the desired flow rates. The effect of O/A ratio on percentage uranium recovery from the aqueous phase was studied by varying flow rates of the organic and aqueous phases while keeping the total flow rate the same. The raffinate was analyzed for uranium concentration to quantify percentage extraction. The two phases in the dispersion coming out of the microbore tube were separated and the extract phase (loaded organic) was subsequently fed to the second microchannel (750 μm diameter microbore tube connected to a 750 μm diameter PTFE microfluidic T-junction) for direct precipitation in which it was contacted with ammonium hydroxide. The end of the microbore tube was connected to a product collector. A three phase mixture was obtained in the product collector. The solids were separated by filtration,

washed thoroughly with water and dried. Ammonium hydroxide solution and the lean organic phase present in the filtrate were separated and analyzed for uranium content by using ICP-OES. Experiments were carried out for different values of residence time which was varied by varying the flow rate. The effects of residence time, O/A ratio and concentration of ammonium hydroxide solution on percentage uranium recovery, and space-time-yield were studied.

It is worth mentioning here that choking or clogging of the microchannel was not observed during direct precipitation. This is attributed to the fact that the organic phase was the continuous phase in the direct precipitation step. It wetted the PTFE microbore tube and formed a sheath around the aqueous phase drops and thus prevented the solid contained in the aqueous phase drops from coming in contact with the wall of the microbore tube.

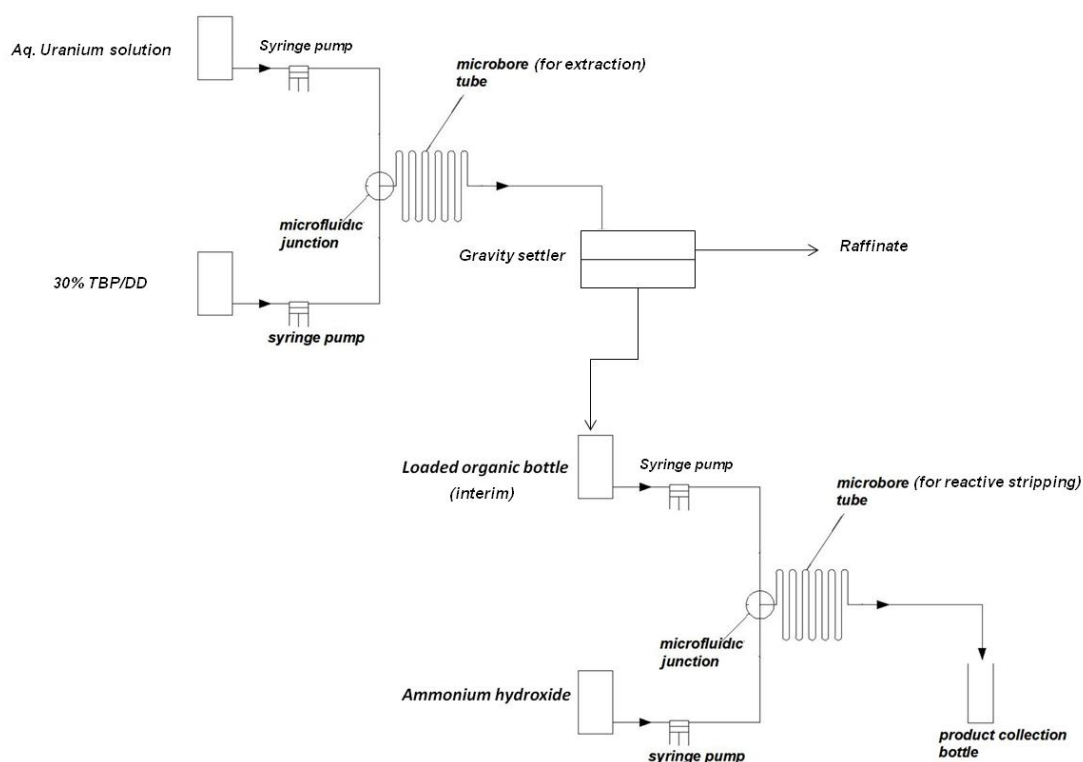


Figure 7.1: Schematic diagram of the experimental setup

7.3 EXTRACTION USING MICROBORE TUBE

Extraction of uranium from the aqueous phase to the organic phase in a microbore tube constituted the first step of the experiments. As the flow in microbore tube was co-current, only a single-stage could be realized. Hence experiments were conducted at high values of O/A ratio so that uranium loss in the raffinate could be minimized. The feed was a lean stream as it is particularly difficult to process using conventional solvent extraction equipment (e.g. mixer-settler, columnar contactors etc.) due to low value of distribution coefficient. The inherent advantages of microchannels like minimal diffusion path lengths as well as very high specific interfacial area make them ideally suited for such applications.

Extraction experiments were conducted using a 750 μm diameter microbore tube of 7.36 m length. Flow velocity (based on total volumetric flow rate) was kept constant such that the residence time obtained was 19.5 sec. Feed concentration in all experiments was maintained constant at 860 ppm. O/A was varied by varying flow rates of the organic phase and the aqueous phase by using respective syringe pumps. Fig. 7.2 shows the percentage extraction of uranium as well as the final uranium concentration in the raffinate phase (C_{exit}) for different values of O/A ratio.

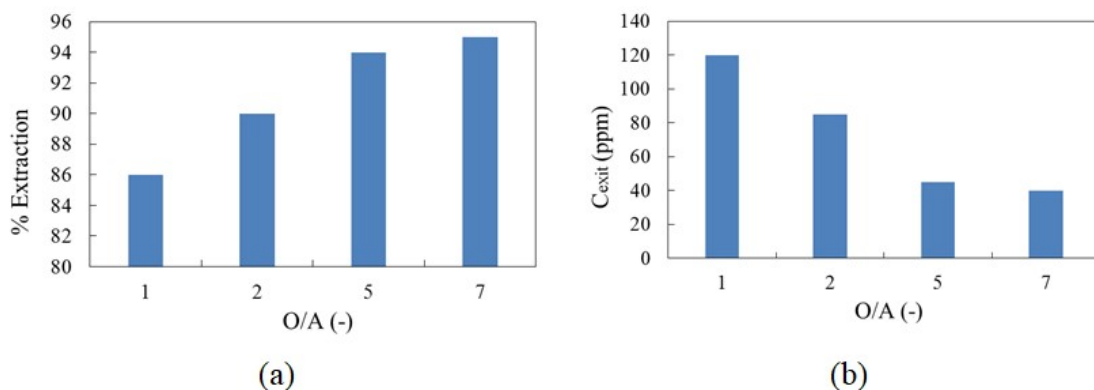


Figure 7.2: Effect of O/A ratio on (a) % uranium extraction and (b) uranium concentration in the raffinate

It can be observed that percent extraction of uranium increases with an increase in O/A ratio. Uranium concentration in the raffinate consequently reduces with an increase in O/A ratio. Increase in percent extraction with increase in O/A ratio is attributed to the presence of a large excess of extracting phase which ensures dilution of the extracted uranium in the extracting phase and thus a large driving force for extraction of uranium from the aqueous phase to the organic phase.

Almost 90% of the initial uranium concentration could be extracted at $O/A = 2$. Corresponding value of uranium concentration in the raffinate phase was 83 ppm. An increase of O/A to 5 could reduce the raffinate uranium concentration to below 50 ppm. However, to maintain organic inventory at a modest value and to ensure that uranium concentration in the organic phase (loaded) is not too low for further experiments on direct precipitation in microchannels, $O/A = 2$ was selected for extraction step. If uranium concentration is too low in the loaded organic phase, very high O/A ratio will be needed to concentrate and precipitate uranium in the aqueous phase during direct precipitation experiments. At higher O/A ratio in direct precipitation, the concentration of the uranium extracted in the aqueous phase will be high which will adversely affect the concentration gradient that drives the mass transfer.

7.4 DIRECT PRECIPITATION USING MICROBORE TUBES

In the second step of the experiments, the loaded organic phase was contacted with ammonium hydroxide for direct precipitation in another microchannel.

Preliminary direct precipitation experiments were carried out to identify the conditions in which stable continuous operation could be attained. As the concentration of

uranium in the organic phase was low, ADU precipitation did not start right at the location of the microfluidic junction but occurred down the line in the microbore tube. Both the microfluidic junction and the microbore tube were hydrophobic and hence were preferentially wetted by the organic phase. This ensured that the solids formed (enclosed in the dispersed aqueous phase) did not come in contact with the wall of the microchannel. Thus the microreactor system worked continuously without choking/clogging due to solids. Percent uranium recovery in direct precipitation step was estimated from the difference of uranium concentration in the loaded organic phase and the sum of uranium concentration in the stripped organic phase and the strippant phase. Space-time-recovery (STR, gm/L-day) of the reactor and recovery rates (RR, gm/day) were quantified as per the following expressions.

$$RR = 0.0000144C_oQ_oR \quad (7.1)$$

$$STR = RR/V_r \quad (7.2)$$

Where, C_o is the initial uranium concentration in the loaded organic (ppm), Q_o is the loaded organic flow rate (mL/min), R is the percent uranium recovery (in %) and V_r is the reactor volume (L).

7.4.1 Effect of residence time

The direct precipitation step used in this work is essentially a reactive step in which there exists a concentration gradient of uranium between the organic phase and the aqueous phase along the entire length of the microbore tube. Hence, unlike a typical stage-wise solvent extraction or stripping process there is no equilibrium limitation. Thus, theoretically, in a single microbore tube the entire uranium present in the loaded organic phase can be removed. This technique thus obviates the need of multi-stage

operation typically required in stripping of uranium from loaded organic using acidified water (0.01 N nitric acid).

Residence time or contact time being an important parameter, its role in percentage recovery of uranium from loaded organic phase was studied. As the process is not equilibrium limited, the extent of uranium recovery depends on the residence time. Residence time was varied by varying the flow rate of the phases (maintaining O/A constant). However, as the volumetric flow rate was changed the flow velocity inside the microbore tube also changed. [Fig. 7.3](#) shows the effect of residence time on percent uranium recovery.

Essentially, uranium is first stripped from the loaded organic phase to the aqueous phase (dispersed as slugs/drops in the organic phase) and then it reacts with ammonium hydroxide to form ADU. The overall process involves two steps – mass transfer of uranium from organic phase to aqueous phase and the precipitation reaction occurring inside the slug/drop which is the reaction step. [Fig. 7.3](#) shows that as residence time is increased percentage uranium recovery keeps on reducing except for a small range at very low values of residence time where there is a small increase in percent uranium recovery with increase in residence time. Residence time was varied by changing the flow rate which in turn changed the flow velocity. Thus a high value of residence time is characterized by low velocity. At low velocity slugs formed at the microfluidic junction are longer as shear stress acting on the interface is less which leads to a reduction in specific interfacial area (for the same dispersed phase holdup). Moreover, internal recirculation inside the aqueous phase drops/ slugs is also less at low velocity. These two factors lead to poor mass transfer at low velocities ([Kashid et al., 2011](#); [Sen et al., 2016](#)). This effect is further compounded for dilute systems in

which, due to smaller driving force for mass transfer, the mass transport of uranium from the organic phase to the aqueous phase becomes the rate limiting step. Had the direct precipitation process been kinetically controlled (i.e. reaction of stripped uranium with ammonium hydroxide present in aqueous phase were the rate controlling step) percentage uranium recovery should have increased with increase in residence time. However, the fact that percent uranium recovery reduced with an increase in residence time shows that mass transfer of uranium from the organic phase to the aqueous phase is the rate limiting step in the two-step process of stripping followed by precipitation.

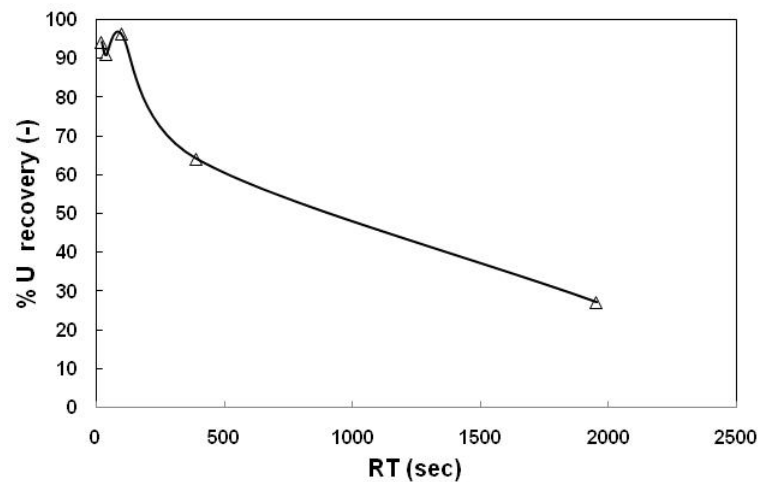


Figure 7.3: Variation of percent uranium recovery from loaded organic with residence time ($O/A=6$; $D_T=0.8$ mm; $L_T=7.35$ m)

This fact is better represented in Fig. 7.4 which shows the variation of percentage uranium recovery with velocity. Fig.7.4 also shows the variation of concentration of uranium in the lean organic phase, space-time-recovery (STR) and recovery rate (RR) of uranium with velocity. RR and STR are obtained from Eq. (7.1) and Eq. (7.2).

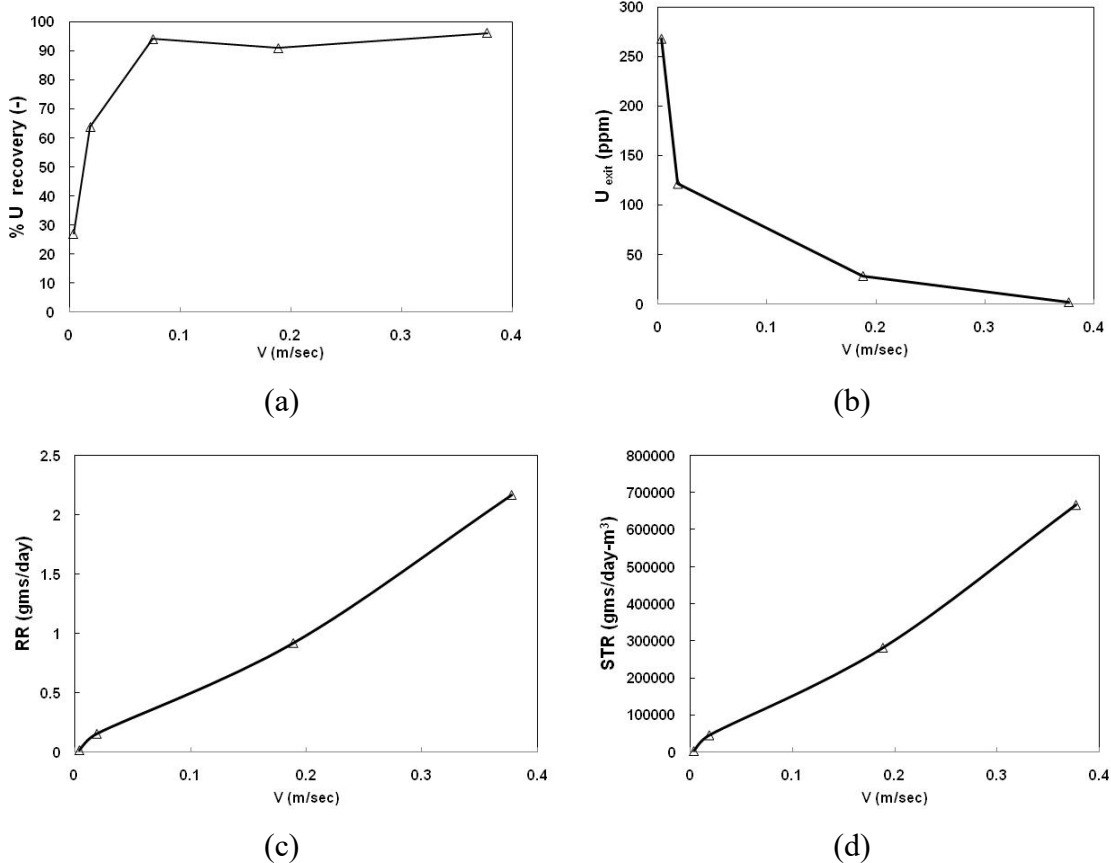


Figure 7.4: Effect of velocity on (a) percent uranium recovery from the organic phase (b) uranium concentration in the lean organic phase (c) recovery rate (d) space-time-recovery. ($O/A=6$; $D_T=0.8$ mm; $L_T=7.35$ m)

As is observed from Fig. 7.4(a), an increase in flow velocity leads to an increase in percentage recovery of uranium from the organic phase. A corresponding reduction in uranium concentration in the lean organic phase is also noted in Fig. 7.4(b). Values of STR and RR keep on increasing with increase in flow velocity. This is because RR and STR are directly proportional to volumetric flow rate (according to Eq. 7.1 and Eq. 7.2) which in turn is proportional to the flow velocity.

An important result is that about 95% uranium recovery from the loaded organic can be attained with in a very short contact time of 19.5 sec for an O/A ratio of 6. Corresponding value of STR, as high as 1382160 gm/m³-day, can be attained while

ensuring a uranium concentration of about 2 ppm in the lean organic phase and about 123 ppm in the aqueous phase exiting the reactor.

7.4.2 Effect of O/A ratio

Fig. 7.5 shows the effect of O/A ratio on percentage uranium recovery from the organic phase, space-time-recovery and recovery rate. As O/A ratio was varied, total volumetric flow rate was maintained constant thereby keeping total flow velocity and residence time the same. It is observed that percentage recovery reduced with increasing O/A ratio. Similar trend is also observed for the recovery rate (RR) as well as space-time-recovery (STR).

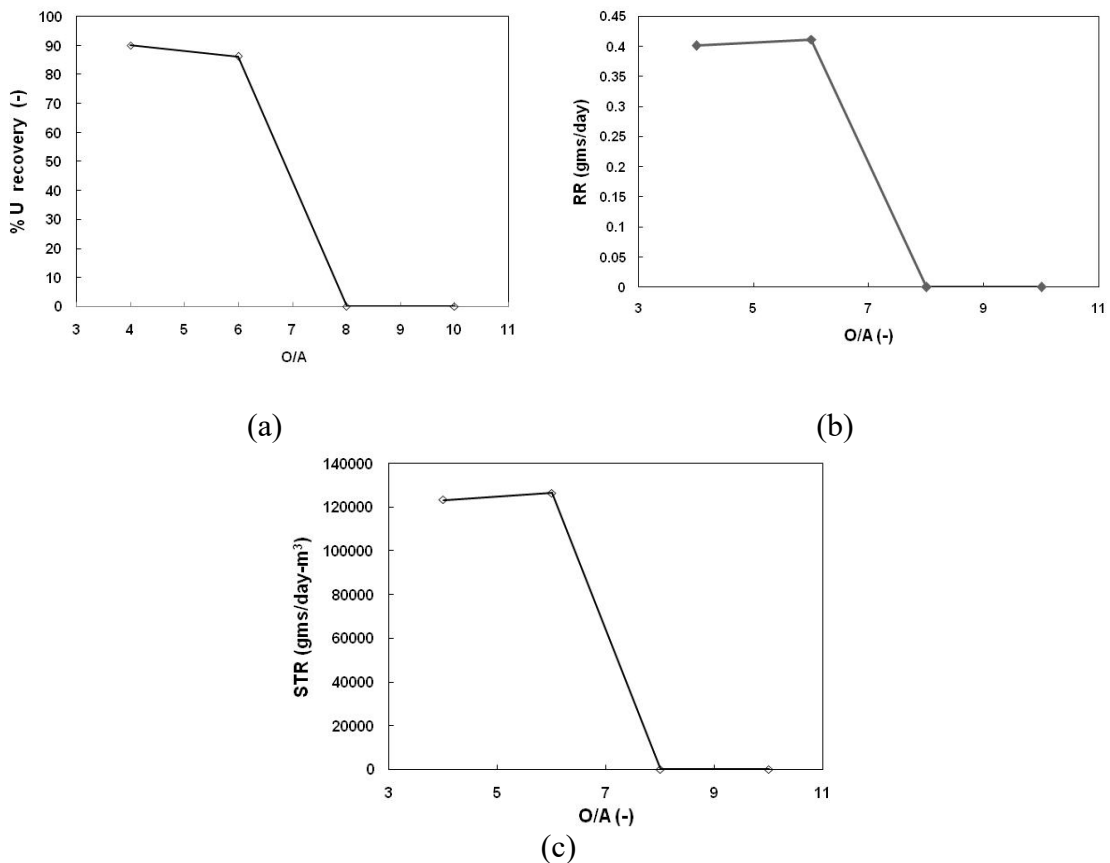


Figure 7.5: Effect of O/A ratio on (a) percentage uranium recovery from loaded organic (b) recovery rate (c) space time recovery ($v=0.037$ m/sec; $D_T=0.8$ mm; $L_T=7.35$ m)

Values of O/A were kept high to ensure precipitation from loaded organic containing low concentration of uranium. Hence O/A ratio was varied in the range from 4 to 10. This ensured that uranium present in the loaded organic phase is contacted with a relatively smaller volume of the aqueous phase containing ammonium hydroxide leading to higher concentrations of uranium in the aqueous strip phase which would, in turn, lead to efficient precipitation of ADU.

More than 90% recovery of uranium from the organic phase could be attained when O/A and residence time were 4 and 195 sec, respectively. Corresponding values of RR and STR were 0.4 gm/day and 123335 gm/day-m³ respectively. However, it is interesting to note that as the O/A ratio is increased beyond 6, percentage uranium recovery reduces to almost zero with a corresponding increase in uranium concentration in the lean organic phase. Similar trends are also observed for RR and STR for which an increase in O/A leads to significant reduction in RR and STR. This is attributed to the fact that with an increase in O/A ratio, two consecutive aqueous phase drops/slugs are separated by a large volume of organic phase. Thus the uranium present in the central regions of the organic phase (continuous phase) has a longer path to traverse to come in contact with the aqueous phase (dispersed phase) and get stripped to the aqueous phase. In other words, an increase in O/A ratio reduces the phase fraction of the dispersed aqueous phase leading to a reduction in specific interfacial area. This adversely affects mass transfer in the microchannel.

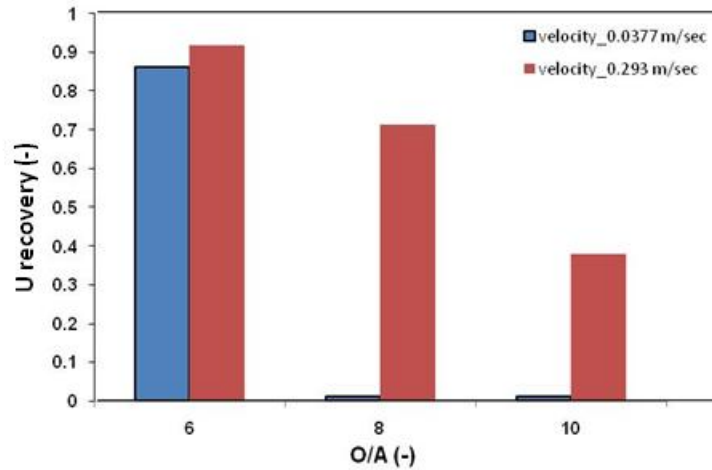


Figure 7.6: Effect of O/A and flow velocity on percent uranium recovery

Fig. 7.6 shows the variation of percentage uranium recovery from loaded organic phase with O/A ratio for two different values of flow velocity. It is clearly observed that an increase in flow velocity leads to an enhancement in percentage uranium recovery for all O/A ratios. This is due to the fact that mass transfer of uranium from the organic phase to the aqueous phase is enhanced at higher velocities. This is similar to the observations made in Fig. 7.4.

One important point to be noted is that the organic flow rate used in one of the direct precipitation experiments (organic phase flow rate of 6.67 mL/min, total volumetric flow rate of 7.77 mL/min, total flow velocity of 0.293 m/sec) is the same as that used in the extraction studies. This means that under the above mentioned condition, the loaded organic generated in the extraction step can be processed in the direct precipitation step sequentially and continuous processing with recycle of the organic phase can be achieved. Thus the extraction step can process a lean uranium stream at a total (combining both organic and aqueous phases) throughput of 10 mL/min ($O/A=2$). The uranium concentration in the feed stream can be reduced from 860 ppm to 86.5 ppm signifying 89.93% recovery of uranium within a residence time of 19.5 sec. The

loaded organic phase can be separated using a gravity settler and injected using a syringe pump into the second microreactor dedicated for the direct precipitation step. In this step 91.74 % of the uranium in the organic phase can be removed as ADU with uranium concentration in the stripped organic being only 31 ppm. This can be achieved with in a residence time as short as 25 sec, O/A ratio being 6. Corresponding values of space time recoveries attained in extraction and direct precipitation stages are 1141373 and 1047163 gm U/day-m³ respectively. Under these conditions, the uranium content in the raffinate of the extraction stage is 86.5 ppm while uranium content in stripped organic and the aqueous phase coming out from the reactor are 31 ppm and 4.5 ppm, respectively. Considering the fact that the overall loss of uranium form the entire process is through aqueous route (organic phase being recycled) an overall recovery of 89.78% can be attained.

7.4.3 Effect of concentration of ammonium hydroxide

[Fig. 7.7](#) shows the effect of concentration of ammonium hydroxide in the strip phase on percentage uranium recovery, recovery rate and space-time-recovery. While ammonium hydroxide concentration was varied, other parameters like residence time and O/A ratio were kept constant. Experiments were conducted with two different concentration of ammonium hydroxide – commercial (specific gravity of 0.91) and diluted (25% commercial ammonium hydroxide and 75% DM water). Results are shown for two different values of O/A ratios (6 and 10).

It is once again observed from [Fig. 7.7](#) that percentage uranium recovery is almost zero for O/A ratio of 10. Moreover, percentage uranium recovery, RR and STR at O/A of 6 are not affected by ammonium hydroxide concentration in the strip phase.

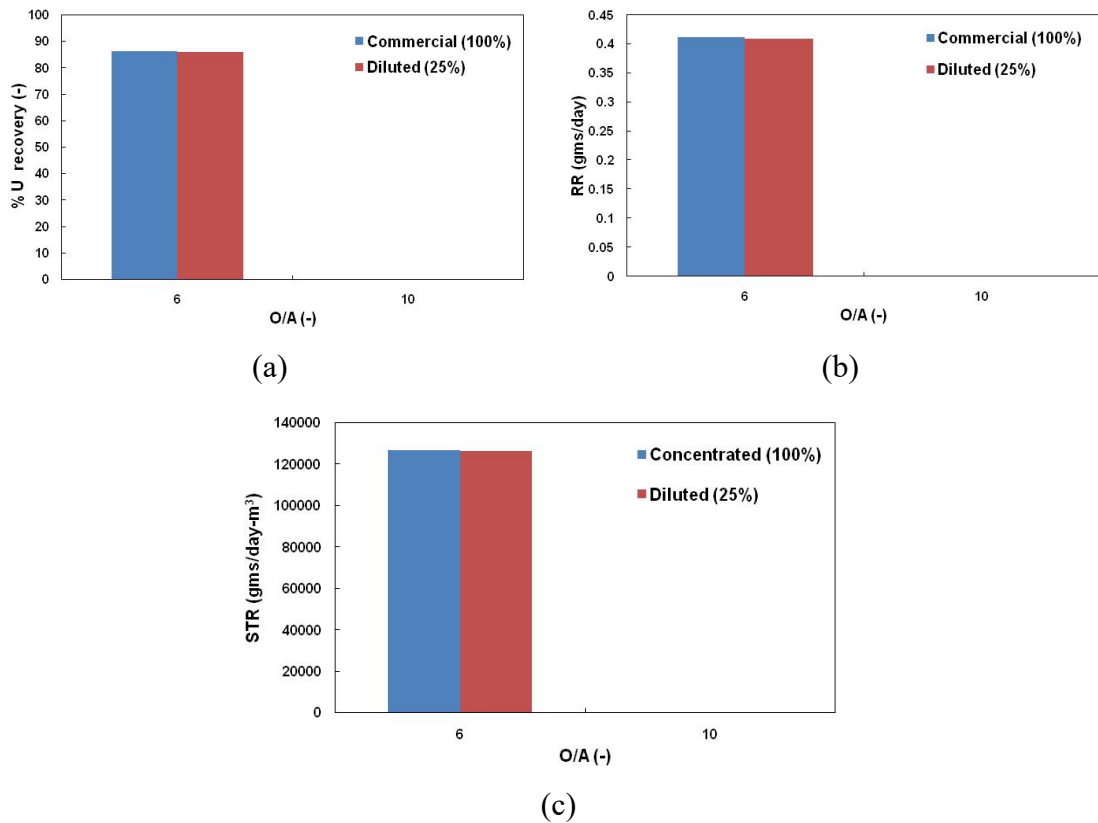


Figure 7.7: Effect of O/A ratio and ammonium hydroxide concentration on (a) percent uranium recovery from loaded organic (b) recovery rate and (c) space time recovery ($v=0.037$ m/sec; $D_T=0.8$ mm; $L_T=7.35$ m)

This is primarily attributed to the fact that the major resistance in the overall process of direct precipitation, mass transfer of uranium from the organic phase to the aqueous phase is rate limiting. Whenever uranium comes in contact with the aqueous phase it immediately reacts with the ammonium hydroxide present in the aqueous phase. Hence the concentration of ammonium hydroxide does not play a major role. This observation also reinforces the idea that the primary resistance offered is that due to interphase mass transfer and not the precipitation kinetics. Had the kinetics been the rate limiting step, an increase in concentration of ammonium hydroxide would have

enhanced the uranium recovery. Having said so, it is important to mention that the concentration of ammonium hydroxide should always be higher than the stoichiometric amount necessary for complete precipitation of uranium present in the loaded organic.

One important observation is that it is not necessary to use commercial (concentrated) ammonium hydroxide to obtain a high degree of precipitation of uranium from the loaded organic in a single microbore tube. Even a diluted ammonium hydroxide strip phase is sufficient. This not only reduces the cost of ammonium hydroxide but also reduces the generation of ammonium nitrate secondary waste.

7.4.4 Reusability of organic phase

In the experiments conducted in this study, the organic phase was contacted with concentrated ammonium hydroxide solution. This is specific to the direct precipitation processes in which uranium is removed from the loaded organic by contacting it directly with concentrated/diluted ammonium hydroxide solution. In conventional stripping in which stripping and precipitation are separately conducted, the organic phase does not come in contact with the ammonium hydroxide solution. Hence, it is important to check whether the contact with ammonium hydroxide has any adverse effect on the reusability of the organic phase.

To establish the reusability of the organic phase, batch solvent extraction and direct precipitation experiments were carried out multiple times using the same organic phase. [Fig. 7.8](#) shows the value of distribution coefficient (K_D) for extraction of uranium from the aqueous phase to the organic phase after each set of extraction and direct precipitation experiments.

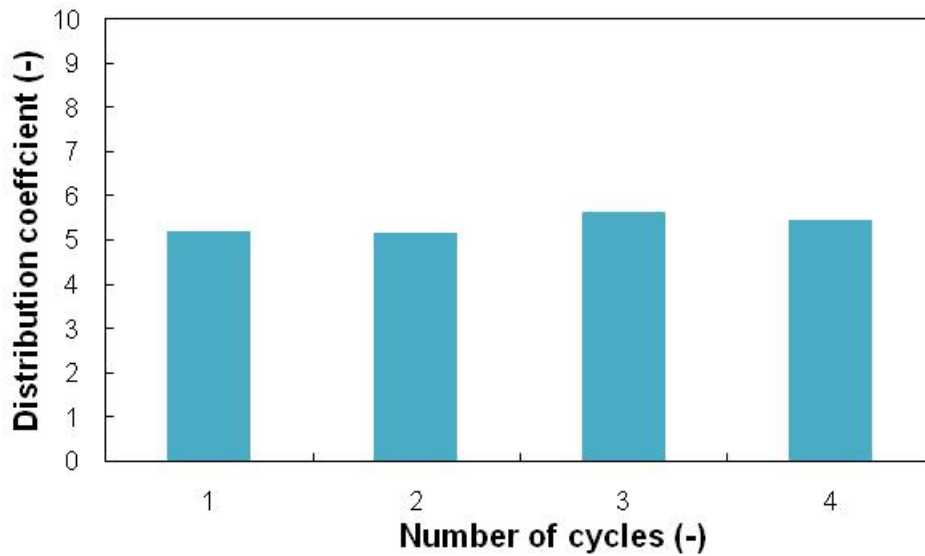


Figure 7.8: Distribution coefficient value measured after repeated contact of organic phase with ammonium hydroxide solution

It can be observed that value of distribution coefficient is almost constant over four cycles. Hence the capability of the organic phase to remove uranium during extraction remains unaffected after repeated contacts with concentrated (commercial) ammonium hydroxide. As observed in [Fig. 7.7](#), even a dilute ammonium hydroxide solution (25%) is able to remove more than 90% uranium from loaded organic. Hence it can be safely said that the organic phase will remain suitable for reuse when diluted ammonium hydroxide will be used for direct precipitation process because even with concentrated ammonium hydroxide there is no variation in values of distribution coefficient after four cycles.

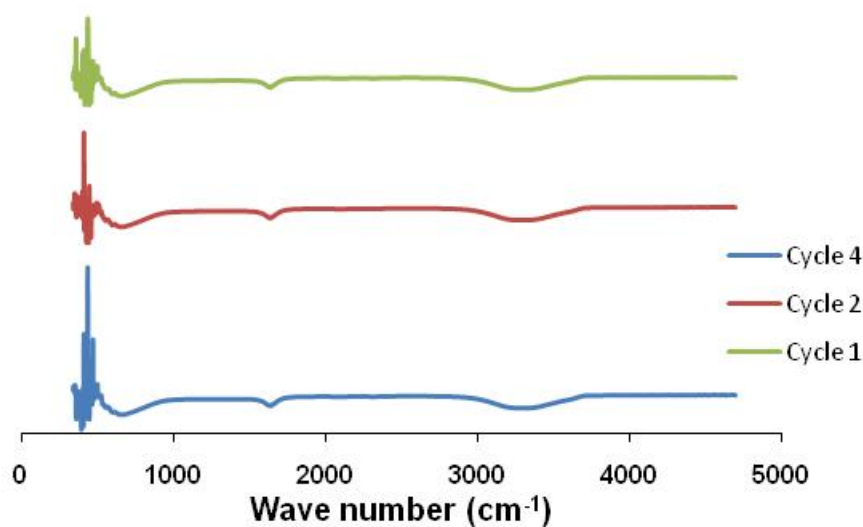


Figure 7.9: FT-IR spectrum of the fresh and recycled organic phase

Fig. 7.9 compares the FT-IR spectrum of the fresh organic phase (30% TBP in dodecane) *vis-à-vis* those of after second and fourth cycles. As is clear from Fig. 7.9, the functional groups in the organic phase remain the same even after repeated contact with concentrated ammonium hydroxide. This substantiate the observation of Fig. 7.8 that distribution coefficient is invariant even after repeated contact of the organic phase with concentrated ammonium hydroxide.

7.5 CONCLUSIONS

A continuous microfluidic method to extract uranium from a lean aqueous stream and reactive precipitation of the loaded organic to directly get ammonium diuranate is presented. The proposed process combines two different steps – multi-stage stripping step using dilute acid and precipitation step - in a single microbore thus simplifying and intensifying the overall process. The effects of different operating parameters such as residence time, flow velocity, O/A ratio and concentration of ammonium hydroxide strippant on percent uranium recovery, space-time-recovery and recovery rates were

studied. An increase in flow velocity was observed to enhance the recovery of uranium from the loaded organic where as an increase in O/A ratio beyond 6 significantly reduced the recovery of uranium from the organic phase. These results indicated that the overall process of stripping and precipitation was mass transfer controlled. A set of operating conditions is identified for which lean aqueous stream could be processed at a total throughput of 10 mL/min (O/A=2) such that about 90% of uranium present in the aqueous feed stream is picked up by the organic phase which is subsequently processed in the direct precipitation step at an O/A ratio of 6 for about 92% recovery of uranium from the organic phase in the form of ADU. Corresponding values of space-time-recovery (STR) attained in the extraction and direct precipitation steps are 1141373 and 1047163 gm U/day-m³ respectively. Recovery rates (RR) for the extraction and direct precipitation steps are 3.71 and 3.41 gm U/day, respectively. It is worth mentioning that under this condition, total rate of uranium loss (in raffinate as well in the aqueous phase exiting the direct precipitation step) is 0.2928 mg/min which corresponds to an overall recovery of 89.78%. No significant effect of dilution of the ammonium hydroxide in the strippant phase on uranium recovery was observed which showed that a dilute ammonium hydroxide stream was good enough to remove more than 90% of the uranium loaded in the organic phase. Further, reusability of the organic phase was also demonstrated over four cycles.

REFERENCES

- Acke, D. R.; Stevens, C. V. (2007). A HCN-based reaction under microreactor conditions: industrially feasible and continuous synthesis of 3, 4-diamino-1 H-isochromen-1-ones. *Green Chemistry*, 9(4): 386-390.
- Al-Rawashdeh, M.; Fluitsma, L. J. M.; Nijhuis, T. A.; Rebrov, E. V.; Hessel, V.; Schouten, J. C. (2012a) Design criteria for a barrier-based gas-liquid flow distributor for parallel microchannels. *Chemical Engineering Journal*, 181-182: 549-556.
- Al-Rawashdeh, M.; Yu, F.; Nijhuis, T. A.; Rebrov, E. V.; Hessel, V.; Schouten, J. C. (2012b) Numbered-up gas-liquid micro/milli channels reactor with modular flow distributor. *Chemical Engineering Journal*, 207-208: 645-655.
- Amaral, J. C. B. S.; Antônio de Morais, C.(2016) Study of Zirconium and Hafnium Separation by Solvent Extraction Technique from Nitric and Hydrochloric Solutions with Acid, Basic and Neutral Extractants. *World Journal of Engineering and Technology*, 4: 138-150.
- Aoki, N.; Tanigawa, S.; Mae, K.(2011)A new index for precise design and advanced operation of mass transfer in slug flow. *Chemical Engineering Journal*, 167: 651-656.
- Bannock, J. H.; Phillips, T. W.; Nightingale, A. M.; Demello, J. C. (2013) Microscale separation of immiscible liquids using a porous capillary. *Analytical Methods*, 5(19): 4991-4998.
- Ban, Y.; Hotoku, S.; Tsutsui, N.; Suzuki, A.; Tsubata, Y.; Matsumura, T. (2016) Uranium and Plutonium Extraction by N,N-dialkylamides using Multistage Mixer-settler Extractors. *Procedia Chemistry*, 21: 156-161.

- Benz, K.; Jäckel, K. P.; Regenauer, K. J.; Schiewe, J.; Drese, K.; Ehrfeld, W.; Hessel, V.; Löwe, H. (2001) Utilization of micromixers for extraction processes. *Chemical Engineering Technology*, 24(1): 11-17.
- Bremond, N.; Thiam, A. R.; Bibette, J. (2008) Decompressing emulsion droplets favors coalescence. *Physical Review Letters*, 100(2): 024501.
- Breisig, H.; Schmidt, M.; Wolff, H.; Jupke, A.; Wessling, M. (2017) Droplet-based liquid–liquid extraction inside a porous capillary. *Chemical Engineering Journal*, 307: 143-149.
- Castell, O. K.; Allender, C. J.; Barrow, D. A. (2009) Liquid-liquid phase separation: Characterisation of a novel device capable of separating particle carrying multiphase flows. *Lab on a Chip*, 9: 388–396.
- Cervera-Padrell, A. E.; Morthensen, S. T.; Lewandowski, D. J.; Skovby, T.; Kiil, S.; Gernaey, K. V. (2012) Continuous hydrolysis and liquid-liquid phase separation of an active pharmaceutical ingredient intermediate using a miniscale hydrophobic membrane separator. *Organic Process Research and Development*, 16: 888–900.
- Charpentier, J. C. (1981) Mass-transfer rates in gas-liquid absorbers and reactors. *In Advances in chemical engineering*, 11: 1-133.
- Cherlo, S. K. R.; Kariveti, S.; Pushpavanam, S. (2010) Experimental and numerical investigations of two-phase (liquid– liquid) flow behavior in rectangular microchannels. *Industrial Engineering Chemistry Research*, 49: 893-899.
- Ciceri, D.; Perera, J. M.; Stevens, G. W. (2014) The use of microfluidic devices in solvent extraction. *Journal of Chemical Technology and Biotechnology*, 89: 771–786.

- Darekar, M.; Sen, N.; Singh, K. K.; Mukhopadhyay, S.; Shenoy, K. T.; Ghosh, S. K.(2014a) Liquid–liquid extraction in microchannels with Zinc–D2EHPA system. *Hydrometallurgy*, 144: 54-62.
- Darekar, M.; Singh, K. K.; Govalkar, S. S.; Joshi, J. M.; Mukhopadhyay, S.; Shenoy, K. T. (2014b) Extraction of Uranium from Dilute Solutions using Microbore Tubes. *BARC Newsletter*, 338: 9-14.
- Darekar, M.; Singh, K. K.; Mukhopadhyay, S.; Shenoy, K. T.; Ghosh, S. K.(2014c) Solvent extraction in microbore tubes with UNPS - TBP in dodecane system. *Separation and Purification Technology*, 128: 96-105.
- Dehkordi, A. M. (2001) Novel type of impinging streams contactor for liquid– liquid extraction. *Industrial & engineering chemistry research*, 40(2): 681-688.
- Dehkordi, A. M. (2002) Liquid–liquid extraction with chemical reaction in a novel impinging-jets reactor. *AIChE journal*, 48(10): 2230-2239.
- De Menech, M.; Garstecki, P.; Jousse, F.; Stone, H. A. (2008) Transition from squeezing to dripping in a microfluidic T-shaped junction. *Journal of Fluid Mechanics*, 595: 141-161.
- Desigan, N.; Velavendan, P.; Pandey, N. K.; Rao, R. S.; Vijayakumar, V.; Mudali ,U. K.; Natarajan, R.(2012)Solvent Extraction Studies of Gadolinium in Tri-Butyl Phosphate. *Procedia Chemistry*, 7: 295-301.
- Dessimoz, A. L.; Cavin, L.; Renken, A.; Kiwi-Minsker, L. (2008) Liquid liquid two-phase flow patterns and mass transfer characteristics in rectangular glass microreactors. *Chemical Engineering Science*, 63: 4035-4044.

- Duan, W.; Zhao, M.; Wang, C.;Cao, S.(2014) Recent Advances in the Development and Application of Annular Centrifugal Contactors in the Nuclear Industry. *Solvent Extraction and Ion Exchange*, 32: 1-26.
- Edwards, C. R.; Oliver, A. J.(2000) Uranium processing: A review of current methods and technology. *The Journal of the Minerals, Metals & Materials Society*, 52: 12-20.
- Fan, F.; Bai, J.; Fan, F.; Yin, X.; Wang, Y.; Tian, W.; Wu, X.; Qin, Z.(2014) Solvent extraction of uranium from aqueous solutions by α -benzoinoxime. *Journal of Radioanalytical and Nuclear Chemistry*. 300: 1039–1043.
- Fang, L.; Yong-hao, L.; Shi-ming, Y. (2008) Analytical and experimental investigation of flow distribution in manifolds for heat exchangers. *Journal of Hydrodynamics*,20(2): 179-185.
- Fernandes, J. B.; Sharma, M. M. (1967) Effective interfacial area in agitated liquid-liquid contactors. *Chemical Engineering Science*, 22(10); 1267-1282.
- Fu, T.; Wei, L.; Zhu, C.; Ma, Y. (2015) Flow patterns of liquid–liquid two-phase flow in non-Newtonian fluids in rectangular microchannels. *Chemical Engineering and Processing: Process Intensification*, 91: 114-120.
- Günther, A., Jensen, K. F. (2006). Multiphase microfluidics: from flow characteristics to chemical and materials synthesis. *Lab on a Chip*, 6(12): 1487-1503.
- Gupta, U.C.; Jayaraj, R.N.; Meena, R.; Sastry, V.S.; Radhakrishna, C.; Rao, S.M.; Sinha, K.K.(1997) Nuclear fuel fabrication - developing indigenous capability. *Proceedings of the fifth international conference on CANDU fuel*, 1: 170-180.
- Hellé, G.; Mariet, C.; Cote, G. (2014) Liquid-liquid Two-Phase Microflow Patterns and Mass Transfer of Radionuclides. *Proceedings of the 9th IEEE International*

- Conference on Nano/Micro Engineered and Molecular Systems* April 13-16, 2014, Hawaii, USA. 157-162.
- Hellé, G.; Mariet, C.;Cote, G.(2015) Liquid-liquid extraction of uranium (VI) with Aliquat® 336 from HCl media in microfluidic devices: Combination of micro-unit operations and online ICP-MS determination. *Talanta*,139: 123–131.
- Holbach, A.; Kockmann, N. (2013) Counter-current arrangement of microfluidic liquid-liquid droplet flow contactors. *Green Processing and Synthesis*, 2: 157–167.
- Hessel, V.; Löwe, H.; Hardt, S. (2004). *Chemical micro process engineering: fundamentals, modelling and reactions* (Vol. 1). John Wiley & Sons.
- Hotokezaka, H.; Tokeshi, M.; Harada, M.; Kitamori, T.; Ikeda,, Y. (2005) Development of innovative nuclide separation system for high level radioactive waste using microchannel chip- extraction behavior of metal ions from aqueous phase to organic phase in microchannel. *Progress in Nuclear Energy*, 47(1-4): 439-447.
- Jiang, F.; Drese, K.F.; Hardt, S.; Küpper, M.; Schönfeld, F.(2004) Helical flows and chaotic mixing in curved micro channels. *AIChE Journal*, 50(9): 2297-2305.
- Ji, X.Y.; Ma, Y. G.; Fu, T. T.; Zhu, C. Y.; Wang, D. J. (2010) Experimental investigation on liquid volumetric mass transfer coefficient for upward gas–liquid two phase flow in rectangular microchannels. *Brazilian Journal of Chemical Engineering*, 27(4): 573-582.
- Kannan, K.; Rudramurthy, R. (2010) Experimental and numerical analysis of laminar and low turbulent flow distribution in inlet dividing header of shell and tube heat exchanger. *Journal of Hydrodynamics*, 22(4): 494-502.

- Kashid, M. N.; Agar, D. W. (2007a) Hydrodynamics of liquid-liquid slug flow capillary microreactor: flow regimes, slug size and pressure drop. *Chemical Engineering Journal*, 131: 1-13.
- Kashid, M. N.; Agar, D. W.; Turek, S. (2007b) CFD modelling of mass transfer with and without chemical reaction in the liquid-liquid slug flow microreactor. *Chemical Engineering Science*, 62(18-20): 5102-5109.
- Kashid, M. N.; Harshe, Y. M.; Agar, D. W. (2007c) Liquid-Liquid Slug Flow in a Capillary: An alternative to suspended drop or film contactors. *Industrial & Engineering Chemistry Research*, 46(25): 8420-8430.
- Kashid, M. N.; Renken, A.; Kiwi-Minsker, L. (2011) Gas-liquid and liquid-liquid mass transfer in microstructured reactors. *Chemical Engineering Science*, 66: 3876-3897.
- Kies, F. K.; Benadda, B.; Otterbein, M. (2004) Experimental study on mass transfer of a co-current gas-liquid contactor performing under high gas velocities. *Chemical Engineering and Processing: Process Intensification*, 43(11): 1389-1395.
- Kolehmainen, E.; Turunen, I. (2007) Micro-scale liquid-liquid separation in a plate-type coalescer. *Chemical Engineering and Processing: Process Intensification*, 46(9): 834-839.
- Kralj, J. G.; Sahoo, H. R.; Jensen, K. F. (2007) Integrated continuous microfluidic liquid-liquid extraction. *Lab on a Chip*, 7: 256-263.
- Kumar, S.; Kumar, B.; Sampath, M.; Sivakumar, D.; Mudali, U. K.; Natarajan, R. (2012) Development of a micro-mixer-settler for nuclear solvent extraction. *Journal of Radioanalytical and Nuclear Chemistry*, 291(3): 707-800

- Kumar, S.; Kumar, B.; Sinha, P. K.; Sampath, M.; Sivakumar, D.; Mudali, U. K. (2017) Extraction of uranium from simulated highly active feed in a micromixer-settler with 30% TBP and 36% TiAP solvents. *Journal of Radioanalytical and Nuclear Chemistry*, 311: 2111–2116.
- Lan, W.; Jing, S.; Li, S.; Luo, G. (2016) Hydrodynamics and mass transfer in a countercurrent multistage microextraction system. *Industrial & Engineering Chemistry Research*, 55(20): 6006-6017.
- Li, S.; Jing, S., Luo, Q.; Chen, J.; Luo, G. (2012) Bionic system for countercurrent multi-stage micro-extraction. *RSC Advances*, 2(29): 10817-10820.
- Liu, G.; Wang, K.; Lu, Y.; Luo, G. (2014) Liquid–liquid microflows and mass transfer performance in slit-like microchannel. *Chemical Engineering Journal*, 258: 34-42.
- Liu, H.; Li, P.; Lew, J. V. (2010) CFD study on flow distribution uniformity in fuel distributors having multiple structural bifurcations of flow channels. *International Journal of Hydrogen Energy*, 35: 9186-9198.
- Logtenberg, H.; Lopez-Martinez, M.J.; Feringa, B.L.; Browne, W.R.; Verpoorte, E.(2011) Multiple flow profiles for two-phase flow in single microfluidic channels through site-selective channel coating. *Lab Chip*, 11: 2030–2034.
- Luo, L.; Fan, Z.; Gall, H. L.; Zhou, X.; Yuan, W. (2008) Experimental study of constructal distributor for flow equidistribution in a mini cross flow heat exchanger (MCHE). *Chemical Engineering and Processing: Process Intensification*, 47: 229-236.
- Mathuthu, M.; Mokhine, N. D.;Stassen, E.(2019) Organic solvent extraction of uranium from alkaline nuclear waste. *Journal of Radioanalytical and Nuclear Chemistry*. 319: 687-693.

- Menzies, I. A.; Rigby, F.(1961) Separation of thorium from uranium and rare earth phosphate-xylene elements by solvent extraction with tri-n-butyl. *Journal of Applied Chemistry*, 11: 104-113.
- Misek, T.; Berger, R.; Schröter, J. (1985). Standard Test Systems for Liquid-Liquid Extraction. European Federation of Chemical Engineering. Working Party on Distillation, Absorption and Extraction, Eds.: The Institution of Chemical Engineers, Rugby, United Kingdom.
- Mohan, V. M.; Kumar, C. S.; Sujatha, V.; Prasad, P. R.; Sarveswarao, S. (2010) Mass transfer correlation development for the presence of entry region coil as swirl promoter in tube. *International Journal of Thermal Sciences*, 49(2): 356-364.
- Moulin, P.; Rouch, J. C.; Serra, C.; Clifton, M. J.; Aptel, P. (1996) Mass transfer improvement by secondary flows: Dean vortices in coiled tubular membranes. *Journal of Membrane Science*, 114(2): 235-244.
- Naphon, P.; Wongwiset, S. (2006) A review of flow and heat transfer characteristics in curved tubes. *Renewable and Sustainable Energy Reviews*, 10(5): 463-490.
- Naphon, P. (2007) Thermal performance and pressure drop of the helical-coil heat exchangers with and without helically crimped fins. *International Communications in Heat and Mass Transfer*, 34(3): 321-330.
- Natarajan, R.; Raj, B.(2007) Fast reactor fuel reprocessing technology in India. *Journal of Nuclear Science and Technology*, 44: 393–397.
- Neira, M.; O'Keefe, T. J.; Watson, J. L. (1992) Solvent extraction reagent entrainment effects on zinc electrowinning from waste oxide leach solutions. *Minerals Engineering*, 5(3-5): 521-534.

- Okubo, Y.; Toma, M.; Ueda, H.; Maki, T.; Mae, K. (2004) Microchannel devices for the coalescence of dispersed droplets produced for use in rapid extraction processes. *Chemical Engineering Journal*, 101: 39-48.
- Okubo, Y.; Maki, T.; Aoki, N.; Khoo, T. H.; Ohmukai, Y.; Mae, K. (2008) Liquid–liquid extraction for efficient synthesis and separation by utilizing micro spaces. *Chemical Engineering Science*, 63: 4070 – 4077.
- Prabhanjan, D. G.; Raghavan, G. S. V.; Rennie, T. J. (2002) Comparison of heat transfer rates between a straight tube heat exchanger and a helically coiled heat exchanger. *International Communications in Heat and Mass Transfer*, 29(2): 185-191.
- Priest, C.; Zhou, J.; Klink, S.; Sedev, R.; Ralston, J. (2012) Microfluidic solvent extraction of metal ions and complexes from leach solutions containing nanoparticles. *Chemical Engineering & Technology*, 35(7): 1312-1319.
- Roy, A.; Darekar, M.; Singh, K. K.; Shenoy, K. T.; Grover, R. B. (2018). Drop formation at nozzles submerged in quiescent continuous phase: an experimental study with TBP-dodecane and nitric acid system. *Nuclear Science and Techniques*, 29(6): 88.
- Rebrov, E. V.; De Croon, M. H. J. M.; Schouten, J. C. (2001) Design of a microstructured reactor with integrated heat-exchanger for optimum performance of a highly exothermic reaction. *Catalysis Today*, 69(1-4): 183-192.
- Saito, M.; Yin, L. J.; Kobayashi, I.; Nakajima, M. (2005) Preparation characteristics of monodispersed oil-in-water emulsions with large particles stabilized by proteins in straight-through microchannel emulsification. *Food Hydrocolloids*, 19(4): 745-751

- Salim, A.; Fourar, M.; Pironon, J.; Sausse, J. (2008) Oil-water two-phase flow in microchannels: Flow patterns and pressure drop measurements. *The Canadian Journal of Chemical Engineering*, 86: 978-988.
- Sattari-Najafabadi, M.; Nasr Esfahany, M.; Wu, Z.; Sunden, B. (2018) Mass transfer between phases in microchannels: A review. *Chemical Engineering and Processing - Process Intensification*, 127: 213-237.
- Sarkar, S.; Singh, K. K.; Shankar, V.; Shenoy, K. T. (2014). Numerical simulation of mixing at 1–1 and 1–2 microfluidic junctions. *Chemical Engineering and Processing: Process Intensification*, 85: 227-240.
- Sarkar, P. S.; Singh, K. K.; Shenoy, K. T.; Sinha, A.; Rao, H.; Ghosh, S. K. (2012) Liquid–liquid two-phase flow patterns in a serpentine microchannel. *Industrial & Engineering Chemistry Research*, 51: 5056-5066.
- Scheiff, F.; Mendorf, M.; Agar, D.; Reis, N.; Mackley, M. (2011) The separation of immiscible liquid slugs within plastic microchannels using a metallic hydrophilic sidestream. *Lab on a Chip*, 11(6): 1022-1029.
- Schneider, M. A.; Maeder, T.; Ryser, P.; Stoessel, F. (2004). A microreactor-based system for the study of fast exothermic reactions in liquid phase: characterization of the system. *Chemical engineering journal*, 101(1-3): 241-250.
- Sen, N.; Darekar, M.; Singh, K. K.; Mukhopadhyay, S.; Shenoy, K. T.; Rao, H.; Ghosh, S. K. (2014) Solvent extraction and stripping studies in microchannels with TBP nitric acid system. *Solvent Extraction and Ion Exchange*, 32(3): 281-300.
- Sen, N.; Singh, K. K.; Mukhopadhyay, S.; Shenoy, K. T.; Ghosh, S. K. (2013) Continuous, solvent free, high temperature synthesis of ionic liquid 1-butyl-3-methylimidazolium bromide in a microreactor. *BARC Newsletter*, 334: 20-23.

- Sen, N.; Singh, K. K.; Mukhopadhyay, S.; Shenoy, K. T. (2016) On continuous, solvent-free synthesis of ionic liquid [BMIM]Br in a microbore tube. *Journal of Radioanalytical and Nuclear Chemistry*, 307(2): 1001-1009.
- Shin, C.; Kim, J.; Kim, J.; Kim, H.; Lee, H.; Mohapatra, D.; Ahn, J.; Ahn, J.; Bae, W., (2009) Recovery of nitric acid from waste etching solution using solvent extraction. *Journal of Hazardous Materials*, 163: 729-734.
- Singh, K. K.; Mahajani, S. M.; Shenoy, K. T.; Ghosh, S. K.(2008) CFD modeling of pump-mix action in continuous flow stirred tank. *AIChE Journal*, 54(1): 42-55.
- Singh, K. K.; Renjith, A. U.; Shenoy, K. T. (2015). Liquid–liquid extraction in microchannels and conventional stage-wise extractors: a comparative study. *Chemical Engineering and Processing: Process Intensification*, 98: 95-105.
- Sivaramakrishna, M.; Raut, D. R.; Nayak, S. K.; Nayak, S. K.; Mohapatra, P. K. (2019) Extraction of plutonium (IV) from acidic feeds using several diamides with a tri-phenyl pyridine centre. *Journal of Radioanalytical and Nuclear Chemistry*. 320: 245-253.
- Smirnov, A. L.; Skripchenko, S. Y.; Rychkov, V. N.; Pastukhov, A. M.; Shtutsa, M. G. (2013). Uranium stripping from tri-n-butyl phosphate by hydrogen peroxide solutions. *Hydrometallurgy*, 137: 18-22.
- Sugiura, S.; Nakajima, M.; Tong, J.; Nabetani, H.; Seki, M. (2000) Preparation of monodispersed solid lipid microspheres using a microchannel emulsification technique. *Journal of Colloid and Interface Science*, 227(1): 95-103.
- Su, Y.; Zhao, Y.; Chen, G.; Yuan, Q.(2010) Liquid–liquid two-phase flow and mass transfer characteristics in packed microchannels. *Chemical Engineering Science*, 65(13): 3947-3956

- Takebayashia, Y.; Suea, K.; Yodaa, S.; Furuyaa, T.; Maeb, K.(2012) Direct carbonylation of nitrobenzene to phenylisocyanate using gas–liquid slug flow in microchannel. *Chemical Engineering Journal*, 180: 250-254.
- Tamagawa, O.; Muto, A. (2011) Development of cesium ion extraction process using a slug flow. *Chemical Engineering Journal*, 167(2-3): 700-704.
- Tonkovich, A.; Kuhlmann, D.; Rogers, A.; McDaniel, J.; Fitzgerald, S.; Arora, R.; Yuschak, T. (2005) Microchannel technology scale-up to commercial capacity. *Chemical Engineering Research and Design* 83(6): 634-639.
- Torab-Mostaedi, M.; Ghaemi, A.; Asadollahzadeh, M.;Pejmanzad, P.(2011) Mass transfer performance in pulsed disc and doughnut extraction columns. *Brazilian Journal of Chemical Engineering*. 28; 447 - 456.
- Tsaoulidis, D.; Dore, V.; Angeli, P.; Plechkova, N. V.; Seddon, K. R.(2013a) Dioxouranium(VI) extraction in microchannels using ionic liquids. *Chemical Engineering Journal*, 227: 151-157.
- Tsaoulidis, D.; Dore, V.; Angeli, P.; Plechkova, N. V.; Seddon, K. R.(2013b) Extraction of dioxouranium (VI) in small channels using ionic liquids. *Chemical Engineering Research and Design*, 91(4): 681-687.
- Tsaoulidis, D. (2014) Studies of intensified small-scale processes for liquid-liquid separations in spent nuclear fuel reprocessing, PhD dissertation, UCL (University College London).
- Vansteene, A.; Jasmin, J.; Cote, G.; Mariet, C.(2018) Segmented Microflows as a Tool for Optimization of Mass Transfer in Liquid–Liquid Extraction: Application at the Extraction of Europium (III) by a Malonamide.*Industrial & Engineering Chemistry Research*, 57: 11572-11582.

- Veliscek-Carolan, J. (2016) Separation of actinides from spent nuclear fuel: A review. *Journal of Hazardous Materials*, 318: 266–281.
- Verma, R. P.; Sharma, M. M. (1975) Mass transfer in packed liquid—liquid extraction columns. *Chemical Engineering Science*, 30(3): 279-292.
- Veser, G. (2001). Experimental and theoretical investigation of H₂ oxidation in a high-temperature catalytic microreactor. *Chemical Engineering Science*, 56(4): 1265-1273.
- Wang, K.; Luo, G. (2017). Microflow extraction: A review of recent development. *Chemical Engineering Science*, 169: 18-33.
- Wang, T.; Xie, T.; Xu, C.(2019) Microextractors applied in nuclear-spent fuel reprocessing: Micro/mini plants and radiochemical analysis. *Critical Reviews in Environmental Science and Technology*, 39: 1-31.
- Weeranoppanant, N.; Adamo, A.; Sapparaiuly, G.; Rose, E.; Fleury, C.; Schenkel, B.; Jensen, K. F.(2017) Design of Multistage Counter-Current Liquid-Liquid Extraction for Small-Scale Applications. *Industrial and Engineering Chemistry Research*, 56: 4095–4103.
- Willersinn, S., Bart, H. J. (2015) Reactive mass transfer in a membrane-based microcontactor. *Chemical Engineering and Processing: Process Intensification*, 95: 186-194.
- Wu, Z.; Yang, F.; Zhang, Z.; Bao, Z. (2014) Magnesium based metal hydride reactor incorporating helical coil heat exchanger: Simulation study and optimal design. *Applied Energy*, 130: 712-722.

- Yagodnitsyna, A. A.; Kovalev, A. V.; Bilsky, A. V. (2016) Flow patterns of immiscible liquid-liquid flow in a rectangular microchannel with T-junction. *Chemical Engineering Journal*,303; 547-554.
- Zhang, J.; Qin, Z.; Deng, D.; Liao, J.; Wei, X.; Zhang, N.(2016) A novel method for the online measurement of impurities in uranium by coupling microfluidics with ICP-MS. *Journal of Analytical Atomic Spectrometry*. 31: 934-939.
- Zhang, X.; Stefanick, S.; Villani, F. J. (2004). Application of microreactor technology in process development. *Organic process research & development*, 8(3): 455-460.
- Zhao, M.; Cao, S.; Duan, W. (2014) Effects of some parameters on mass-transfer efficiency of a ϕ 20 mm annular centrifugal contactor for nuclear solvent extraction processes. *Progress in Nuclear Energy*, 74: 154-159.
- Zhao, Y.; Chen, G.; Yuan, Q. (2006) Liquid-liquid two-phase flow patterns in a rectangular microchannel. *AIChE Journal*,52: 4052-4060.
- Zhao, Y.; Chen, G.; Yuan, Q. (2007) Liquid-liquid two-phase mass transfer in the T-junction microchannels. *AIChE Journal*, 53(12): 3042-3053.
- Zhao, Y.; Su, Y.; Chen, G.; Yuan, Q. (2010) Effect of surface properties on the flow characteristics and mass transfer performance in microchannels. *Chemical Engineering Science*, 65: 1563-1570.
- Zhiwei, F.; Xingui, Z.; Lingai, L.; Weikang, Y. (2009) Numerical investigation of constructal distributors with different configurations. *Chinese Journal of Chemical Engineering*17(1): 175-178.
- Zhu, C.; Li, C.; Gao, X.; Ma, Y.; Liu, D. (2014) Taylor flow and mass transfer of CO₂ chemical absorption into MEA aqueous solutions in a T-junction microchannel. *International Journal of Heat and Mass Transfer*, 73: 492-499.

Thesis Highlight

Name of the Student: Mayur Ramesh Darekar

Name of the CI/OCC: BARC

Enrolment No.: ENGG01201404004

Thesis Title: Liquid-liquid two-phase flow and mass transfer in microchannels

Discipline: Engineering Sciences

Sub-Area of Discipline: Chemical Engineering

Date of viva voce: 21/07/2020

There are several advantages of carrying out solvent extraction in microchannels. In microchannels, the size of the dispersed phase is restricted leading to high specific interfacial area and high overall volumetric mass transfer coefficients. The quality of dispersion can be precisely controlled, which helps in fast settling thereby reducing the size of phase disengagement section. Scale-up of solvent extraction in microchannel is relatively easier as throughput is increased by numbering-up approach.

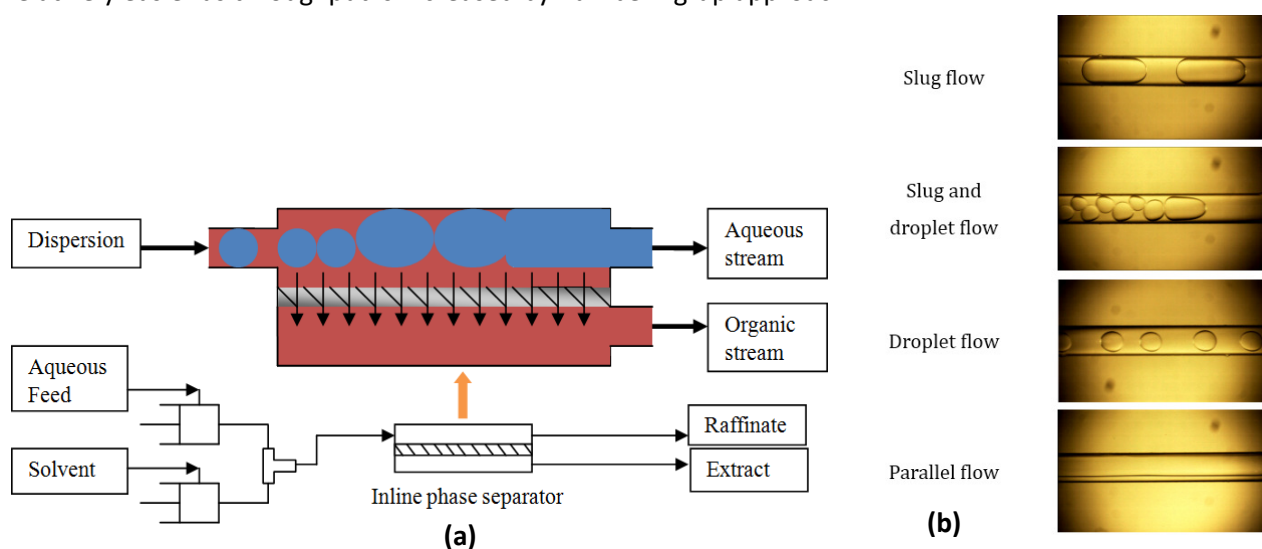


Figure 1. (a) In-line phase separator housing a metallic mesh (b) Different flow patterns in Y-junction microchannel

The liquid-liquid two-phase hydrodynamics in a microchannel is very complex as different flow patterns are possible. Specific interfacial area and overall volumetric mass transfer coefficient in a microchannel depend on the type of flow pattern. Flow pattern affects liquid-liquid phase separation also. Therefore, mass transfer and phase separation is significantly affected by the prevailing hydrodynamics. Experimental work carried out in this research aimed at understanding hydrodynamics, mass transfer and phase separation for solvent extraction in microchannels. Generalized flow regime maps for liquid-liquid two-phase flow in Y-junction microchannels are obtained. Methodology to identify an optimum configuration for solvent extraction in microchannel at a desired throughput for a given liquid-liquid system is proposed. A novel monoblock distributor having in-built microfluidic junctions for realizing higher throughputs using numbering-up approach is conceptualized and tested. Intensification of phase separation of a liquid-liquid dispersion generated at a microfluidic junction is explored by using an in-line phase separator housing a metallic mesh (Figure 1). Finally, a complete intensified process of recovery of uranium from lean streams comprising of extraction, and direct precipitation from loaded organic is demonstrated by using microchannels.